Multi-scale simulation of fluvio-deltaic and shallow marine stratigraphy

Rory Dalman

Multi-scale simulation of fluvio-deltaic and shallow marine stratigraphy

Multi-schaal simulatie van fluvio-deltaische en ondiep mariene stratigrafie (met een samenvatting in het Nederlands)

ter verkrijging van de graad van doctor
aan de Technische Universiteit Delft,
op gezag van de Rector Magnificus prof. dr. ir. J.T. Fokkema,
voorzitter van het College voor Promoties
in het openbaar te verdedigen op 12 juni 2009 om 14:00 uur
door
Rory Alan Forbes DALMAN

doctorandus in de Geologie
geboren te 's Gravenhage

Dit proefschrift is goedgekeurd door de promotor:
Prof. dr. S.B. Kroonenberg

Copromotor:
Dr. G.J. Weltje

Samenstelling promotiecommissie:

Rector Magnificus, voorzitter
Prof. dr. S.B. Kroonenberg, Technische Universiteit Delft, promotor
Dr. G.J. Weltje ,Technische Universiteit Delft, copromotor
Prof. dr. S.M. Luthi, Technische Universiteit Delft
Prof. dr. ir. M.J.F. Stive, Technische Universiteit Delft
Prof. dr. P.L. de Boer, Universiteit Utrecht
Prof. dr. P.M. Burgess, Royal Holloway University of London
Prof. dr. ir. A. Veldkamp, Wageningen Universiteit en Researchcentrum
Prof.dr. J.J.G. Reijmer, Technische Universiteit Delft, reservelid

The research described in this thesis has been supported by the Delft University of Technology, speerpunt Earth and speerpunt Water

Printed by Wöhrmann Print Service, Zutphen
ISBN 978-90-8570-292-4

Voor Christa en Findlay

Contents

Multi-scale simulation of fluvio-deltaic and shallow marine stratigraphy

Chapter 1
Introduction

Scope

In general, the objective of modelling stratigraphy is to determine the underlying rules or laws governing the complex interplay of processes. Some form of long-term self-organisation is present, as the ultimate averaging or accumulation of processes usually ends in a predictable and recognisable end product. By using the expertise gained in short term (decadal-scale) modelling and extrapolating these models, an improved stratigraphic model incorporating morphodynamic features is obtainable. Numerical modelling of stratigraphy has reached the stage in which simulation of continental-margin evolution over long time spans is feasible. Existing numerical models are capable of producing realistic-looking stratal patterns in a range of environments from fluvio-deltaic to slope-basin settings, in response to external forcing by tectonics, sea level and climate. Many of these models are dedicated to a single environment and/or restricted to a 2D subspace (cross section or plan view). The next logical step is to extend and couple such models so as to produce a comprehensive 3D model of a continental margin.

The aim of this thesis is to illustrate how a sediment dispersal system spanning several sedimentary environments can be represented in a dynamic model. The ultimate aim in the discipline of sedimentary system dynamics is to approach a full source to sink representation of the system; this thesis is a step towards this goal. The areas described here are restricted to fluvial and shallow marine processes. Ultimately coupling of different models for sediment production in the drainage basin and the inclusion of subaqueous gravity flows may allow a larger scope.

Why numerical modelling?

No direct experimentation is feasible on time scales longer than several decades. This means that sedimentary geology, as does evolutionary biology and astronomy, suffers from the classic inverse problem. That is, the result (stratigraphy) is known, but the process (sediment deposition and erosion) itself not. There are several ways in which we can deal with this problem. We can interpolate current processes to geologically relevant time scales (i.e. the present is the key to the past), but this is likely to lead to a bias towards high-frequency processes even in situations where low-frequency, high-magnitude processes dominate the system. Conceptual models allow us to qualitatively understand the interaction in a sedimentary system. Yet these model types cannot be adequately tested, as they are mostly qualitative. This means that the relative influence of controls can, at best, be indicated in comparative terms of less and more since the output of the models only varies in direction (i.e. positive or negative). Another option is to use scale, laboratory models of the system, which result in a useful qualitative understanding of large-scale phenomena (e.g. glacio-eustatic forcing of river-shelf systems). This method is feasible, and indeed used successfully for certain scale-invariant processes, however for clastic sedimentary systems upscaling issues

concerning the flow dynamics and sediment transport make comparisons with real-world settings problematic. A very promising method to deal with the inverse problem is to create a mathematical or numerical model of the sedimentary processes, based on conjectures of the physics or abstractions thereof. Although this method of modelling is as subjective as the other methods of explaining stratigraphy and sedimentary architecture, it does generate quantitative results and consequently the results can be evaluated quantitatively.

Although numerical models may answer many theoretical questions, they cannot be used efficiently and properly without quantitative field data. The explicit nature of the model results and current 3D graphics output increase the possibility of bias towards believing in model results. Theoretical model results should always be tested using field data, to confirm or disprove the hypothesis.

Conversely, numerical models can be used to explain field data. Using multiple scenarios, one can determine the probability of each scenario, by carefully evaluating the goodness of fit between model output and field data. This does require an extensive field dataset and careful evaluation of the definition of goodness-of-fit for each region of study. Although there are severe limits to the validation of models and theories in the earth sciences (Oreskes et al, 1994), well-researched areas may still retain enough information to make at least an order of magnitude estimation of the forcing mechanisms. Another benefit of numerical models is that they are inherently good teaching tools due to their interactive nature (Flemings and Grotzinger, 1996).

Classification of dynamic sedimentary system models

Several model types are available that allow for investigation of sediment dynamics. I will discuss several themes here in order to give the reader a brief overview of the possibilities and the relative strengths and weaknesses of each approach. Purely object-based models are not discussed here, as they do not provide information on the relation between stacking architecture and the sedimentary processes and forcing mechanisms involved.

n-dimensional models, (n=1,2 or 3)

Many modelling efforts have focussed on cross sections, partially to reduce complexity but also because sequence stratigraphy is very much biased towards 2D due to its origins in the interpretation of seismic lines. This has resulted in a useful representation of sequence-stratigraphic and smaller-scale continental shelf processes. However, in 2D simulations sediment will always leave or enter the system laterally and out-of-plane variations are not taken into account, thus making comparison to real-world settings difficult. To fully understand lateral variation we must model these systems in 3D, especially in areas where multiple processes occur (Fagherazzi & Overeem, 2007). A prime example is the Danube Delta where the most active distributary discharges a river plume into a limited delta area, and therefore fluvial processes are dominant. In locations of the delta that receive less sediment directly, the deposits are reworked by waves and form beach ridges (Bhattacharya & Giosan, 2007).

In order to illustrate the difference at the most fundamental level (conservation of mass) in behaviour of 2D vs. 3D systems, two very simple geometric models were created and run. Both models have a presumed constant foreset angle, no fluvial aggradation, and no erosion. Sediment is added at the foreset and shoreline progradation is merely dependent on the sediment volume available and the depth of the clinoform toe. In the 3D version the topset of the clinoform is assumed to be semi-circular and sediment is distributed linearly based on accommodation space. The progradation rates have been made non-dimensional, as a good comparison between 2D and 3D surfaces and volumes is impossible. Figure 1.1 shows the rollover point/shoreline migration through time. Both models use an initial bathymetry with a constantly slope, therefore progradation rates slows as

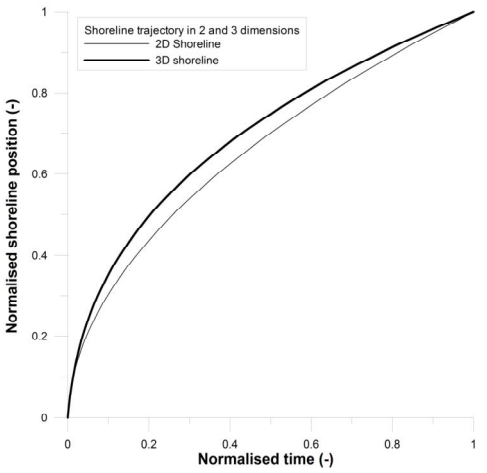

Figure 1.1; The rollover point migration as a measure for progradation rate in a two-dimensional and a three-dimensional geometrical model.

the clinoform toe reaches deeper water and accommodation space increases. There is a very clear discrepancy in behaviour between the 2D and 3D results, due to the spatial distribution of sediments and the widening of the delta front. Note that the 3D shoreline is a cross-section down dip. 2D models are often assumed to represent a cross-section through sediment, but these experiments clearly show that a quantitative comparison is difficult for laterally discontinuous sedimentation patterns.
Although the stratigraphy and the sedimentary environments studied in this thesis are fully three dimensional, the processes acting on it can be adequately represented using a 2D (plan view) generalization. Hydrodynamic flow and associated sediment suspension is often represented using a depth-averaged algorithm. This significantly improves upon computational efficiency and simplifies algorithm design.

Process-based vs. behaviour orientated – on the origins of the models
Models are based on assumptions. These assumptions can be derived from intuitive estimations or from basic physics. The basis for model principles has led to a spree of classifications.
Process-based models are usually defined as being derived from first principles, that is human-scale physical laws. Obviously there are still many assumptions necessary in these models. A prime example is the necessary sediment transport equations, which is still difficult to predict under ideal circumstances (Karim, 1998). Also they require very accurate initial and boundary conditions, which are very difficult to derive anywhere outside of the very recent past. The other end of the spectrum of model complexity is inhabited by behaviour-orientated, process-response or rule-based models. These model types are defined as being derived from certain rules that approximate the behaviour of the system or simplify fundamental laws.
The presumption in this classification is that one set of physical laws is applicable to a wide range of scales. Yet, rather high-level processes that occur on large spatio-temporal scales may be quite accurately represented using only a few crucial low-level processes (Paola, 2000). Thus the classification of model complexity can only be properly assessed in relation to the scale on which the processes work. i.e. on low-level processes (10 years, 10's kilometres), physical processes will need to be assessed on a very detailed level. On the other hand, high level processes (10,000's years, 100's kilometres) may be modelled using much more simplified process representation. Both model types can still be classified as process based, as long as all necessary processes are represented on the spatio-temporal scale of the field of study.
Consequently, our search for the most accurate model does not necessarily imply choosing the most complex model. Quite often many smaller scale, high-frequency, low-magnitude processes are completely overshadowed by low-frequency, high magnitude events. Thus allowing much simplification of the model's foundation without sacrificing its accuracy.

Coupled vs. uncoupled models
Most numerical, sedimentary models are either simplified basin-scale models, which assume that some form of diffusion adequately represents sediment transport, or single-environment models that focus on specific sedimentary processes. The former

type of model might be a reasonable choice for large spatio-temporal scales (Paola, 1992), but is not sufficient to adequately mimic meso and micro scale deposits. The latter type of models often do satisfactorily represent the physical processes, but are not embedded in a larger framework of basin-scale processes, such as spatio-temporal variations in sediment supply, sea level and subsidence. Coupling of the two types of models is therefore not without difficulty, as all large-scale variations must be translated to local boundary conditions and input parameters for the single environment models, without the possibility to generate feedback between the sedimentary architecture predicted by the single environment models and the sequence-stratigraphic architecture of the entire basin fill. This effectively impedes any analysis of the responses of local systems to autogenic vs. allogenic perturbations on the basin scale. A more promising approach is to directly incorporate the small-scale processes and stratigraphic/architectural elements into a large-scale basin-filling model, so as to ensure that the relation between the two scales may be examined directly.

Time constraints of implementation and of computer runtime and perceived complexity have resulted in the dominance of many single-environment models. Conceptual models have also suffered from this, as there are few people well versed in the study of wide ranging facies.

However, our lack of knowledge should not discourage us in studying the interaction between sedimentary environments, rather it should be seen as an encouragement. As in any natural system, the boundary or interface between two phases is where most problems and most interesting features occur. Coupled modelling is particularly necessary in deltas where the interaction between the marine and continental systems is especially apparent. Single environment models will always need external conditions to emulate the link with the `other´ environment and are consequently prone to seem extremely dependant on allogenic forcing.

Nested models

Hierarchy Theory (Haigh, 1987; Capobianco et al, 1998) partitions nature into "naturally occurring" levels that share similar time and space scales, and that interact with higher and lower levels in systematic ways. Each level in the hierarchy sees higher levels as intrinsic boundary conditions and the lower levels as intrinsic (or sub-grid scale) processes.

Niedoroda et al (1995) compare the problems in modelling the full range of boundary layer and sediment dynamics to the recognition in thermodynamics that the behaviour of systems comprised of very large numbers of molecules cannot be approached through Newtonian physics. The subgrid processes in this case are on a molecular scale, obviously much too small to model on our "human" level of interest. However, many small-scale processes (albeit on a higher level than the molecular scale) are very important to the large-scale development of clastic continental shelf shelf systems. Therefore models described in this thesis aim to fit this philosophy into a pragmatic modelling approach. The goal is to create a relatively fast sedimentary process model, which includes many different processes. As computational efficiency and many high-level processes are mutually exclusive we model many of these processes intrinsically

(sub-grid). In this way we try to assign sufficient clout to small-scale processes, so that they are able to influence the large-scale system.

Numerical models of sedimentary systems

This paragraph provides a brief overview of some notable modelling efforts, most are single environment models and have been grouped accordingly. This review does not aim to provide a complete picture, as several review papers have summarized recent numerical modelling efforts (Christieblick & Driscoll, 1995; Paola, 2000; Fagherazzi & Overeem, 2008).

Most relatively simple models are based on the assumption that sediment dynamics can be represented by some form of diffusion (most recent examples; Bowman & Vail, 1999; Granjeon & Joseph, 1999). Usually these models are used to mimic hundreds to thousands of meters of stratigraphic deposits, which would result in an unreasonable amount of calculation time for more complex calculations. Moreover, when comparing deposits on these scales, diffusion is an adequate representation of long-term averaged sediment transport (Paola, 1992). On the other end of the spectrum of dynamic models are the fluid mechanics models, which encompass a solution to a form of the Navier-Stokes equations and from the associated bed interaction derive the associated sediment dynamics. The most representative of these types of model is Delft3D (Roelvink and Van Banning, 1994), which is useful for relatively short-term, small spatial scale studies. Current research (Storms et al, 2008) focuses on longer term, stratigraphic applications of Delft 3D.

Most other models fall somewhere in between these two extremes of diffusive transport or fluid mechanical bed interaction. The next couple of paragraphs summarize some recent efforts for single-environment models and ends with an overview of coupled-environment models.

Fluvial

In numerical models on the continental-margin scale, sediment transport in fluvio-deltaic channel networks is typically calculated by the combination of a method for routing water across the grid to determine local discharge, and a sediment-transport routine which calculates how much sediment is actually transported (Howard, 1994; Granjeon & Joseph, 1999; Clevis et al., 2003). The channel network itself is not resolved, and consequently, such large-scale models cannot be directly compared to small-scale alluvial architecture models, in which processes such as avulsions are considered to be the dominant control on channel-belt evolution. Leeder, 1978; Mackey & Bridge, 1995; Karssenberg et al., 2001 are well-known examples of the latter and are the so-called LAB models (Paola, 2000), which have provided valuable insights into the relation between alluvial processes and the stratigraphic record (cf. Shanley & McCabe, 1993). Quantitative understanding of floodplain processes has, especially in modelling of sedimentary systems, been represented by assuming some form of exponentially decreasing overbank sedimentation (Leeder & Bridge, 1979; Mackey & Bridge, 1995; Karssenberg et al, 2001).

Deltaic

Harbaugh & Bonham-Carter (1970) were some of the first geologists to recognize the potential application of computers. Amongst many other problems, they pioneered delta modelling in a 2D-depth averaged model, but were hampered by a lack of graphics output. Many successors did not reach this level of complexity.
Many models partially cover marine geomorphological sedimentary evolution, yet few address the problems occurring on geological timescales in 3D space. Several large-scale basin filling models are usually simplified, representing marine processes as diffusion (e.g. Granjeon & Joseph, 1999; Clevis et al., 2003, Meijer, 2002). This approach may be appropriate for generalized sequence stratigraphic conceptual studies and comparisons. However, when we wish to analyse the relative influence of fluvial processes and waves or study the sedimentary architecture in greater detail, we must include several processes. Notably small grain-size fractions can be transported far from the river-mouth. In most cases they are transported by hypopycnal plumes, which due to slow mixing may transport the finer grains far offshore. Oblique currents will distort the plume and the sediment distribution accordingly. Subsequently, large storm waves influence the newly deposited sediments. The increase in near bed orbital velocity allows the sediment beds to become mobile, even resulting in resuspension under sufficiently energetic conditions. Resuspended sediments may be transported by wave-induced or other currents and may take several days to settle. Thus the eventual resting place of the fine sediments is an accumulation of high energetic storm events and subsequent low energetic transportation.

Waves/shoreface
Previous modelling efforts of long-term shoreface evolution have mostly focused on the coastal profile (e.g. Niedoroda et al, 2003; Storms et al, 2002; Stolper et al, 2005, Swenson et al, 2005, Cowell et al, 1995, Niedoroda at al, 1995). This approach certainly has its value < for short time scale modelling (i.e. decades to centuries), however on geological time scales the external forcing and consequent interaction with the surrounding sedimentary and possibly anthropogenic environments necessitates a dynamic linkage. Local changes in sediment supply, subsidence or wave regime may upset this model response, as cross-sections cannot account for out-of-plane variations. Niedoroda et al (2003) linked a set of two-dimensional transect models to create a three-dimensional model of the Coastal Systems Tract, their focus is mainly on the morphodynamic response on relatively short-term, low amplitude sealevel cycles.

Coupled Models
Two notable coupled models are the Sedsim-Wave model (Tetzlaff, 2004; Martinez, 1987; Martinez & Harbaugh, 1993) and Sedflux 2.0 (Hutton et al, 2008). The former contains hydrodynamical representation of marine processes; it focuses on relatively small-scale features, but the source code is not open and cannot be used for scientific study. The latter is an aggregated stratigraphic/morphodynamic model and incorporates an abstracted channel switching routine, wave induced sediment transport, hypo- and hyperpycnal plume deposition and mass wasting. The Meijer (2002) QDSSM model may be considered a coupled model as it represents marine

processes purely diffusively and couples an advective fluvial routing scheme to represent fluvial processes more accurately. Slingerland et al (1994) provided an in depth review of modelling sedimentary processes in several different environments and noted the idea that these may be linked, resulting in a coupled interacting model.

Simclast a multi-level, coupled model:

SimClast is a basin-scale 3D stratigraphic model, which allows several interacting sedimentary environments. We developed it from 2004 to 2008 at Delft University of Technology and implemented part of the Meijer (2002) code for accounting, loading and storing algorithms. SimClast is a fully plan view 2D, depth-averaged model, allowing the complex interaction between fluvial and wave influences on deltaic and shoreface development to be studied. It focuses on theoretical experiments, as quantitative experiments are intrinsically difficult to recreate in real world settings. Yet there lies the great strength of numerical modelling, as we can improve upon the understanding of these systems by focussing on the process forming and removing the deposits. The modelling applications focus especially on the erosional and nondepositional events as these probably represent the greatest amount of "stratigraphic time".
Short-term, high-resolution processes are coupled with the long-term stratigraphic model by nesting a parameterised version of the high-resolution processes. We extrapolate physical and empirical relationships of the geomorphological development and implement these. A necessary constraint on these long-term models is a relatively large grid sizing (i.e. km scale), as the area to be modelled is on the scale of continental margins and the modelling time is on the scale of many millennia. Areas of special importance are modelled by implementing sub-grid scale processes into a large-scale basin-filling model; this refines the model dynamics and the resulting stratigraphy.
Processes included are; fluvial channel dynamics and overbank deposition, river plume deposition, open marine currents, wave resuspension, nearshore wave induced longshore and crosshore transport. This combined modelling approach allows insight into the processes influencing the flux of energy and clastic material and the effect of external perturbations in all environments. Many governing processes work on relatively small scales, e.g. in fluvial settings an avulsion is a relatively localised phenomenon, yet they have a profound effect on fluvial architecture. This means that the model must mimic these processes, but at the same time maintain computational efficiency. Additionally, long-term models use relatively large grid sizing (km scale), as the area to be modelled is on the scale of continental margins. We solve this problem by implementing the governing processes as sub-grid scale routines into the large-scale basin-filling model. This parameterization greatly refines morphodynamic behaviour and the resulting stratigraphy. SimClast recreates realistic geomorphological and stratigraphic delta behaviour in river and wave-dominated settings.

Outline of the thesis
This thesis can be divided in two distinct sections. Chapters 2 to 5 narrate the story of the construction, the theoretical background and relationships of the clastic stratigraphic/morphodynamic model. Chapters 6 and 7 are theoretical applications of the model on the response of fluviodeltaic systems to several autogenic and allogenic forcing mechanisms.

Model development
Chapters 2 details the modelling of fluvial channel and overbank processes. Fluvial channels are modelled in one gridcell with the possibility of crevasse. Subgrid distribution of sedimentation mimics alluvial ridge aggradation and overbank deposition. Avulsions are modelled one dimensionally by calculating the flow and sediment transport at prospective avulsion nodes.

Chapter 3 focuses on the implementation of floodplain processes. Specifically differential compaction, groundwater table, peat growth and multi-cellular overbank deposition.

Chapters 4 describes the modelling of shallow marine wave and current influenced processes for the suspended load sediment transport. Rivers deliver sediment and water to the sea, where the river momentum spreads the suspended sediment in a plume. Multiple plumes and longshore current hydrodynamics are calculated using a potential flow routine. Subsequent sedimentation due to fallout uses the removal rate principle.

Chapter 5 records the nearshore marine processes in wave-influenced systems, being littoral and crosshore transport. Waves are modelled using linear Airy and Stokes wave theory. Deepwater wave height is derived from a Gaussian distribution to represent natural storm variability. The asymmetric waves preferentially transport the sands (bedload fraction) shorewards and the fines (suspended load fraction) offshore. In combination with a littoral drift routine this allows waves to rework and transport sediments.

Applications
Stratigraphic models can be used to test and adapt conceptual models of generalized systems. A special focus of applications in this thesis is how we can distinguish between autogenic and allogenic forcing. In chapter 6 we establish a base case for fluvially dominated deltas, without any change in boundary conditions. This allows us to determine the inherent behaviour of systems, which in turn allows us to distinguish allogenically induced vs. autogenic processes and deposits in real-world settings. Chapter 7 aims to improve the understanding of the relation between wave-dominated fluvio-deltaic and coastline evolution and the stratigraphic record under conditions of varying sealevel and sediment supply.

Chapter 2
Sub-grid parameterization of fluvio-deltaic processes and architecture in a basin-scale stratigraphic model

Published as; Dalman, R.A.F. & Weltje, G.J., 2008. *Sub-grid parameterization of fluvio-deltaic processes and architecture in a basin-scale stratigraphic model.* Computers & Geoscience, v. 34-10, p. 1370-1380.

"If it keeps on rainin', levee's goin' to break; And the water gonna come in, have no place to stay"
-Kansas Joe McCoy and Memphis Minnie-

Abstract
We present a parameterization of fluvio-deltaic drainage network evolution and alluvial architecture in a basin-scale 2-DH model. The model setup is capable of producing convergent and divergent channel networks. Major elements are the alluvial-ridge aggradation and the coupled overbank deposition, the dimension and style of the channel belt and the sub-grid stratigraphic expression. Avulsions are allowed to develop out of randomly instigated crevasses. Channel stability is modelled one dimensionally by calculating the flow and sediment transport at prospective avulsion nodes. The ultimate fate of crevasses (failed avulsion, successful avulsion, stable bifurcation) depends on the ratio of cross-valley and in-channel gradients in the local neighbourhood of the grid cell under consideration and on the amount and distribution of the suspended sediment load in the water column. The sub-grid parameterization yields implicit knowledge of the alluvial architecture, which may be analysed stochastically. Stochastic realisations of the alluvial architecture allow us to investigate the relationship between basin-fill architecture and small-scale alluvial architecture, which is likely to improve geological reservoir modelling of these notoriously complex deposits. Modelling results under conditions of time-invariant forcing indicate significant quasi-cyclic autogenic behaviour of the fluvio-deltaic system. Changes in avulsion frequency are correlated with the number and length of distributary channels, which are in turn related to alternating phases of progradational and aggradational delta development. The resulting parasequences may be difficult to distinguish from their allogenically induced counterparts.

Introduction
In numerical models on the continental-margin scale, sediment transport in fluvio-deltaic channel networks is typically calculated by the combination of a method for routing water across the grid to determine local discharge, and a sediment-transport routine which calculates how much sediment is actually transported (Howard, 1994; Granjeon & Joseph, 1999; Clevis et al., 2003). The channel network itself is not resolved, and consequently, such large-scale models cannot be directly compared to

small-scale alluvial architecture models, in which processes such as avulsions are considered to be the dominant control on channel-belt evolution (Leeder, 1978; Mackey & Bridge, 1995; Karssenberg et al., 2001). Well-known examples of the latter are the so-called LAB models (Paola, 2000), which have provided valuable insights into the relation between alluvial processes and the stratigraphic record (cf. Shanley & McCabe, 1993). However, these models are not embedded in a larger framework of basin-scale processes, such as spatio-temporal variations in sediment supply, sea level and subsidence. Coupling of the two types of models is therefore not without difficulty, as all large-scale variations must be translated to local boundary conditions and input parameters for the LAB models, without the possibility to generate feedback between the alluvial architecture predicted by the LAB models and the sequence-stratigraphic architecture of the entire basin fill. This effectively impedes analysis of the responses of alluvial systems to autogenic vs. allogenic perturbations on the basin scale. A more promising approach is to directly incorporate the small-scale processes and stratigraphic/architectural elements into a large-scale basin-filling model, so as to ensure that the relation between the two scales may be examined directly.

The algorithm presented in this contribution is an attempt to bridge the gap between discrete architecture models and basin-scale stratigraphic models, which may be considered a logical step forward in model development (Paola, 2000). We propose a

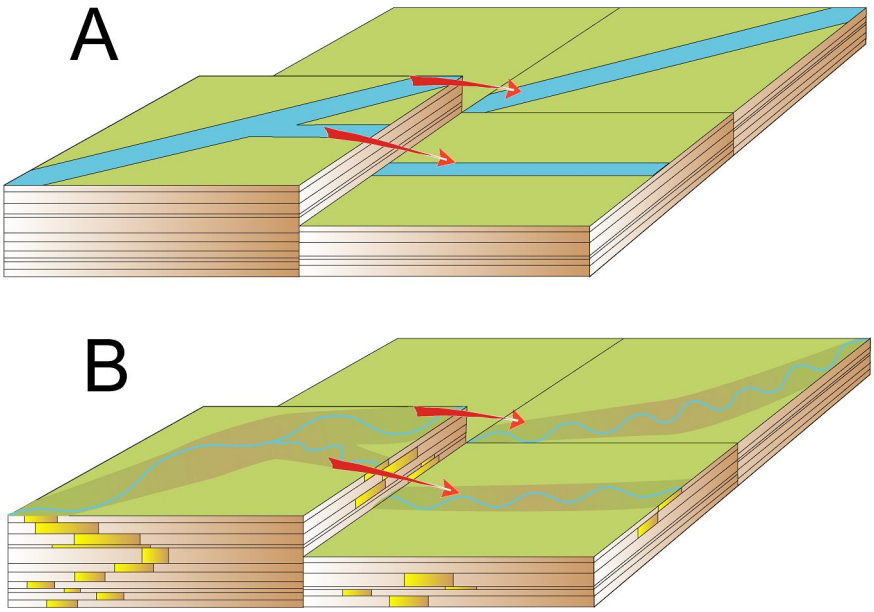

Figure 2.1; Channel network representations. (A) typical large-scale model with homogeneous grids (Meijer, 2002); (B) Sub-grid parameterization proposed in this paper. Note the alluvial ridge, fluvial style and dimensions, changes in sinuosity and the subdivision overbank/floodplain in the stratigraphic record.

sub-grid parameterization of alluvial processes and stratigraphy for application in a large-scale basin-filling model (Figure 2.1). Parameterization refers to the method of replacing processes that are too small scale or complex to be explicitly represented in the model by simplified expressions. Sub-grid sediment transport and channelisation are derived from physical equations, capable of producing convergent and divergent drainage networks, trunk channels and most importantly, detailed representations of avulsions and bifurcations. This permits investigation of the natural variability of the basin-scale drainage system and its responses to allogenic vs. autogenic forcing through multiple model runs, without sacrificing speed of computation. A major advantage of this method is the possibility to visualize and investigate the sub-grid alluvial stratigraphy produced implicitly by the parameterization, in order to attain the level of detail required for geological reservoir modelling.

Model description

The architecture of the basin-scale model is based on Meijer (2002). Marine processes

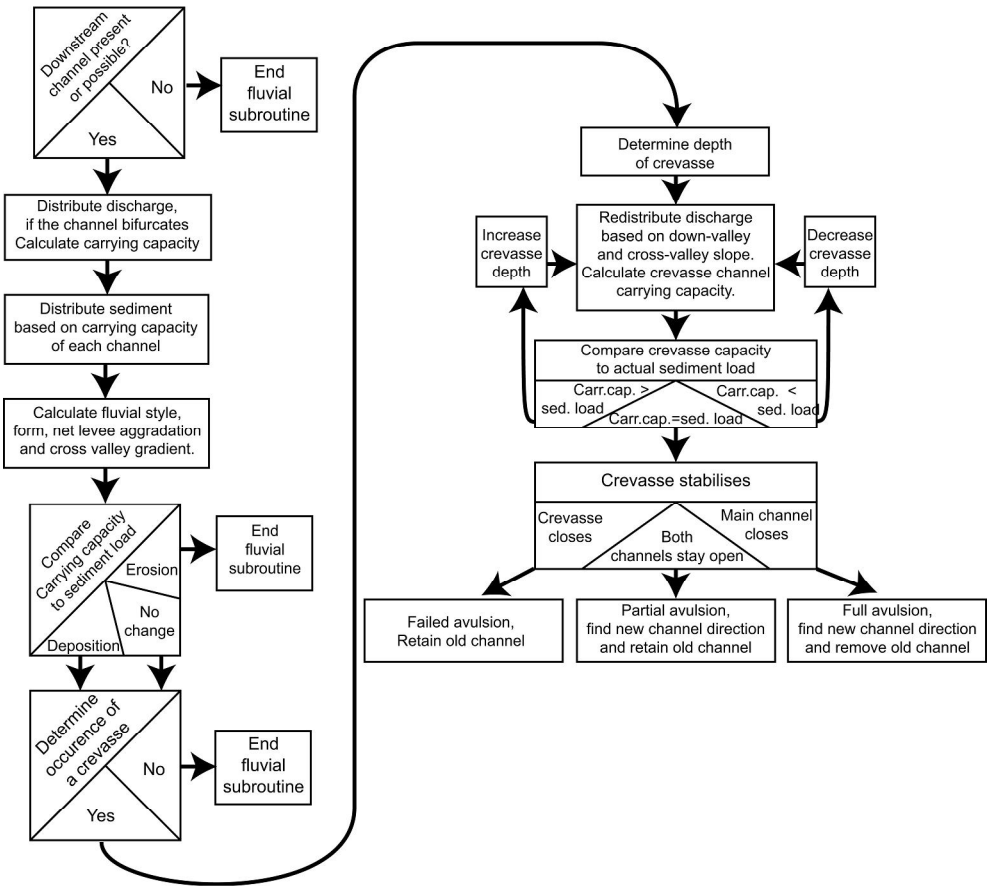

Figure 2.2; Flow chart of the fluvial parameterization routine.

in this model, comprising a simplified plume routine with diffusion-based mass wasting, have been retained for the purpose of this study. A new algorithm was developed to represent subaerial fluvio-deltaic processes (compare Figure 1A and 1B). A flowchart of the routines developed to calculate liquid discharge, sediment transport and channel evolution is illustrated in Figure 2.2.

Discharge routing

Discharge routing is a complex morphodynamic problem, which has been largely ignored in large-scale stratigraphic modelling. In most basin-scale (and many sub-basin scale) fluvio-deltaic models, the direction and amount of liquid discharge routed to neighbouring cells is determined with one of two methods. The steepest-descent method, whereby all water draining from one cell is moved to only one neighbouring cell, is generally used to represent convergent (tributary) systems (Figure 2.3). This results in a system where one trunk channel develops (Fagherazzi et al, 2004; Howard, 1994), which may be regarded as an adequate representation of e.g. bedrock-channel networks in fluvial drainage basins, but it cannot be used for the purpose of modelling fluvial valleys and coastal plains (Figure 2.3). Such (potentially) divergent distributary systems are commonly created by means of a diffusive routing algorithm, in which water is routed to all lower-lying neighbouring cells in quantities proportional to the slopes. The simplest approach is to distribute discharge linearly proportional to the slopes (e.g. Clevis et al., 2003). A more sophisticated method, in which the steeper slopes are given a slight advantage in discharge proportion, was proposed by Freeman (1991) to compensate for the preferential direction artefacts caused by square grid cells:

$$f_j = \frac{s_j^p}{\sum_{j=1}^{n} s_j^p} \qquad (1)$$

Where f_j is the fraction of discharge routed towards cell j with slope s_j; n is the total number of downstream cells. The compensation for the square grid bias is provided

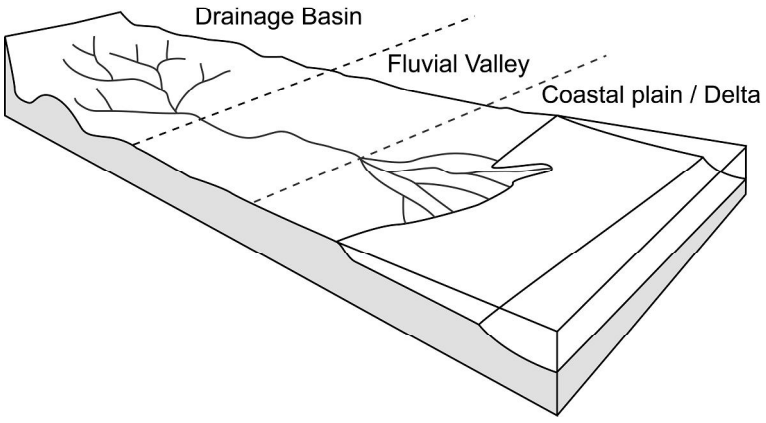

Figure 2.3; Drainage network types as components of the fluvio-deltaic system (after Schumm, 1977).

by parameter p, which is set to 1.1.
The use of Equation 1 results in an approximation of sheet flow, i.e. diffuse drainage patterns without distinctive channels (e.g. Meijer, 2002). Although the drainage patterns created by this method appear to be representative of distributary networks, this approach does not permit implementation of small-scale fluvial processes believed to control the evolution of such networks. Clearly, both methods are poorly suited to modelling of the entire range of fluvio-deltaic channels on time scales shorter than several hundred millennia (Paola et al, 1992).
In order to recreate more realistic channel patterns, we have developed an algorithm in which liquid discharge is routed with one of two methods. We have defined a threshold flux of $6.25*10^{-7}$ m^3s^{-1}/m^2 , which translates to a minimum bankfull discharge of 10 m^3s^{-1}(Van Den Berg, 1995), assuming a gridcell size of 16 km^2 and a maximum of one channel per gridcell. The threshold flux is used to determine whether a channel is likely to develop in each gridcell. If the threshold flux is not exceeded, discharge is assumed to be unconfined (overland flow) and follows the diffusive method of Freeman (1991) as distinctive channels do not form. The second routing method is employed in cases where a channel is already present in a grid cell or the threshold flux is exceeded, in which case an active channel is created. If erosion occurs in the designated channel segment, the channel is assumed to be stable as it will not be able to escape its entrenched valley. If the channel segment is depositional or in equilibrium the channel is also assumed to remain in place, yet crevasses may occur. The evolution of such channels is discussed further in the *Channel stability* paragraph below. If the threshold discharge is not exceeded or an avulsion is successful the channel segment is abandoned.

This method captures the essence of drainage-network evolution, as it allows the channel pattern to be preserved where necessary. The implementation of crevasse channels, which may develop into successful avulsions, failed avulsions, or stable bifurcations (see below) permits the development of distributary networks. Once multiple channels have developed in a single grid cell, discharge at bifurcations is distributed between channels with the routine of Freeman (1991). This approach results in a self-organising discrete drainage network, comprising both tributary as well as distributary channels, in which small-scale fluvial processes have been implemented.

Channel Forming Discharge
Channel dimensions are determined from the channel-forming discharge, which is usually approximated by the bankfull discharge (Knighton, 1998). As the model employs mean discharges over time steps of one year, the bankfull discharge (Q_b) is unknown and must be derived from the mean discharge ($\overline{Q}$), using a power-law relationship calibrated to data of 192 rivers worldwide (Van Den Berg, 1995; Boogaart et al , 2003):

$$Q_b = 25\ \overline{Q}^{0.75} \quad (2)$$

Channel style and dimension

Channel style (meandering or braided) is derived from stream power (Van Den Berg, 1995), which depends on down-valley slope, median grain size and bankfull discharge. The hydraulic geometry theory introduced by Leopold & Maddock (1953) relates rectangular channel dimensions to bankfull discharge:

$$W_b = k_{wb} Q_b^{M_{wb}} \quad (3)$$

Where W_b is the bankfull width (m), and k_{wb} and M_{wb} are dependent upon channel style. Boogaart et al (2003) approximated these two parameters as k_{wb}= 3.65 and M_{wb}=0.50 for meandering rivers and k_{wb}= 3.81 and M_{wb}=0.69 for braided rivers. The bankfull channel depth is consequently obtained from mean width/depth ratios for meandering and braided rivers, 18.9 and 305.2, respectively (Boogaart et al, 2003).

Water flow and sediment transport

The flow velocity is needed to calculate bed shear stresses and shear velocities for sediment transport. We use the Darcy-Weisbach Equation to compute the mean flow velocity, as it employs a non-dimensional friction coefficient (cf Mannings' Equation) and is dependent only on wetted channel depth and slope. Subsequently, bed shear stress and velocity are calculated using the reduced hydraulic radius conjecture (Einstein, 1950).

Bedload transport rates are calculated using the modified Bagnold bedload transport Equation (Bridge & Dominic, 1984):

$$i_b = \frac{c}{\tan\alpha}\left(U_* - U_{*c}\right)\left(\tau_0 - \tau_c\right) \quad (4)$$

Where i_b is the bedload sediment transport, and U_* and U_{*c} the effective and critical shear velocity. τ_0 and τ_c are the effective and critical shear stress, respectively. Coefficients c and $\tan a$ represent bed roughness and dynamic friction, whose ratio ($c/\tan a$) has been empirically derived as 10 (Slingerland et al, 1994). The concentration profile and transport rate of the suspended load are derived using the Rouse Equation (Rouse, 1937):

$$\frac{C_y}{C_h} = \left(\frac{D-y}{y}\frac{h}{D-h}\right)^{\frac{w}{\kappa U_*}} \quad (5)$$

Where C_y is the sediment concentration at flow height y, C_h is the sediment concentration at flow height h, h is the height of the moving bed layer, D is the water depth, w is the fall velocity for the relevant grain size and κ is the von Karman constant (0.4 for clear water). The sediment concentration at flow height h is calculated by assuming that grains in suspension have a concentration in the moving bed layer predicted by the bedload equation (Slingerland et al, 1994):

$$C_h = \frac{i_b}{U_b h g} \qquad (6)$$

Where U_b is the near-bed velocity and g is the gravitational constant.
Sediment distribution at bifurcations is complicated by asymmetric flow in meanders and effects of downstream boundary conditions (Kleinhans & Stouthamer, 2005), as well as differentiation of bedload and suspended load. In our model we assume that the crevasse stabilizes within one time step (i.e. one year), permitting a stable bifurcation to form. In such a case, sediment is distributed over the channels in proportion to the sediment transport capacities of the downstream channel segments. This may result in a slight overestimation of bifurcation stability, but viable alternative solutions (cf Ikeda et al, 1981) are considered too complex to be incorporated in the model.

Alluvial ridge and overbank aggradation
The dimensions of grid cells used in our basin-scale stratigraphic model (4 by 4 km) are required to be much larger than the widths of most channel belts. In order to determine the sub-grid geomorphological and stratigraphic evolution of the channel belt we redistribute the sediment deposited in each grid cell (Figure 2.4) according to the exponential overbank-aggradation equation (Pizzuto, 1987; Mackey & Bridge, 1995):

$$r_z = ae^{-bz_c/z_m} \qquad (7)$$

Where r_z is the overbank-aggradation rate at cross-valley distance z_c , a is the channel belt aggradation rate, b is the overbank-aggradation exponent, z_c/z_m is the normalised distance away from the edge of the channel belt at maximum distance z_m. A crucial assumption in this sub-grid redistribution model is the limited lateral extent of overbank aggradation relative to the dimensions of the grid cell. This implies that floodplain deposition is limited to the cell through which a channel flows, which is valid presuming grid cell dimension is at least 4 by 4 km. The implicit sub-grid morphology allows us to track the superelevation and cross-valley gradient of the alluvial ridge.

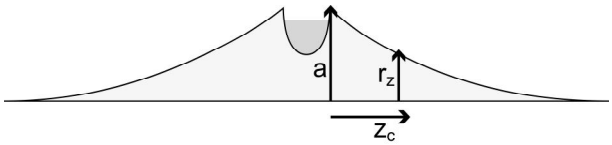

Figure 2.4; Cartoon cross section of an aggrading channel system. Most sediment is deposited in and around the channel and decreases exponentially outwards. a is the total aggradation of the alluvial ridge, r_z is the aggradation at distance z_c from the alluvial ridge.

Channel belts widen over time, due to meandering, crevasse splays etc. We model this by assuming that new channel belts have a width equal to the channel width. Channel-belt widening is calculated as follows (Bridge, 2003):

$$\frac{\partial m_{cur}}{\delta t} = E\left(m_{cb} - m_{cur}\right) \qquad (8)$$

Where m_{cur} is the current channel belt width, m_{cb} is the maximum channel belt width and E is the bank erodibility. The maximum channel belt width is given by:

$$m_{cb} = 59.86D^{1.8} \qquad (9)$$

Channel stability

Channel stability is determined by evaluating the ratio of sediment load to transport capacity. Channels are unconditionally stable as long as they incise. Aggrading channels and channels that are in equilibrium (at grade) are conditionally stable, i.e. they may be subject to avulsion or bifurcation.

Avulsions are triggered by events such as major floods, which initiate crevasse channels by breaching of levees. Yet the magnitude of these events (e.g. flood intensity) is nearly irrelevant for the subsequent success of the avulsion (cf. Jones & Schumm, 1999). The main controlling factors on evolution of the channel network are the progressive increase in cross-valley slope due to super-elevation of the alluvial ridge (Figure 2.5A), and to a lesser extent the amount of suspended sediment (the concentration profile) in the main channel (Slingerland & Smith, 1998; Overeem & Weltje, 2001). The exact location and timing of crevasses will be of minor importance, because other factors determine whether they are likely to develop into avulsions or bifurcations. Avulsions are therefore modelled by stochastically instigating crevasses by means of uniform random deviates. Each cell containing one or more channels is a candidate at every time step. The probability of a crevasse occurring is set to 0.5.

We assume that the new configuration will reach equilibrium within one time step. The equilibrium crevasse channel is calculated iteratively, using bracketing and bisection. We start with an initial guess for the crevasse depth. The water above the level of the crevasse is redistributed over the old channel and the new crevasse channel (Figure 2.5B) according to the algorithm of Freeman (1991). The cross-valley gradient is calculated by subtracting the crevasse depth from the amount of alluvial ridge aggradation. From Equation 3 we derive the channel geometry of the crevasse channel and the sediment transport capacity is calculated using Equations 4, 5 and 6. The sediment transport capacity is compared to the sediment load received from the main channel. Note that bedload transported by the main channel will rarely reach the crevasse due to the jump in height. As the suspended sediment is concentrated preferentially in the lowermost part of the flow, a small crevasse channel will receive water with a comparatively low concentration of suspended sediment, which implies a high probability that this channel will incise. As erosion continues and the crevasse

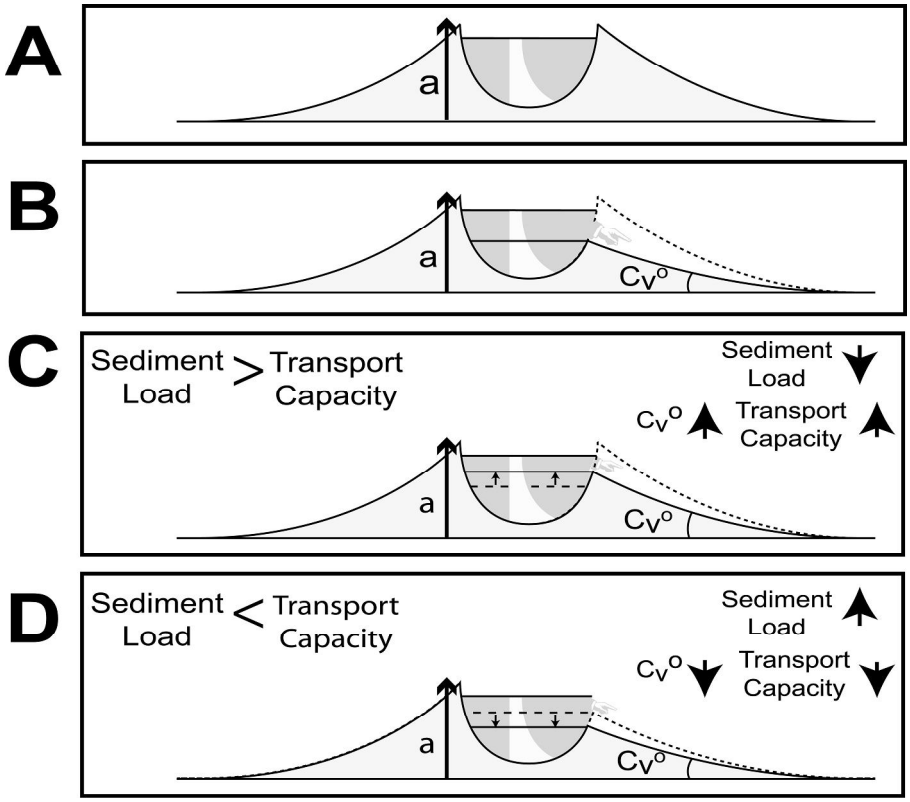

Figure 2.5; Development and stabilisation of a crevasse. (A) Cross section of stable channel; concentration of suspended sediment decreases upward in the water column. (B) Depth of the crevasse (lip) is determined randomly. Discharge above the crevasse lip is redistributed over the old channel and the crevasse channel. Sediment transport capacity of the crevasse channel is compared to the sediment load received from the main channel. (C) Sediment load exceeds transport capacity, the crevasse is unstable and will heal (partially), (D) Transport capacity exceeds sediment load, the crevasse incises.

deepens, the cross-valley gradient decreases and more suspended sediment is available for redistribution on the floodplain (Slingerland & Smith, 1998; Overeem & Weltje, 2001). If the sediment load is greater than the transport capacity the crevasse is unstable and will heal (Figure 2.5C), whereas the crevasse will incise if the transport capacity is greater than the sediment load (Figure 2.5D). Hence, the avulsion process is self-stabilising, as the increase in transport capacity due to a steeper slope is balanced by a decrease in sediment load delivered from the main channel and vice versa.

If the discharge of the equilibrium crevasse channel does not exceed the threshold discharge defined above, the avulsion has failed. A partial avulsion (bifurcation) occurs when the newly created and the old channel each receive more discharge than the

threshold discharge. A full avulsion occurs if the discharge received by the old channel does not exceed the threshold discharge. If the avulsion has partially or fully succeeded, the new channel follows the path of steepest descent of the inter-gridcell gradients.

Sub-grid stratigraphy and architectural elements

The calculations of discharge and sediment transport through the drainage network are carried out without the need to specify the exact location of channels within grid cells. Hence, the alluvial stratigraphic record of each cell is exclusively stored in terms of architectural elements. The sub-grid stratigraphic data stored for each grid cell are the depth, size and shape of the channel belt and the amount of overbank deposits. These data are stored after the channel belt is abandoned, which allows the lithostratigraphic expression of the channel belt (i.e. its exact location) to be stochastically determined. Multiple stochastic realizations of sub-grid alluvial stratigraphy may thus be obtained from a single model run. An example of a stochastic realisation of the sub-grid stratigraphy in the proximal reaches of the fluvial domain is illustrated in Figure 2.6.

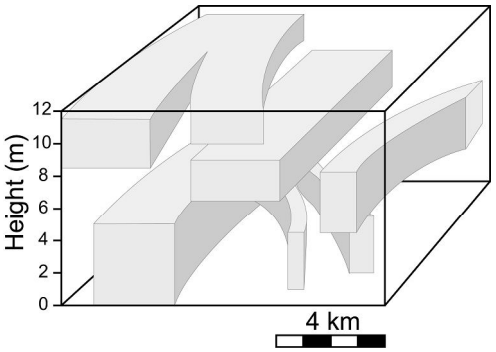

Figure 2.6; A realisation of the alluvial sub-grid stratigraphy of nine gridcells in the upper reaches of the system; coarse-grained channel belt deposits are visualized, overbank fines are invisible.

Example model run

The model was run in order to illustrate the relationship of fluvio-deltaic morphological evolution to spatio-temporal patterns of erosion and sedimentation. The model run was conducted under time-invariant forcing, i.e. constant sea level, liquid discharge (1000 m^3 s^{-1}) and sediment load (4 * 10^6 m^3 $year^{-1}$). Two grain-size fractions were used (1 μm and 500 μm). Sediment entered the model domain from the head of a fluvial valley of 50 cells long and 4 cells wide, which was connected to a rectangular grid of 50 cells wide and 75 cells long. The initial topography comprised a low gradient fluvial valley and continental shelf (both 0.0002) and a continental slope (0.002).

Geomorphological/hydrological results

The basin-scale model creates discrete delta lobes fed by a single channel and displays autogenic lobe switching due to avulsions at the apex of the delta. The low down-valley slope on the delta plain reduces the transport capacity of the main channels and allows rapid superelevation to develop. Hence, a multi-channel delta system (Nile

Delta type) will develop depending on sediment load and down-valley gradient (see Figure 2.7 for examples).
Regional avulsions upstream from a delta lobe may result in its complete abandonment. The example (Figure 2.8) shows a series of gradual and rapid avulsions that result in the generation and subsequent abandonment of delta lobes some 80 km apart. A secondary effect of these regional avulsions is the abandonment of large sections of the delta plain. This results in alternating phases in which the delta plain is occupied by a single distributary (Figure 2.8C) and multiple distributaries (Figure 2.8B).

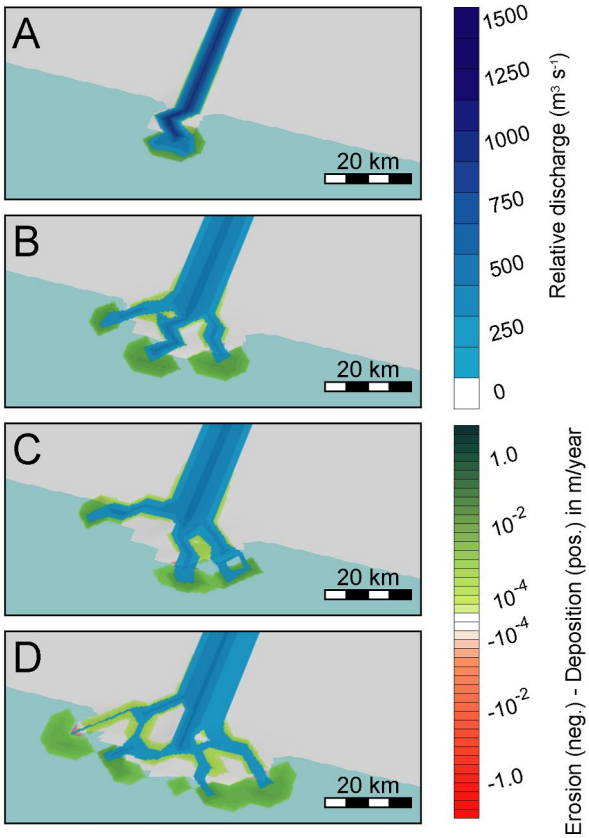

Figure 2.7; Hydrological and geomorphological development at the start of the initial run of delta development. For a stratigraphic overview and timing see Figure 8. (A) After 200 years the delta has prograded slightly into the basin, with one single channel. (B) After 500 years, the delta has developed two extra channels resulting in three distinct delta lobes. Due to the declining down channel slope the delta is able to gradually change into a multi-channel delta system (C: 700 years; D: 1000 years). Note the apparent backstepping of the delta apex as the area occupied by the delta plain increases through progradation and onlap.

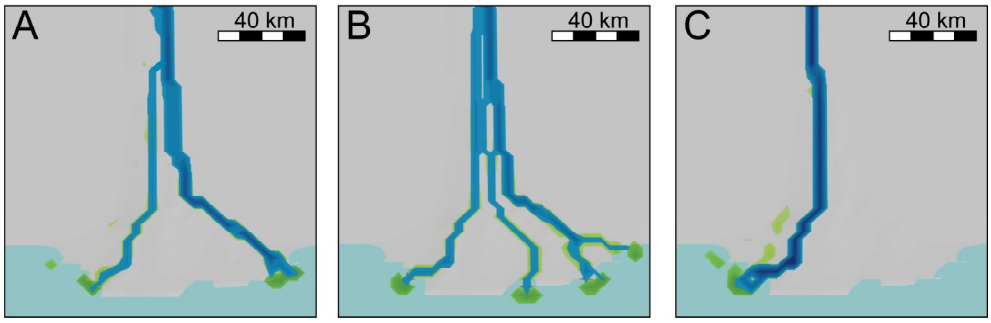

Figure 2.8; Hydrological and geomorphological development of the influence of upstream (nodal) avulsions on deltaic development. The legend is the same as Figure 7. (A) At 5700 years into the simulation, a large two-channel system has developed resulting in two well-separated delta lobes. Note the right channel carries 90 % of the discharge. (B) At 5800 years, a large multi-channel delta has developed resulting in a decreased discharge in the main channel. (C) At 5900 years only one single channel remains.

Stratigraphic results

Patterns of erosion and deposition are illustrated by combining Wheeler and avulsion diagrams (Figure 2.9). Most avulsions and bifurcations occur in the delta, where down-valley gradients are low and sediment load is small. The extent of delta-plain area covered by channels appears to be linked to avulsion rate. Initially, one single channel feeds the delta and multiple channels can develop only after this channel has aggraded sufficiently to permit successful avulsions. These multiple channels distribute the sediment over a larger area and avulsion rates decrease. Continuation of this process results in a large increase in delta-plain area, both through progradation and onlap (backstepping). The delta apex migrates upstream as the area of the delta plain increases, effectively shortening the fluvial valley (Figure 2.3). This is illustrated by the geomorphological evolution (Figures 2.7 and 2.8) and by the Wheeler/avulsion diagram (Figure 2.9). After a certain period of time, a major upstream avulsion occurs. As a result of this nodal avulsion, the central area is bypassed and the discharge is concentrated into one efficient channel system, which completes the "cycle". Repeated periods of drainage network growth alternating with nodal avulsions result in a depositional pattern similar to an "inverted Christmas tree" (Figure 2.9).

A secondary effect of nodal avulsions on delta development is created by storage of sediment in the fluvial valley as the river attempts to attain its graded profile, which starves the downstream area of the basin of sediment and decreases the rate of delta-front progradation.

Discussion and conclusions

The model presented is intended to simulate most channel processes relevant on time scales longer than 100 years. On a basin scale, these processes might initially seem irrelevant, yet their effects can be profound, as evidenced by the near-instantaneous delta lobe switching over some 100 km within a time span of 200 years (Figure 2.8).

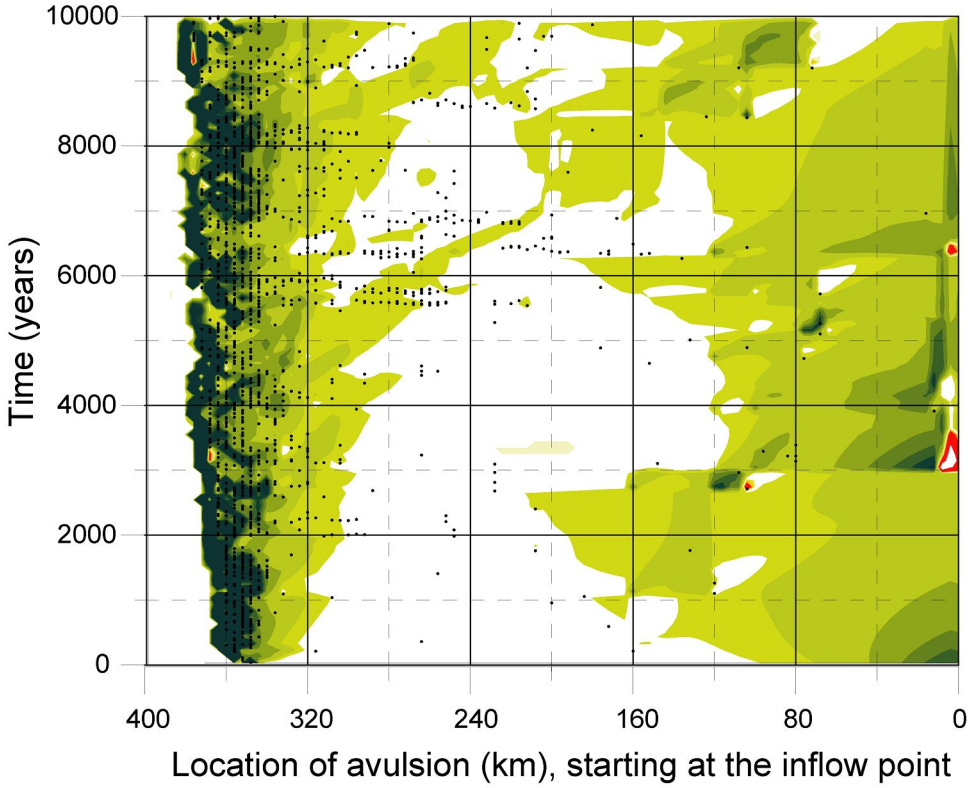

Figure 2.9; Chronostratigraphy (see Figure 2.7 for legend) and avulsions (black dots) of the entire grid summed along strike. Note rapid progradation of the delta in the first 500 years, which slows significantly as the delta front widens. Most avulsions occur in the delta area where down-valley gradients are lowest and sedimentation is highest.

Our study on the development of river-dominated low-angle shelf deltas clearly shows an initial increase in the number of distributaries (Figure 2.7). Yet contrary to popular theory (Olariu & Bhattacharya, 2006), the number of distributaries may decrease during progradation of the delta, notably after major nodal point avulsions (Figure 2.8). The model underestimates the number of terminal distributaries, as it does not include mouthbar deposition and subsequent channel splitting in the river-mouth areas. Nonetheless, an increase of the number of terminal distributaries by splitting of coastal channels will be restricted to the scale of a single delta lobe. On the scale of the entire delta (i.e. several delta lobes), a quasi-cyclic autogenic increase and decrease of distributaries is expected.

Owing to the fixed hydraulic geometry relationships of the channels in the model, the number of distributary channels reflects the efficiency of the dispersal system. One major channel with a specified discharge will have a larger suspended load sediment transport capacity than several smaller channels with the same total discharge. The increase in total hydraulic radius results in increased friction and subsequent deposition on the delta plain. Thus aggradation is more likely to occur during periods

with multiple distributary channels, whereas periods with a single or few distributary channels are associated with rapid delta-front progradation. In bedload-dominated systems the sediment transport efficiency is somewhat more complicated (cf Nanson & Huang, 1999), as bedload transport is mainly dependent on flow depth.

In our experiments, the graded profile is continually extended due to delta progradation, which prevents the system from reaching an equilibrium profile. These numerical experiments may be regarded as representations of fluvial-dominated settings, in view of the absence of shallow-marine processes. Lengthening of the fluvio-deltaic profile is much less conspicuous in wave-influenced systems where a significant proportion of sediment delivered to river mouths is reworked and moved alongshore. Changes in the channel network continually influence sedimentation and erosion patterns, due to fluctuations of the total sediment transport capacity. The sediment transport capacity associated with a given amount of discharge flowing through one channel will be different from the capacity of a system in which the same amount of discharge flows through multiple channels (assuming similar style, grain size and gradient). Therefore, a nodal avulsion provoked by aggradation in a low-efficiency multiple-channel system results in the abandonment of this system. A single channel system replaces the system, which results in a highly efficient profile. Conversely, as this highly efficient single channel system develops, aggradation on the delta plain due to loss of energy at the shoreface allows partial avulsions to occur, which produces a backstepping system of multiple channels (see Figure 2.9). Thus, the self-adjusting influence of avulsions results in a dynamic equilibrium around the "graded" profile, which represents a one-dimensional abstraction of the spatially distributed channel network. In our model, the spatially averaged fluvio-deltaic profile fluctuates between a relatively efficient system and a less efficient system, which allows autogenic fluctuations in sedimentation patterns to occur on a regular basis (Figure 2.10).

The modelling results show that alluvial-plain and delta-front parasequences are created during phases of predominant aggradation and progradation, respectively. Such parasequences are fully explained by autogenically induced phases of distributary channel rearrangement, which emerge as a robust feature of self-organisation in the model. Further experiments are required to investigate the possibility of distinguishing between autogenically and allogenically induced parasequences.

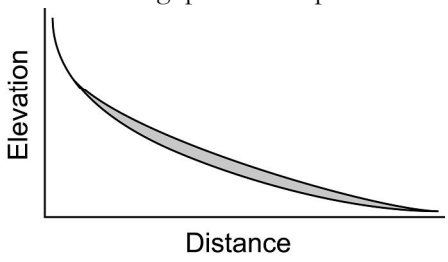

Figure 2.10: Conceptual graph of the dynamic equilibrium around the spatially averaged graded profile. The shaded area represents the area between the most (lower) and least (upper) efficient channel network.

In petroleum geology, exploitation of fluvial reservoirs is notoriously challenging, due to their generally low net-to-gross ratio and complex architecture. The difficulty of conditioning the current generation of LAB-type alluvial architecture models to well data (cf. Karssenberg et al., 2001) seems at least partly attributable to the fact

that their alluvial architecture is stochastically generated without the benefit of basin-scale geological constraints on these realisations. The model presented above may contribute to a better understanding of such reservoirs through its integrated simulation of basin-scale sequence-stratigraphic architecture and reservoir-scale alluvial architecture. One of the possibilities to be explored is to run the model with the intent to approximate large-scale basin-fill properties (based on geological background information about sea level, sediment supply, subsidence, initial topography, and so forth), after which it may be stochastically optimised to mimic the sub-grid (reservoir-scale) properties of selected parts of the basin fill in the direct vicinity of well locations. This approach promises a simultaneous increase in the geological credibility of stochastically simulated fluvial reservoir models and a significant reduction of the time needed to attain an acceptable goodness of fit to well data.

The holistic approach to channel network modelling presented in this paper seems robust enough to allow a wide variety of scenarios to be examined. Clearly, the autogenic system dynamics observed in this preliminary study need to be studied further, by numerical and physical modelling as well as in the field. This may require the implementation of variable discharges and the effects of floods (i.e. channel-forming discharge).

Applications of the model on the source-to-sink scale will require several additions. Future versions will include drainage basins, more realistic floodplain processes, and a near-shore module with sub-grid parameterization of delta-front morphology and marine processes. The overarching conclusion of our numerical experiments is that repeated "storage-and-release" events in the fluvial system appear to be a direct consequence of channel-network evolution. This raises some doubts about the general validity of one-dimensional equilibrium-profile models of fluvial systems that do not account for such "out-of-plane" variations.

List of Notations

a	Channel belt deposition rate at alluvial ridge (m yr^{-1})
b	Overbank aggradation exponent (-)
c	Bed roughness coefficient (-)
C_h	Sediment concentration at flow height h (kg m^{-2})
C_y	Sediment concentration at flow height y (kg m^{-2})
D	Water depth (m)
E	Bank erodibility (yr^{-1})
f_j	Fractional discharge routed towards cell direction j (-)
i_b	Bedload sediment transport as immersed weight passed per unit width (kg m^{-1})
$\varkappa$	The von Karman constant (-)
$k_{w/b}$	Hydraulic geometry width coefficient (-)
m_{cb}	Maximum channel belt width (m)
$M_{w/b}$	Hydraulic geometry width exponent (-)
n	Total number of downstream cells (-)
p	Square grid compensation parameter (-)
Q_b	Bankfull discharge (m^3s^{-1})
$\bar{Q}$	Mean discharge (m^3s^{-1})
$r_{z\varkappa}$	Overbank aggradation rate (m yr^{-1})
s_j	Slope towards cell j (-)
$tan\ a$	Dynamic friction coefficient (-)
τ_0	Effective shear stress (N m^{-2})
τ_c	Critical shear stress (N m^{-2})
U_*	Effective shear velocity (m s^{-1})
U_{*c}	Critical shear velocity (m s^{-1})
w	fall velocity for the relevant grain size (m s^{-1})
W_b	Bankfull channel width (m)
z_i	Distance away from the edge of the channel belt (m)
z_m	Maximum sedimentation distance from the edge of the channel belt (m)

Chapter 3

Towards dynamic floodplain interaction in a stratigraphic model

Abstract

Numerical models of fluvial systems have primarily focussed on channel processes. Yet, floodplain processes such as differential compaction, peat growth and overbank deposition directly influence the channel network. This paper describes a first-order approach to modelling these processes in a dynamic numerical model. The one-dimensional, sub-grid approximation of overbank deposition described by Dalman & Weltje (2008/Chapter 2) has been replaced by a two-dimensional, multi-cellular approximation. This addition to the floodplain routines allows us to use the model on basin to reservoir scale. Other floodplain processes included are; compaction, peatland dynamics and groundwater. Compaction of recently deposited sediments effectively reduces the elevation of abandoned delta lobes. This provides a mechanism for flooding surfaces to occur in coastal zones. The peatland dynamics add and stabilise the fluvial channels ands contributes considerably to the deposited volumes in a delta.

Introduction

In numerical modelling of fluvial systems attention has been primarily focussed on channel processes. Floodplain processes have not received as much attention (Jerolmack & Paola, 2007). Previous models (Leeder & Bridge, 1979; Mackey & Bridge, 1995; Karssenberg et al, 2001; Dalman & Weltje, 2008 (Chapter 2, this thesis) accurately model in-channel processes but simplify overbank sedimentation to exponentially decreasing sedimentation away from the channel, and ignore other floodplain processes. However the associated superelevation of channels influences the occurrence of avulsions and the sedimentary architecture. Avulsions determine the channel occurrence interval on the floodplain and therefore channel density and interconnectedness. Differential compaction, peat growth and overbank deposition will directly influence the superelevation of the channels. Additionally, bank erodibility will be highly variable in different floodplain deposits, which will have a large influence on the channel network morphology (Jerolmack & Mohrig, 2007).

The addition of discrete floodplain processes to the model proposed by Dalman & Weltje (2008; Chapter 2, this thesis) will allow higher-resolution modelling than previous versions, because overbank sedimentation can be distributed over multiple cells. This opens up the possibility of reservoir-scale modelling exercises, using a discretization scale of 200 m. The method of distribution of these fine-grained deposits in a numerical model partially determines the ratio of the cross-valley to down-valley gradient. Peat formation will also influence fluvial processes (Van Asselen et al, 2009), as peat may accrete rapidly and decrease bank erodibility. Creating additional volumes of deposits on the floodplain by incorporating peatland dynamics in the model will increase the elevation of the floodplain relative to the elevation of

the channel and consequently decrease the cross-valley gradient. Peat growing on the floodplain has a high porosity and significant compaction of peat occurs even at very shallow burial depths (Nadon, 1998). Consequently, the topographic elevation of the floodplain in areas where peat growth occurs can change considerably as a result of compaction. This paper describes the steps necessary for emulating these crucial processes. Full understanding of the implications of these modifications will require more study.

Modelling floodplain processes

This section describes the most important processes that influence floodplain deposition and morphology, specifically peat growth, local groundwater level and overbank deposition during floods.

Peatland dynamics

Depending on floodplain drainage and climate, peat can significantly influence elevation, erodibility and compaction of floodplain deposits. Under favourable circumstances, peat can grow fast enough to keep up with very high in-channel aggradation rates, which rules out any significant superelevation of the channel. Additionally, peat growth will inhibit lateral erosion due to consolidation of the floodplain substrate and its high intrinsic competence.

Peatlands can be found in areas where the climatic regime is characterized by an annual water surplus that depends on the balance between precipitation and evaporation. In many regions, temperature exerts a strong influence on primary productivity of peat. Peatland dynamics are a function of the balance between the growth of living plants at the surface and in the oxic upper layer (acrotelm) on the one hand and the decomposition of peat in both the acrotelm and the anoxic layer below (catotelm) on the other hand. All of these processes relate positively to temperature. Thus, peatland dynamics result from complex and non-linear relations of thermal and moisture conditions (Yu et al., 2001).

We assume the boundary between the catotelm and acrotelm to be equal to the relative water table depth (WTD). While this may not be completely accurate, this assumption complies with the level of complexity desired in our model. The peatland dynamics are modelled purely one-dimensional, i.e. peat only grows upwards, independent of surrounding gridcells. Therefore, peat growth is possible in any area where the WTD is within tolerable conditions (i.e. not too high, which drowns the peat, and not too low, which dries the peat). Peatlands can start and continue to grow at shallow and relatively stable ground water table depths. Once clastic deposits cover the peat it will stop growing and be subject to compaction and erosion only. Thermal conditions during simulation are assumed to favour peat growth, and parameter values can be chosen in such a way that they represent realistic growth and decomposition rates under specific temperature conditions.

Hilbert et al. (2000) developed a simple peatland dynamics model that incorporates external factors (groundwater table) and internal factors (soil specific decomposition rates). In our model the relative WTD is defined as the distance between the yearly average position of the water table and the land surface. The differential equation for change in height [dH/dt; m year^{-1}] is the difference between the rate of growth [G; m year^{-1}] and the rate of decomposition [D; m year^{-1}] (Figure 3.1):

$$\frac{dH}{dt} = G - D \qquad (1)$$

Peat growth is modelled as a quadratic function of the relative WTD. The minimum and maximum values of the WTD act as boundaries in between which peat growth can take place. After Hilbert et al. (2000):

$$G = k\left(WTD - WTD_{min}\right)\left(WTD_{max} - WTD\right) \text{ for } WTD_{min} \le WTD \le WTD_{max} \quad (2)$$

where k [m yr^{-1}] controls the maximum rate of growth. Growth is confined to the zone between the lower boundary WTD_{min} (-0.2 m) and upper boundary WTD_{max} (0.4 m). Outside this range no peat growth will occur. The decrease in height due to decomposition is defined as:

$$\begin{aligned} D &= -r_1 WTD + r_2(H_p + WTD) \text{ for } WTD < 0 \\ D &= r_2 H_p \qquad\qquad\qquad\quad \text{for } WTD > 0 \end{aligned} \quad (3)$$

In which r_1 and r_2 are the decomposition rate in the acrotelm and catotelm [yr^{-1}] respectively, and H_p is the active peat layer height [m].

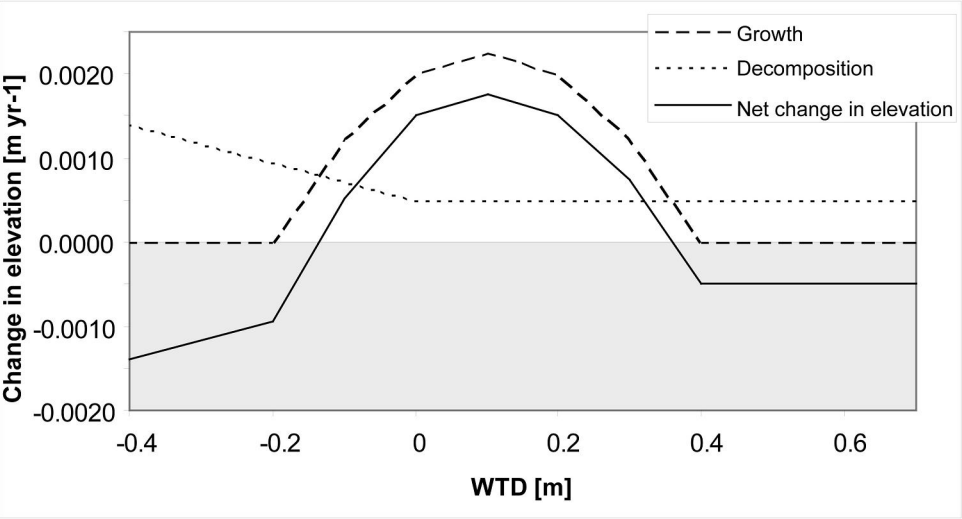

Figure 3.1: Growth, decomposition and change in height for a peat layer with a constant peat height of 0.1 m, k = 0.0025 m yr^{-1}, r_1 = 0.0025 yr^{-1}, r_2 = 0.00025 yr^{-1}, WTD_{min} = -0.2 m and WTD_{max} = 0.4 m (table 1)

Groundwater table

To model peat growth, the relative ground water table is incorporated in the model. Water table fluctuations are caused by many factors including precipitation, evapotranspiration, drainage, seepage, and all kinds of soil characteristics (e.g.

Bierkens and Te Stroet, 2007). As a full incorporation of all these effects would be prohibitively complex we propose a method to incorporate the groundwater table that only uses variables whose values are dynamically available in the model, such as topographic elevation, sea level and channel location.
King (1899) recognized the close relationship between the water table depth and the topography. When gravity drives the flow of groundwater from higher towards lower elevations, the phreatic surface is a subdued replica of the land surface (Desbarats et al., 2002). The conceptual *base water table* (BWT) is modelled as a replica of the topography on the continent, a constant depth (dBWT) below the land surface. The BWT is a long-term steady state result of recharge (precipitation minus overland flow and evapotranspiration) and discharge processes. The value of dBWT can be changed during simulation to represent fluctuations in discharge and climate. Wherever surface water is present, either the sea or a fluvial channel, the groundwater table has the same elevation as the surface water (Kehew, 2006). A continuous phreatic surface is defined with the BWT as the starting point and pull-up effects around surface water (Figure 3.2). The elevation of the WTD in a transition zone between BWT and surface water is modelled with a 2-D explicit linear diffusion scheme. The value of the diffusion coefficient is assumed to be constant in the horizontal plane and can be chosen in such a way that it is proportional to the expected width of the transition zone of the surface water: highest width for the sea (c_s), lower for the channels (c_{ch}) (Figure 3.2). The diffusion coefficient for the influence of a channel is proportional to the mean bankfull discharge across the grid:

$$c_{ch} = a \cdot \frac{\sum_{C=1}^{n_{fluv}} W_b \cdot D_b}{n_{ch}} \qquad (4)$$

With W_b and D_b the bankfull width and depth respectively in grid cell *C*; n_{fluv} is the total number of grid cells in the continental (fluvial) environment, *a* is a conversion constant, and n_{ch} the total number of grid cells where a channel is present. The diffusion routine results in an interaction of multiple surface water phenomena and increases the area of pull-up of the WTD from the BWT, but cannot create a WTD higher than the surface water with the highest elevation.

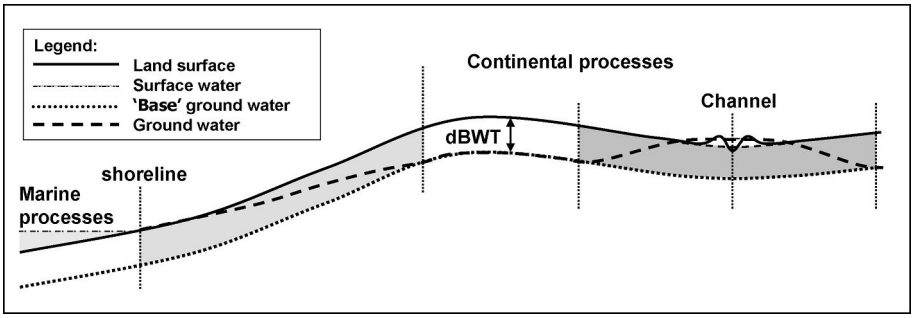

Figure 3.2: Schematic cross-section showing the ground water table (WTD) and the transition zones between the base water level (BWT) and the surface water of the sea and channel.

Compaction

Peat can have a porosity ranging from 83% to 96% and can, consequently, undergo rapid compaction even under small loads (MacFarlane, 1969; Nadon, 1998). To prevent overestimating the effects of peat deposition in the model, compaction is incorporated.

Compaction can be addressed with a simplified approach that characterizes the essence of the compaction process (Bahr et al., 2001). A number of physically reasonable assumptions are applied in this model to simplify the calculations. Compaction is modelled vertically, horizontal stresses are assumed to be negligible and only mechanical compaction occurs. The matrix, including peat, is assumed to be incompressible. Compaction only occurs by reduction of the pore space, and the density of the matrix is constant. Exponential porosity reduction during burial is calculated using the equation of Sclater and Christie (1980), based on the original work of Athy (1930):

$$\phi = \phi_0 e^{-mZ} \tag{5}$$

Where ϕ_0 is the initial porosity, Z is the depth in km and m is an empirically derived constant. The constant m can be related to the initial porosity by the following equation:

$$m = 0.03 \cdot e^{4.52 \cdot \phi_0} \tag{6}$$

The constant m is a curve-fitting constant in the original Sclater-Christie equation and as such based on the empirical relation between initial porosity and burial porosity (Sheldon and Retallack, 2001). Time dependent compaction is assumed to be unimportant for our time and spatial scale.

Peat grows in the continental environment with a very high initial porosity. However, it can be eroded, transported, and deposited again later in the simulation. The transported peat, here referred to as clastic peat, has a deposition porosity in the same order as sand, if grain sizes are similar. Porosity reduction is exponential, but behaves almost linear in the shallow subsurface.

Since the initial porosity is different for each facies, the compaction behaviour is different as well. Facies with a high initial porosity, such as peat, will contribute more to the total compaction than facies with a low initial porosity. The compaction algorithm scans through the entire stratigraphic record and updates the porosity of the facies according to their burial depth. Accordingly the compaction routine greatly increases run time, as each stratigraphic unit must be accessed during each time interval.

Compaction in the model mainly reduces the volumes of peat that have grown in the continental environment. The volume reduction of by compaction decreases the impact of peatland dynamics on the alluvial system.

Overbank sedimentation

Sediment deposition decreases exponentially with distance from the natural levee (Pizzuto, 1987; Mackey and Bridge, 1995; Middelkoop and Asselman, 1998). The sand fraction of these deposits decreases from 0.9 at the levee to 0.05 in the proximal floodplain. At distances larger than 50 to 100 m from the river channel, the deposits consist essentially of clay and silt (Middelkoop and Asselman, 1998). The exponential decrease therefore depends mainly on the sand deposition on the levee. Exponential decrease in sediment deposition can be modelled by turbulent diffusion.

Here a method is proposed to distribute sediments from the channel across the grid cell boundaries, referred to as inter-cellular deposition. In previous model versions (see Chapter 2/ Dalman & Weltje, 2008) overbank deposition occurred only in the cell where the channel was located. Sediment was distributed using one-dimensional linear diffusion in one single gridcell. This assumption limits the lower size of the discretization. To alleviate this problem the sediment is now allowed to be distributed over the floodplain using two-dimensional linear diffusion, representing flood deposits. The clay fraction available for overbank deposition is calculated as the difference between total deposition and the deposition of the fractions with a higher settling velocity in the grid cell. The overbank deposits are distributed over all neighbouring grid cells located down slope on the floodplain using a 2-D explicit linear diffusion scheme. Naturally, the total mass balance needs to be maintained during this process. Consequently, clay is removed from the channel and accommodation space in the channel is filled more slowly.

Note that the Dalman & Weltje (2008) model uses a cross-valley gradient calculated in each gridcell containing an active channel to determine the stability of the channel. The distribution of overbank deposits requires the cross-valley gradient to be computed by comparing the elevation of the channel and the surrounding gridcells.

Results

The processes described above are illustrated by modelling the development of a time-invariant low-angle shelf delta over several thousand time steps of one year. We use a discretization of 1 by 1 km.

Overbank deposition is illustrated at several time intervals in Figure 3.3. The net change in elevation includes compaction in the subsurface. The mud deposition decreases exponentially away from the channel when the local topography is still flat (Figure 3.3a). As time progresses, avulsions cause the abandonment of old channel-belt complexes and produce remnant morphological features on the alluvial or delta plain. These features force subsequent overbank deposits around the elevated areas, producing irregular deposits (Figure 3.3b and 3.3c). Note that overbank deposition is currently dependent on in-channel deposition, which causes most overbank deposits to occur on the floodplain. The overbank deposition smoothes the floodplain morphology (see Figure 3.3c) and encases abandoned sandy channel deposits in clays.

The effects of the compaction routine can also be observed in Figure 3.3. The net decrease in surface elevation at the coastline is caused by the compaction of marine muds, which starts off as a highly porous material with high compaction rates. This effect is obscured at sites with high sedimentation rates (i.e. near river mouths), where the sedimentation rate exceeds the compaction rate. Only after these areas are abandoned does the compaction effect become clear.

The groundwater modelling (Figure 3.4a) shows the relative influence of surface water on the groundwater table. The highest elevation of the groundwater table is in the near shore delta plain due to the vicinity of both the sea and the distributary channels.

Peat accumulation (Figure 3.4b) is notably patchy due to its sensitivity to large fluctuations in groundwater table. Further inland, away from the stabilising influence of the salt wedge, avulsions change the local groundwater table sufficiently to kill off active peat accumulation, either through drowning or by lack of water. The model inherently mimics the pull-up of groundwater in peat and allows large peat mounds to form.

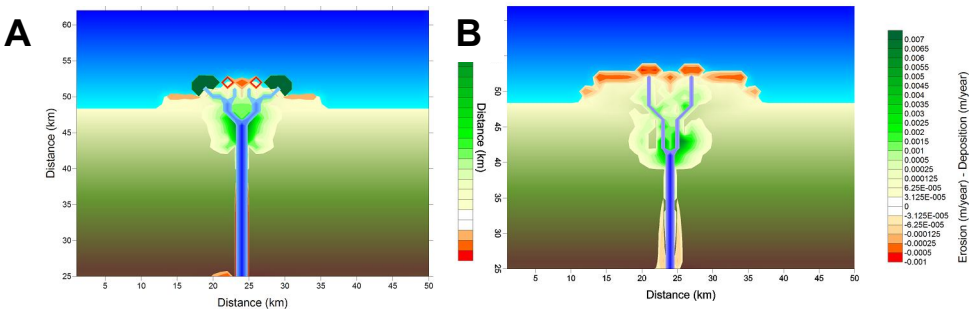

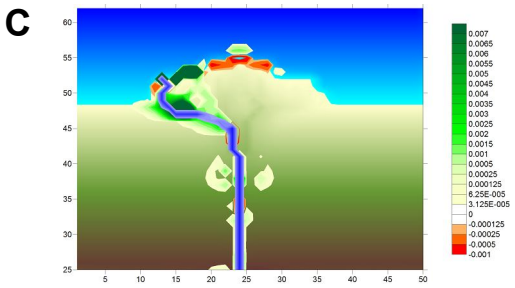

Figure 3.3 A; Channel network, sedimentation and net topography after 300 years.
B; Channel network, sedimentation and net topography after 1000 years. Note that the progradation has increased the fluvial profile sufficiently for most sediment to become stored on the delta plain.
C; Channel network, sedimentation and net topography after 2500 years.

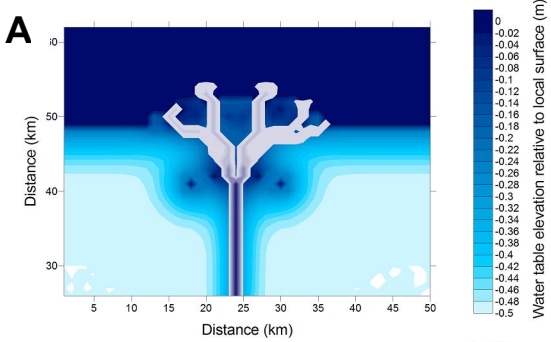

Figure 3.4 A; Surface water and associated relative groundwater table after 500 years into the run. The elevated groundwater table extends significantly further inland than the delta apex.

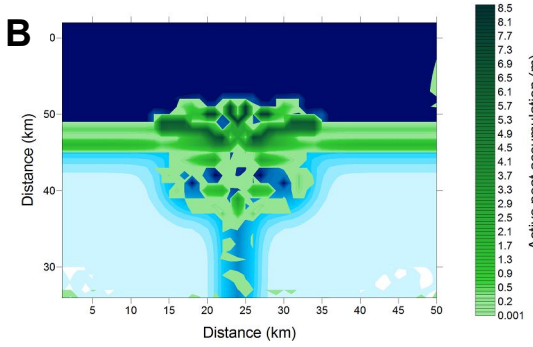

B; Total active peat accumulation. The amount is in meters accumulated, which will have compacted significantly after burial. Note also the lack of active peat in areas where large fluctuations of water level have occurred (just left and right of the delta apex.

Discussion

Overbank deposition

The routines in this paper improve upon the one-dimensional, sub-grid approximantion of overbank deposition described by Dalman & Weltje (2008)/Chapter 2. The one-dimensional approach has been replaced by a two-dimensional, multi-cellular approximation. This method allows much more flexibility in using a wide range of spatial scales for modelling exercises. Our routine uses a direct relationship between in-channel and overbank deposits, because we assume that grains with very low fall velocities will not be deposited in the fast flowing fluvial channel. In most real fluvial systems the overbank deposits are dependent mainly on flood frequency, magnitude, local channel morphology and sediment concentration in the water column. To model this entire spectrum of processes is outside the scope of this work, though some simple modifications will improve the realism of the deposits. By including a percentage of wash load available for overbank deposition during each time step, locally modified by channel morphology and channel elevation, overbank deposition will increase when the channel is superelevated as the floodplain and effectively the accommodation space is large. Conversely, overbank deposition will decrease when channels incise as the accommodation space is restricted to the incised valley area.

Compaction, groundwater and peatland modelling

Compaction of recently deposited sediments effectively reduces the elevation of abandoned delta lobes. This provides a mechanism for flooding surfaces to occur in coastal zones. One phase of delta lobe progradation, consequent abandonment by upstream avulsions and subsequent compaction of the newly deposited materials will result in a progradational sequence capped by a flooding surface, i.e. an autogenic parasequence (see Chapter 6 for a more in-depth discussion on this subject).

As the compaction routine currently requires all stratigraphic units to be processed during each timestep it rapidly hogs all processing time and memory. To prevent this, some simple techniques will need to be implemented. The stratigraphic record can be saved in blocks of minimum thickness, which will decrease the number of records to be accessed. Additionally, the compaction routine can be called only once every n (probably 10) time steps and, the calculated compaction is upscaled linearly. As the compaction is mostly burial-related as opposed to time, and each time step only allows a small amount of sediment to be deposited this will not result in unacceptable errors. Careful analysis of the effect of these jumps especially on sedimentation is necessary to minimize possible artefacts.

The groundwater routine is very simple, yet it does allow us to approximately evaluate the effect surface water on vegetation. Possible improvements might include the local influence of permeability changes. Though this will greatly increase the complexity, as it will require intricate flow calculations through the heterogeneous stratigraphy. For our purposes the current routine suffices, as we only use it to calculate the effect upon vegetation. A more accurate groundwater routine would require a full water balance model, which would include runoff, evapotranspiration, infiltration and groundwater

flow. This would require a detailed architectural description of the subsurface heterogeneities, which is simply not available for most settings.
The peatland dynamics add an extra "infill" of the floodplain, thus stabilising the fluvial channels. Additionally peat growth contributes considerably to the deposited volumes in a delta. The significant impact of peat on the stratigraphic record and alluvial architecture is supported by evidence from field studies in the Rhine-Meuse delta (Van Asselen et al, 2009; Gouw and Erkens, 2007; Berendsen and Stouthamer, 2000; Stouthamer and Berendsen, 2000).

Relative influence of floodplain processes
Discretized explicit overbank sedimentation allows the removal of sediment from the channel gridcells. The main problem in modelling this process does not lie in defining the spatial distribution of sediments, but rather in determining the amount of suspended material available for overbank deposition. Full modelling of this process would require a complete hydrodynamic and climatic reconstruction of the system, as the duration and magnitude of each flood and the sediment distribution in the water column combine to determine the amount of material available for overbank deposition. Therefore we must simplify this process without sacrificing the most important controls. This upscaling problem can be solved if the local channel morphology, suspended sediment load available for overbank deposition and discharge variability (flood frequency and magnitude) can be related to the suspended load in the channel.

Multiscale modelling
The addition of these floodplain routines allows us to use the model on basin to reservoir scale (10^0-10^2 km). Previous restrictions on discretization due to the parameterisation of overbank deposition (see Chapter 2) have been removed. Yet some further improvements can increase the realistic modelling of reservoir architecture. Specifically channel belt dimensions will need to be mimicked more realistically by representing lateral migration of the channels dependent on bank erodibility. This will also have a strong influence on superelevation (see chapter 4), as rapid lateral migration forces the channel to deposit most channel belt deposits horizontally as opposed to vertically. This should result in well-connected sand bodies as opposed to isolated sand bodies encased in clays.

Future work
This pilot study indicates that the model may be used on a variety of scales, using discretizations from 500 to 5000 m. The addition of floodplain processes allows us to test theories of fluvial deposition under different climatic conditions (i.e. change in vegetation) and to assess fluvial architecture under scenarios of sealevel change.

Biogeomorphological processes on decadal time scales influence many longer time scale processes. Our peatland model, albeit simplistic, is a first-order, approximation towards this coupling. Future additions might include several vegetation types, which differ in their sediment capture and bed stabilising features.

This will require a dependence of vegetation type on climate and careful calibration of local groundwater table to the growth rate of vegetation.

Conclusions

The one-dimensional, sub-grid approximantion of overbank deposition described by Dalman & Weltje (2008/Chapter 2) has been replaced by a two-dimensional, multi-cellular approximation. This addition to the floodplain routines allows us to use the model on basin to reservoir scale. Compaction of recently deposited sediments effectively reduces the elevation of abandoned delta lobes. This provides a mechanism for flooding surfaces to occur in coastal zones. The peatland dynamics stabilise the fluvial channels ands contributes considerably to the deposited volumes in a delta.

Chapter 4
Modelling Wave and Current induced Suspended Sediment transport and deltaic Stratigraphy

Abstract

Fluvio-deltaic systems under influence of waves typically show a wide range of stratigraphic and morphological responses to waves and currents. Under sufficient energetic conditions, sediment previously deposited on the shelf may be resuspended and transported. This process effectively segregates the subaerial progradation from the subaqueous clinoform, simultaneously segregating the fine grainsize classes from the sandy grainsizes (which remain near the coastline). This has important implications for clinoform patterns and lithology in the stratigraphic record. Therefore we present a 2DH basin scale model that mimics wave resuspension and advective transport. The model is implicitly linked to a fluvial module, thus permitting the study of feedback and interactions between the marine and continental sedimentary environments. This approach allows us to quantify the stratigraphic response to external and intrinsic forcing under the influence of waves and currents.

Introduction

The vast majority of sediments transported and deposited down rivers and through deltas is mud. The small grainsize and associated insignificant fall velocity make it easy to transport and hard to deposit. Conversely the coarser grains need highly energetic hydrodynamic activity before movement can even be initiated. Therefore we mostly find sands near the channels and near the coastline, but the muds are transported orders of magnitude further from the channels and river-mouth. This is exemplified in the stratigraphic record, where isolated sand bodies may be encased in shale strata. The sand is very informative as it can tell us much about the high-energy areas that produce the highest sediment fluxes. Moreover the sandy sediment archive is relatively easy to read in a geological context, due to the large grainsize and distinctive sedimentary structures. But the muds can tell us more about all the other subtle forcings, lost in the coarseness of the sands. In field geology analysis of muds is rather hard without proxies such as extensive geochemical analysis. So as to better understand the vast amounts of buried markers of natural history we need to model the processes working on geological time scales and interpret the distribution of clastic sediments in the subsurface accordingly. This paper is a first step towards this goal.

Clinoforms are fundamental elements of delta stratigraphy. Most studies have focussed on the sandy parts of the delta, as the understanding of coupling of the sandy and muddy subsystems and associated sedimentary structures is currently insufficient to understand the complex growth of shelf clinoforms. The location of preferential suspended matter deposition is dominantly controlled by the amount of material available, the characteristics of sediment sources and the hydrodynamic energy controlling transport and deposition of the suspended fine particles (McCave,

1972). A particularly striking feature of muddy shelf clinoforms is the extraordinary extension of the fine-grained part of the clinoform, often prograding parallel to the coast (e.g. Cattaneo et al, 2007). The length of this extension may range up to several 100 kilometres, and is related to shore-parallel currents transporting the suspended material for long distances. Yet one single river plume cannot explain the entire length of these features. Using the empirically derived removal rate principle by Syvitski et al (1998) and a very fast thermo-haline current of 1.00 m/s (Nittrouer et al, 2004) and a removal rate constant of 2 per day, we can calculate that for clay-sized particles 90 % of the suspended fine material has been deposited after 100 km. Under more realistic current velocity values of 0.40 m/s, 90% of the suspended material will have fallen out of suspension after only 40 km's and 50 % after a mere 12 km. Therefore these deposits cannot possibly be created by one transport sequence. Rather, the fine material must have been resuspended several times due to currents and/or waves and transported after these discrete resuspension events. Obviously this process will only occur when sediment is deposited above the deepest wave base/depth of closure. Thus these long extensions of muddy shelf clinoforms are very sensitive to the wave regime and especially the inherent variability.

Many models partially cover marine geomorphological sedimentary evolution, yet few address the problems occurring on geological timescales in 3D space. Many large-scale basin filling models are usually (necessarily) simplified, commonly representing marine processes as diffusion (e.g. Granjeon & Joseph, 1999; Clevis et al., 2003, Meijer, 2002). This approach is appropriate for generalized sequence-stratigraphic conceptual studies and comparisons. However, when we wish to analyse the relative influence of fluvial processes and waves or study the sedimentary architecture in greater detail, we must include numerous discrete processes. Notably small grainsize fractions can be transported far from the river-mouth. In most cases they are transported by hypopycnal plumes, which may transport the finer grains far offshore due to slow mixing with seawater. Oblique currents will distort the plume and the sediment distribution accordingly. Subsequently, large storm waves influence the newly deposited sediments. The increase in near-bed orbital velocity allows the sediment beds to become mobile, even resulting in resuspension under sufficiently energetic conditions. Resuspended sediments may be transported by wave-induced, oceanic or thermo-haline currents and may take several days to settle. Thus the eventual resting place of the fine sediments is an accumulation of high-energetic storm events and subsequent low-energetic transportation. The model Sedflux 2.0 (Hutton & Syvitski, 2007) is a notable exception; it contains an accurate plume routine, yet uses a simplified longshore transport routine. This chapter presents a (partial) solution to the three dimensional modelling of wave-current influenced marine systems, integrated in a modular continental margin scale model. We have attempted to create a simplified, fast algorithm albeit with realistic results on long timescales (1 to 100 kyears). The main storm events for each time step will likely resuspend the vast majority of the material. Therefore we can simplify the wave hydro- and sediment dynamics routine to one or two runs per time step.

Model description

The framework of the model is an addition to and partial replacement of the architecture of the model presented by Dalman & Weltje (2008), which itself used the architecture of the QDSSM model presented by Meijer (2002). Marine processes in these previous versions were represented by a very simplified plume routine and a diffusion-based routine for gradient-induced mass wasting. This chapter describes the newly implemented algorithms, which were developed to represent wave- and current effects on marine clastic sedimentation.

As we wish to model the influence of the large-scale oceanic currents and waves on clastic sediments over long time scales, some simplifications must be made. This facilitates fast computation, necessary for the modelling of long-term and large-scale systems. Additionally the unknowns in geological time and space, such as the initial conditions and changing influences, are too large to justify a complex solution. However, some complex processes do result in distinctive grainsize distributions and subsequent genetic units in the stratigraphic record.

Continental sediment and hydro- dynamics (Modified after Dalman & Weltje, 2008 - Chapter 2)

The continental clastic sedimentary system is represented by two algorithms. A two-dimensional diffusion algorithm characterizes hill slope denudation. Fluvial processes and stratigraphy are represented by sub-grid parameterisation for application in the large-scale basin-filling model. Sub-grid sediment transport and channelisation are derived from physical equations, capable of producing convergent and divergent drainage networks, trunk channels and most importantly, detailed representations of avulsions and bifurcations.
The channel network model allows realistic input and more importantly spatial and temporal changes of the liquid and solid discharge entering the marine domain.

Hydrodynamics

Our intent in modelling the hydrodynamic behaviour of the system does not aim to create the most accurate simulation of fluid motion. The focus is on sediment dynamics and stratification; therefore the hydrodynamic routines described below represent only those processes relevant on geological time scales. The hydrodynamics in the model represent three individual processes. River plumes and large-scale oceanic currents are integrated in one combined algorithm, allowing rapid calculation. Wave generation and propagation are modelled independently.

Large-scale currents

The hydrodynamic flow of currents and plumes are modelled using one integrated steady-state potential flow routine. Though this technique ignores fluid viscosity, irrotational flow, compressibility and smaller scale perturbations in the hydrodynamic movement, the resultant water movement is robust, speedy and representative for geological time scales. The integration of the river plumes and the longshore currents in one hydrodynamic algorithm allows us to calculate the deposition from the plume

and the longshore transport of resuspended shelf deposits. Concomitantly, additional plumes do not slow the integrated routine.

A linear, homogeneous form of potential flow is represented by the general Laplace equation:

$$\nabla^2 \phi = 0 \qquad (1)$$

Where ϕ is the velocity potential. In our model, we calculate a two-dimensional flow to represent currents and plumes. Vertical velocities may be ignored, as these are much smaller than the horizontal velocities. The Laplace equation in two dimensions is given as:

$$\frac{\partial^2 \phi}{\partial x^2} + \frac{\partial^2 \phi}{\partial y^2} = 0 \qquad (2)$$

This partial-differential equation may be solved using a finite-difference form. We use the simple, yet robust Gauss-Seidel technique (after Harbaugh & Bonham-Carter, 1970). The input for the flow field is provided by supplying velocities at the grid boundaries. The currents are supplied externally (forced externally) using knowledge of the specific setting.

The resulting velocity potentials at each grid node are used to calculate the component vectors and consequently the resulting flow direction and velocity. The velocity components in the x and y direction are derived from the velocity potentials:

$$v_x = \frac{\partial \phi}{\partial x} \qquad v_y = \frac{\partial \phi}{\partial y} \qquad (3)$$

Where v_x and v_y are the velocity components in the x and y direction, respectively.

Basin scale currents

The routine for large-scale currents, described above, needs in and outflow points to be defined for each computational cycle. These boundary conditions are provided by defining the velocity magnitude and direction where applicable. This may be based on an oceanographic circulation model if sufficient knowledge is at hand to run these models.

Hypopycnal plumes

Most river plumes enter a relatively high density, salty body of water and are composed of low-density fresh water; therefore the dominant plume type is hypopycnal. Albertson et al (1950) derived a model of two-dimensional submerged jets. This model is widely used for dispersing sediment load and was implemented in a numerical model by Syvitski et al (1998).

The plumes entering the marine domain are dynamically integrated by automatically assigning an inflow point with the channel velocity (see Dalman & Weltje, 2008) and direction of flow at the appropriate gridcell. Our model somewhat simplifies the spreading of the 2D jet, assuming lateral spreading occurs. The plume may be diverted and skewed by the longshore currents. On a smaller scale model this might result in a somewhat diffuse plume. Yet when using gridcell sizes of 1 to 4 km, the results are quite acceptable. As this routine allows the resuspended sediment transport to be calculated simultaneously with the plume deposition, it is computationally very efficient. The model can dynamically incorporate a practically infinite number of rivers without slowing the calculations. Depending on grainsize distribution, the largest fraction of the sediment loads entering the marine basin under hydrodynamically inactive periods is dumped within the first tens of kilometres of the coast. This holds for nearly all river plumes, as most have a velocity under 1 m/s when entering the basin. Additionally, wave-current interaction may rework a significant proportion of the fine-grained fraction deposited by the plume (see below).

Waves

In order to calculate the sediment resuspension and movement on a wave-influenced shelf, we need the wave height at each point. The waves in the deep water part of the model may increase in height, yet as they reach the shallower areas bottom friction will slow them and decrease the wave height. Figure 4.1 illustrates the principle of the propagation and consequent shoaling of waves at different water depths.

As the largest amount of sediment is eroded and consequently deposited during the extreme events, usually only one event is modelled per time step (one year). This is easily modified if necessary to a number of events limited only by computational capacity or usefulness.

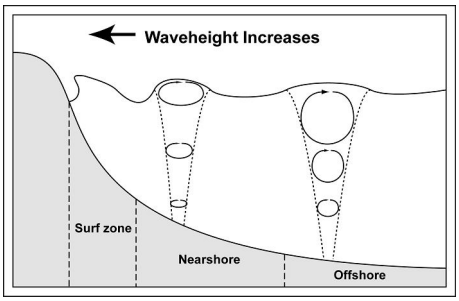

Figure 4.1; Cartoon of the changes in wave height, length and orbital motions in the offshore (water depth larger than one half wavelength), the nearshore and the surfzone (waves break). Each marine gridcell is assigned to one of these three sub-environments.

Deepwater wave generation

Waves at the model boundary can either be provided as input or generated in the model. Wave height may be calculated based on wind velocity and the distance over which this wind blows (the fetch length). The fetch can be provided as input, or it may be calculated in the wave generation-routine if the entire basin is encapsulated in the model. In order to approximate the significant wave height, the Corps of Engineers have derived several semi-empirical relationships (CERC, 1984).

Firstly we need to approximate the wind stress factor U_A, which provides the stress exerted by the wind on the water velocity:

$$U_A = 0.71U^{1.23} \quad (4)$$

Where U is the wind velocity (m/s). In waters deeper than the wave base the wave height (H_s) follows the relationship:

$$H_s = 1.6*10^{-3}\left(\frac{U_A^2}{g}\right)\left(\frac{gF}{U_A^2}\right)^{1/2} \quad (5)$$

Where, F is the fetch length (m) and g is the gravitational constant. The upward limit of this relationship for fully developed seas (where the storm fetch is no longer limiting the growth of waves) is:

$$H_s = 0.2433\frac{U_A^2}{g} \quad (6)$$

In gridcells where the bathymetry is greater than half the wavelength, bottom friction is negligible and the waves may grow in size.

Wave height alone is insufficient for our purposes. Therefore we use the linear Airy wave theory, which is the simplest of wave theories yet eminently useable for our objectives. The wavelength (L) and phase velocity (C) are defined as:

$$C = \frac{gT}{2\pi}\tanh\left(\frac{2\pi h}{L}\right) \quad L = \frac{gT^2}{2\pi}\tanh\left(\frac{2\pi h}{L}\right) \quad (7 \& 8)$$

Where T (s) is the wave period and h (m) is the water depth. Where the water depth is greater than half the wavelength, the phase velocity C_∞ (m/s) and wavelength L_∞ (m) in deep water approach:

$$C_\infty \approx \frac{gT}{2\pi} \qquad L_\infty \approx \frac{gT^2}{2\pi} \quad (9 \& 10)$$

Shoaling in the nearshore

If waves reach shallower areas (i.e. with water depth $z < L/2$) will transform as they shoal. The wave velocity and length progressively decrease and the height will decrease slightly before increasing as the wave period remains constant (Komar, 1998). By combining equations 8 with 10 and 7 with 9 this results in:

$$\frac{L}{L_\infty} = \frac{C}{C_\infty} = \tanh\left(\frac{2\pi h}{L}\right) \qquad (11)$$

This relationship allows us calculate the wavelength and velocity at water depth h. As equation 11 contains L on both sides it must be calculated iteratively. Noda et al (1974) use the following equation describing the shoaling wave height related to the deep-water wave height H_∞ (m), wave number k (=$2\pi/L$) and water depth h:

$$H = H_\infty \left(\tanh(kh)\left[\frac{2k}{\sinh(2kh)}\right]\right)^{-1/2} \qquad (12)$$

Refraction

When waves enter the nearshore (see Figure 4.1) the direction of propagation may change along with decreasing water depth. As the bottom friction increase associated with the decreasing water depth, the wave celerity decreases. If the waves enter the nearshore at an oblique angle, the change in celerity will be greater for the inshore part of the wave front. As the deeper part of the wave front loses less velocity to friction the wave front will turn (Figure 4.2).

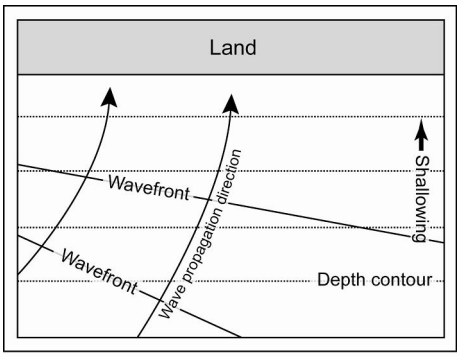

Figure 4.2; Refraction of waves due to relative changes in wave propagation velocity. Note the tendency for the wave front to become more parallel to the shore as the basin shallows.

Refraction is important for the long-term changes in coastal profile. The wave energy is concentrated on protruding headlands, and diverted from embayments. This will increase erosion of the protrusion and allows infilling of the embayments. Through time this process will straighten the shoreline.

In order to mimic this process, we have implemented a wave ray algorithm. This principle uses a finite number of wave rays, lines orthogonal to the wave front and parallel to the wave propagation direction. By interpolation between these lines we can determine the wave direction and consequent focussing of energy at each gridcell. The amount of turning of the wave ray is equal to the velocity gradient (change in velocity) along the wave front. Slingerland et al (1994) derived the change in angle β (°) along the wave ray per unit distance ds (m) as:

$$\frac{d\beta}{ds} = \frac{1}{C}\left(\frac{\partial C}{\partial x}\sin\beta - \frac{\partial C}{\partial y}\cos\beta\right) \qquad (13)$$

Note angle β is measured between the wave ray and the depth contour. Furthermore we need to know the change in distance along the x and y axis:

$$\frac{dx}{dt} = C\cos\beta \quad \text{and} \qquad \frac{dy}{dt} = C\sin\beta \qquad (14 \& 15)$$

The wave velocity C is known for all grid nodes by equation 11, which allows us to calculate the advancing wave ray starting at the deepwater-nearshore boundary.

Koutitas (1988) developed a finite-difference solution scheme to equations 13, 14 and 15, which forms the basis for our algorithm. The routine follows the wave rays as it propagates over distance ds (m); the change in direction β between node n and n+1 is given in the following finite-difference form:

$$\beta^{n+1} - \beta^n = ds\left(\frac{1}{C^n}\frac{\partial C^n}{\partial x}\sin\beta^n - \frac{\partial C^n}{\partial x}\cos\beta^n\right) \qquad (16)$$

Note that the wave ray will commence at the exact location of a gridcell node. As propagation continues the changes in direction β will result in a slight offset in most cases. Under these circumstances the values of C must be interpolated and the exact location of the wave ray node must be calculated relative to a gridcell node.

Evidently the concentration of wave rays will result in changes in wave height and energy. The most pronounced changes in direction and consequently energy is expected at the largest changes in wave propagation velocity and therefore changes in shallow bathymetry (i.e. very near the coast).

Shoaling in the surf zone: Breaking and loss of momentum

Waves lose most of their energy in the surf zone (nearest coast, Figure 4.1) by conversion to turbulence and heat by the breaking waves. Obviously the simplified linear Airy relationships for wave motion described above do not hold in the surf zone. In view of the scale of the model discretization (1 to 5 km) exhaustive modelling of the surf zone waves is unnecessary. Yet the significant distributive and erosive characteristics of the surf zone necessitate a modification of the wave motions in the surf zone cells.

Waves will break when attaining a wave height/water depth (H_s/h) ratio greater than approximately 0.78 (Horikawa 1966). As waves propagate landwards after the breaking process the waves quickly lose energy and wave height (H_s) asymptotically decreases to the "saturated" 0.42h (Horikawa 1966).

The combined hydrodynamics, currents and waves

All processes described above are combined to form a total flow field. In reality the waves and currents influence each other dynamically. For our purposes this is somewhat superfluous, as it would require a full solution to the shallow water equations. On geological timescales most imperfections in the model are vastly smaller than the uncertainties in the boundary conditions. Therefore we model the wave field

and currents independently and only allow interaction through the sediments. Wave induced currents are assumed to be modelled in the explicit current potential flow field, additionally these are usually of quite small scale and therefore irrelevant to our basin scale model.

Sediment transport, erosion and deposition

Sediment erosion, transport and deposition are divided into two routines with differing methods and predominantly different settings. In the offshore and nearshore cells little bedload transport will occur owing to the low persistence of horizontal orbital velocity near the sediment bed (i.e. only high enough during storms). The predominant sediment transport method is by suspended load transport of the smaller grainsize fractions. In the surf zone and upper nearshore, bedload transport may occur, yet the scale of this process (though variable due to dependence on beach slope) is subgrid scale and is discussed further in chapter 5.

Suspended load sediment dynamics is represented by three routines. The (re-) suspension of marine deposits depends on wave influence and to a lesser extent bottom currents. The resuspension event is run through a diffusion routine to represent the diffusive nature of waves. Subsequently the resuspended material is transportation in conjunction with the river-supplied material by the advective motion of the currents. During transportation the sediments gradually fall out of suspension.

Resuspension

Due to the many unspecified constraints in the model, a time-dependent digging algorithm is unpractical. Therefore we assume that the "once-a-year" storm event digs until the bottom shear stress is smaller than the critical shear stress. This is a valid assumption for our purposes as the majority of sediment in the offshore is eroded during these events (Stive & De Vriend, 1995). Moreover the coarse sandy material will scarcely be transported by the longshore currents, resulting in an instantaneous deposition of the sandy material thereby modelling the process of winnowing. This redeposited layer represents the depth of wave reworking. The algorithm uses a bracketing and bisection mechanism to find the stable equilibrium surface, where the bottom shear stress equals the critical shear stress. The amount of resuspended material for the entire marine basin for each grainsize class is calculated before advective or diffusive horizontal transport can take place. This two-layer approach allows the model to mimic supply-limited situations in addition to transport-limited situations. Supply-limited conditions are relatively common on the shelf (Harris & Wiberg, 2001)

To begin with we need to know the critical shear stress τ_{cr} for initiation of suspension transport. The settling velocity (W_s) is calculated after Gibbs et al (1971):

$$W_s = -3\mu + \left(\frac{\left[9\mu^2 + \left(\frac{gD^2}{4} \right) \rho \left(\rho_s - \rho \right) \left(0.0155 + 0.0992D \right) \right]^{0.5}}{\rho \left(0.0116 + 0.0744D \right)} \right) \quad (17)$$

Where D is the grain diameter (m), μ is the dynamic viscosity, ϱ is the density of water, and ϱs is the density of the sediment. The critical shear stress (τ_{cr}) can be derived after Bagnold (1966):

$$\tau_{cr} = 0.64\, \varrho\, W_s^2 \quad (18)$$

We need to determine the bottom shear stress at the seabed under several conditions: wave influenced, current influenced and a combined current-wave interaction. The most important of these is the wave-influenced condition, as the current is relatively slow compared to most storm events and currents have a much lower "carrying capacity". The maximum wave-induced orbital velocity (u_b) is given:

$$u_b = \frac{\pi H_s}{T \sinh\left[k(d - 0.5H_s) \right]} \quad (19)$$

The bottom shear stress is calculated following Li & Amos (2001):

$$\tau_b = 0.5\, \varrho\, f_w\, u_b^2 \quad (20)$$

Where f_w is the wave friction factor calculated following Nielsen (1979).

For the current only conditions, the total current shear velocity (u_{*c}) can be derived from the flow velocity (u_z) at depth (z) using the von Karman-Prandtl equation (see also chapter 2):

$$u_{*c} = \varkappa u_z / \ln(0.3z / 2.5D) \quad (21)$$

Where $\varkappa$ is the von Karman constant (equated to 0.4). The mean velocity at 1 m above seabed is then obtained from (modified from Li & Amos, 2001):

$$u_1 = (u_{*c}/\varkappa) \ln(0.3*1 / 2.5D) \quad (22)$$

The bottom shear stress for steady currents is then calculated as follows:

$$\tau_b = 0.5\, \varrho\, f_c\, u_1^2 \quad (23)$$

Where f_c is the current friction factor.

The combined-flow case is considerably more complex, as the friction factor (f_{cw}) must be calculated iteratively. In cases where the currents are sufficiently powerful to necessitate this, the bottom shear stress is calculated following the SEDTRANS96 method (Li & Amos, 2001). Yet this routine is relatively slow and must be applied several times to each gridcell. To increase the speed of computation we use the wave-only or current-only cases when the velocity ratios are smaller than 0.01. This results in a negligible error and allows a substantial decrease in computation time.

Diffusion

The sediment, which has been eroded, is temporarily kept in suspension by wave action. The suspended particulate matter (SPM) is not expected to stay exactly above its point of origin due to dispersion by wave motion. The model mimics this process by applying an explicit diffusion routine to the suspended particulate matter, excluding the sediment delivered from the rivers in the present time step.

Transport and deposition

Longshore suspended load transport in the onshore and offshore sections is represented using the currents only, as the effective velocity vectors of the waves are mostly orientated crosshore (Bagnold, 1963). Syvitski et al (1988) showed that SPM deposition rate can be estimated using a first-order rate law:

$$dI/dt = -\lambda I \qquad (24)$$

where I is the total mass of SPM in the water column per area and λ is the removal rate constant. The remaining SPM after time step Δt can be related to an earlier time step by integrating to:

$$I_{t+\Delta t} = I_t \, e^{-\lambda \Delta t} \qquad (25)$$

The amount of SPM in each gridcell is known from the erosion routine and the plume input. Unfortunately the time step (Δt) we use in our model is on the order of 1 year, which is useless for the removal rate constants. Therefore we use a variable time step, evaluated between each gridcells. The time step is calculated using the current flow velocity and the size of the gridcells, thus releasing the time necessary for the quantity of SPM to move from one to the other. By repeatedly cycling through the entire model area we continue until all SPM matter is removed and deposited. As the model time steps are sufficiently large to reasonably allow all SPM matter to fall out of suspension this is a realistic assumption.

Algorithm implementation

The marine module of the routine is illustrated in Figure 4.3. The marine module starts as soon as the continental module has finished (thus assuming no offshore to

onshore sediment transport will occur). The marine module receives the necessary bathymetric data, initial river plume velocity and sediment added to the system. Subsequently the program follows the algorithms in the same order as described above. First the combined currents/plume routine is run, followed by the wave calculations. Next the erosion due to waves and currents is calculated in each gridcell. Finally the suspended load is iteratively transported and gradually deposited

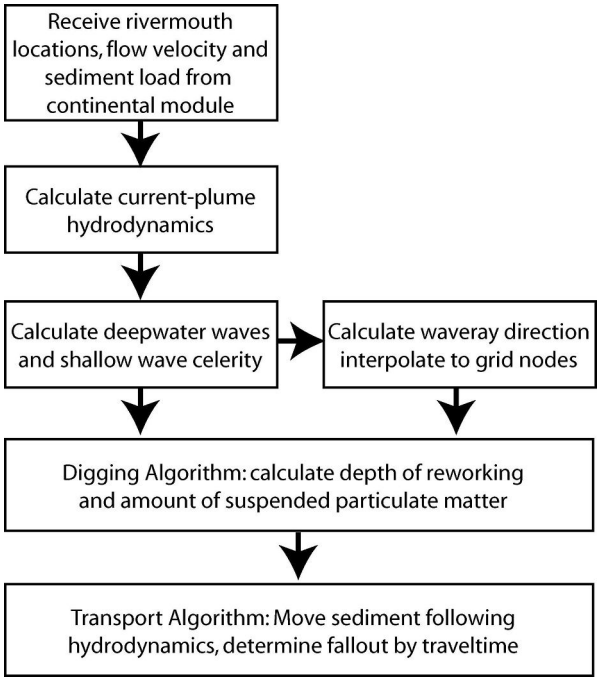

Figure 4.3; Flowchart of the algorithm implementation. Note that each timestep requires new information from the continental module. Storing of stratigraphy and other bookkeeping features are integrated in the overarching model.

Results

The results shown in this section aim to illustrate the capabilities of the marine model in an idealized, synthetic setting and to qualitatively assess the sensitivity to boundary and initial conditions. The first examples show offshore plume deposits under time-invariant forcing. The second set of examples illustrates the interaction between the marine and continental system.

Marine module only

The first example is a purely theoretical exercise that allows the reader to understand the basic working of the marine hydrodynamic and sediment distribution model. The initial bathymetry (Figure 4.4A) is an equilibrium surface for the wave influence. Little or none of the initial surface will be eroded, thus allowing us to focus on the redistribution of the plume deposits. The deepwater waves used in each "storm time step" are the same height (Figure 4.4B in combination with the currents). In this example the plume velocity is fixed to 1 m s^{-1}, the longshore current velocity to 0.2 m

s^{-1}, the deepwater wave height is 3.3 m. To illustrate the resuspension and transport principle we have allowed the plume to deposit fine-grained sediments (grainsize 2 micron) undisturbed during 100 years (Figure 4.4C) at the rate of $1.91*10^9$ kg/year. After this initial deposit, the sediment supply is cut off (e.g., due to a lobe switch on the delta plain) and the wave-current interaction is allowed to rework and transport the deposits. Figure 4.4D and 4.4E show the distribution of the sediments after 1 and 7 storm events respectively.

The initially undisturbed deposits decrease exponentially in height as the distance from the river mouth increases (Figure 4.4C). As the longshore current deflects and turns the plume velocity vectors, the axis of the deposits is dependant on the velocity directions and is also skewed towards the coast. After the first storm event (Figure 4.4D) the deposit axis is stretched somewhat. After 7 storm events (Figure 4.4E) all sediment has moved out of range of the plume velocity vectors. This results in a completely shore-parallel stretched morphology. The depocentre/highest elevation of the resulting sediment body has moved 60 kilometres shore-parallel, within 7 once-a-year storm events. The strong axial-dominated sediment peak is produced by the initial plume depositional mechanism (Figures 4.4C and 4.4D). Yet the continued resuspension events spread the sediment laterally due to the diffusive effect of the waves, resulting in a more uniform crosshore sediment distribution.

Figure 4.5 shows a similar experiment, using the same parameters, except for a very high plume velocity of 2 m s^{-1}. The main change compared to the previous example, is the further offshore spreading of the sediment body by some 5 km's (Figure 4.4B and 4.4C). A secondary effect noticeable (Figure 4.4D) is the loss of sediment beneath the effective wave base or the depth of closure. The depth of the effective wave base is stable in these model runs, as the bathymetry does not vary greatly between time steps and we do not change the deepwater wave height. Thus, as all other factors remain constant, the depth at which the critical shear stress is sufficient to resuspend the deposits is also constant. When sediment is deposited below this bathymetry (here at roughly 12 m depth, at the 55 km mark) it will not be resuspended, and visibly lags. This sediment can be assumed to be deposited permanently.

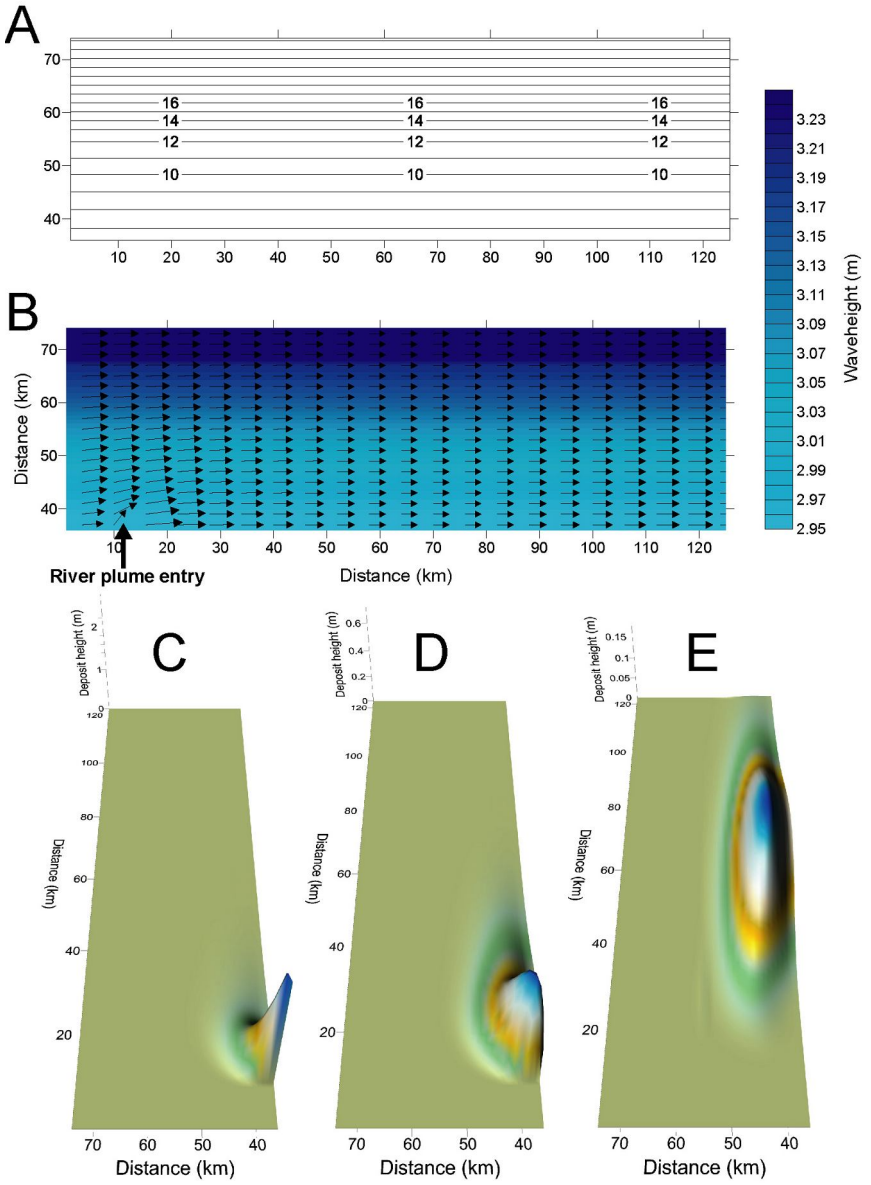

Figure 4.4; Idealized model run. The initial bathymetry (A), the wave height distribution and current flow field (B), The initial deposits (C), and the deposits after 1 (D) and 7 storm events (E) respectively. Note that the vertical scale changes from C to E.

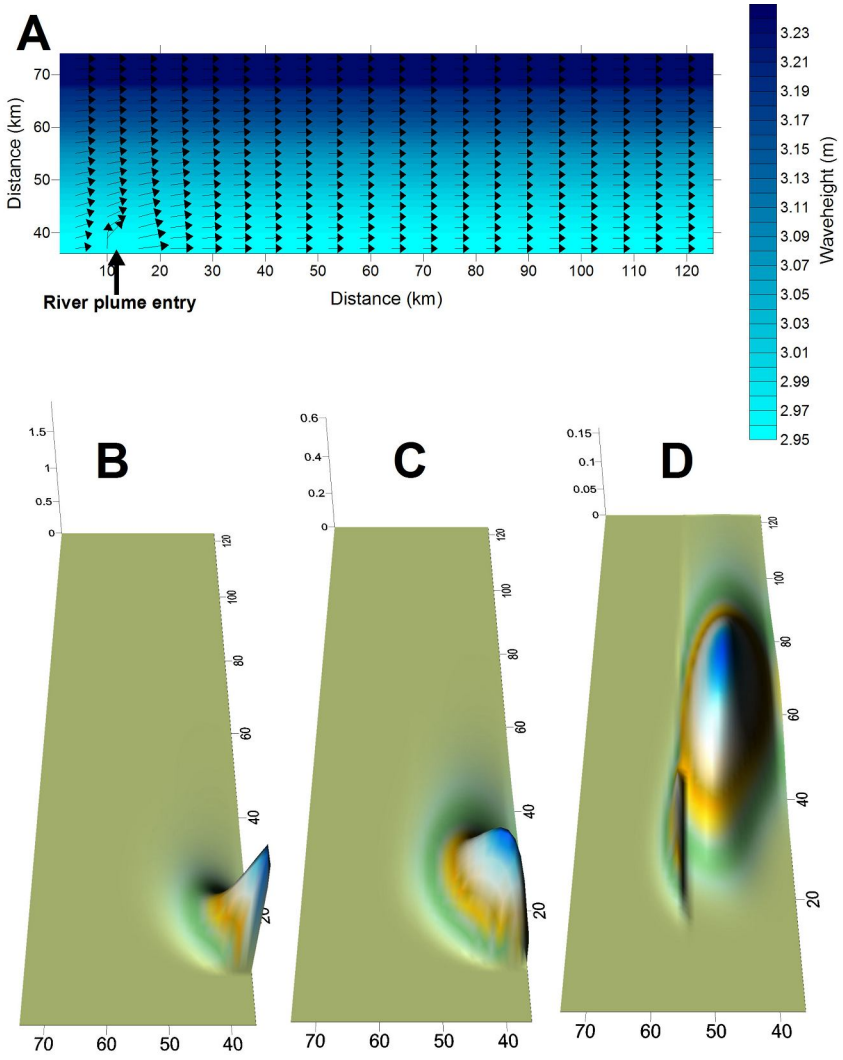

Figure 4.5; Idealized model run with the same parameters as figure 4, barring a plume velocity of 2 m/s. The initial wave height and flow field (A), the initial deposits (B), and the deposits after 1 (D) and 7 storm events (E) respectively. Note that the vertical scale changes from C to E.

Long-term combined continental-marine development

Two runs are presented; both use a steep continental shelf-slope system as initial topography. Liquid and solid discharge are kept constant, liquid at 1500 m^3 s^{-1}.The solid discharge is composed of a clay size fraction (grain diameter $2.*10^{-6}$ m) of $2.*10^9$ kg $year^{-1}$ and a sand fraction (grain diameter $5.*10^{-4}$ m) of $5.*10^8$ kg $year^{-1}$.Sealevel also remains constant, during the 5000 years of runtime (using one year time steps) and a discretization of 1 km.

The first example develops under very high storm wave heights of 7.8 m, in combination with longshore currents of 0.1 m s^{-1}. (Figures 4.6A and 4.7B). The second example is allowed to develop with no wave or longshore current influence. (Figures 4.6B and 4.7A). Both examples show rapid progradation. The wave-dominated delta (Figure 4.6A) is characterized by a steep gradient immediately offshore due to the intense wave action. Excess sediment that moves over gridcell boundaries is removed; therefore we do not see this in the Figures. Figure 4.7B shows a much more gentle delta front and prodelta slope, as this is only influenced by the plume deposition, though several plume deposits are discernable, probably produced during relatively stable river channels or by reoccupation. The side views of the morphological results (Figure 4.7) emphasise this difference. The river-dominated delta shows a very diffuse morphology of several plume deposits overlapping, creating a blanketing prodelta. The wave-dominated delta (Figure 4.7B) shows a sharp drop at the coastline as most of the fine prodelta deposits have been resuspended and transported along the coast.

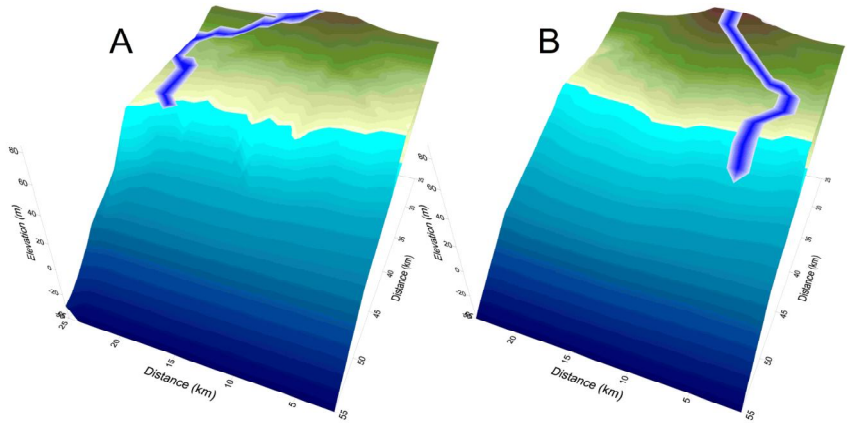

Figure 4.6; Top view of the resulting morphology of delta development after 5000 years under deepwater storm waveheights of 7.8 m, with longshore currents of 0.1 m s^{-1} (A) and no waves or currents (B)

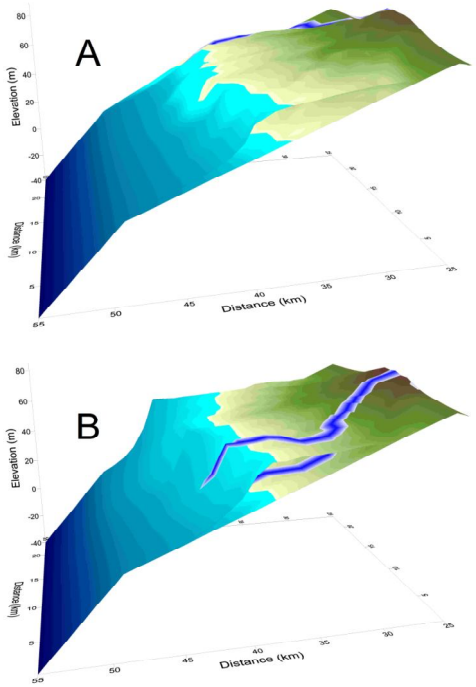

Figure 4.7; Side view of the resulting morphology of delta development after 5000 years under no waves or currents (A) and deepwater storm waveheights of 7.8 m, with longshore currents of 0.1 m s^{-1} (B). The initial topography is plotted below the end morphology.

Discussion and conclusions

The idealized marine plume runs show a clear lengthening and diffusive redistribution of plume deposits. In shallow marine basins, we will therefore expect that the fine-grained sediment will not be deposited permanently. Only one very large (once-in-a-hundred-years) storm is necessary to remove the material and remobilise it until it reaches either a sheltered part of the basin or a very deep part well below the depth of closure. Note that in the "marine only" examples, the storm wave base and therefore the depth of closure is located quite far offshore due to the low angle shelf. Therefore little of the sediment is lost to the depths. In reality, sediment supply will be more continuous than the examples of Figure 4.4 and 4.5. This results in a very elongated mud belt similar to the shore-parallel subaqueous Ganges-Brahmaputra (Michels et al, 1998) and the western Adriatic prodelta (Cattaneo et al, 1998; Nittrouer et al, 2004 etc). These systems are influenced by very different advective hydrodynamic regimes, yet result in very similar patterns of sedimentation. The simple potential flow routine used in this paper can adequately represent these tidal, thermohaline or other currents, thus allowing the modelling of several very different settings.

The steep delta front in the long-term wave-dominated models (Figure 4.6A) seems to form the upper part of the compound-clinoform concept. Due to the strong longshore currents, most fine-grained sediment is moved alongshore, thus making a complete compound clinoform impossible. Most of the sand fraction remains in place (due to the very high removal rate, i.e. it is effectively dumped); this allows the delta front to form the concave-up shape characteristic of wave-dominated coasts.

The fluvial development seems to be influenced quite strongly by the delta front processes. The wave-dominated system shows a much lower angle slope than the river-dominated system. Future experiments are necessary to evaluate the interaction of land and marine processes.

In paleosedimentological reconstructions (i.e. deriving the sediment path) little if any of the climatological and oceanographic history is known. Therefore some calibration of the wave height, or wind strength and frequency is necessary. Yet this can in turn be used to partially validate paleooceanographic and –climatological reconstructions. Therefore the model is eminently useful as a teaching and theoretical tool. Yet when modelling real-world scenarios of the geological past it, as do all dynamic models, requires careful deliberation of the strengths and weaknesses of its predictive capabilities when we wish to formulate firm conclusions.

This modelling effort recreates realistic geomorphological and stratigraphic delta behaviour in river and wave-dominated settings. However, the inherently simplified assumptions in the offshore sediment transport make the model impractical for uses on very short (e.g. yearly) timescales.

Cattaneo et al (2007) propose that the sediment deposited in the bottomset of similar muddy shelf clinoforms may be bounded by bottom currents and other environmental energy. Thus limiting the accommodation space in the bottomset and forcing the sediment to either stay on the foreset or migrate parallel to the shore parallel currents. To better understand these muddy systems future modelling efforts should include bottom currents, Ekman transport and downwelling. This would require a full 3D

approach to the hydrodynamic modelling, making it less suitable to long-term/large scale stratigraphic modelling.
For now the model may be used to study stacking patterns of the muddy subaqueous clinoforms in basinwards and shore parallel directions. Swenson et al (2005) introduced a phase diagram for terrestrially dominated to basin-dominated clinoforms. Their abstracted model shows that an increase in grainsize (amongst others) will result in an expected decrease in subaqueous progradation (i.e. a shorter compound clinoform top set). The model presented in this paper may be used to quantitatively study this gradual shift from Gilbert type to fully wave-dominated deltas and consequently the stratigraphic associations within.

List of Notations

C	Wave phase velocity (m/s)
d	water depth (m)
D	Grain diameter (m)
f_c	Current friction factor
f_{cw}	Combined flow friction factor
f_w	Wave friction factor
H_s	Significant wave height (m)
I	amount of SPM per unit area (kg m^{-2})
F	Fetch length (m)
k	wave number (m^{-1})
L	Wave length (m)
μ	Dynamic viscosity
ϱ	Density of water (kg m^{-3})
ϱ_s	Density of the sediment (kg m^{-3})
ϕ	Velocity potential (m/s)
τ_{cr}	Critical shear stress kg m s^{-2} m^{-2}
T	Wave period (s)
u_1	Mean velocity at 1 m above seabed (m/s)
u_{*c}	Total current shear velocity (m/s)
u_z	Flow velocity (m/s)
U	Wind velocity (m/s)
U_A	Wind stress factor (empirical parameter)
V_x	Velocity component in the x-direction (m/s)
V_y	Velocity component in the y-direction (m/s)
W_s	Settling velocity of a sediment grain (m/s)
z	depth of velocity measurement (m)

Chapter 5

Modelling wave influenced shoreface processes in a basin scale stratigraphic model.

Introduction

Although many coastal processes occur on a higher spatio-temporal resolution than most processes used in basin-filling models, the net effects can be profound. Coastal processes may, under varying circumstances, facilitate erosion or storage of sediments. The coastline forms a buffer zone between the land and sea, which is especially influential in wave-dominated systems. Under strong wave influence sand may be segregated from clays, steep barriers may form next to the low relief shoreface and fine-grained particles are funnelled to the offshore below the deepest wave base. However, one of the most important effects of wave-influenced systems over several sealevel cycles is not the capability to create concave-up cross-shelf profiles and associated graded grainsize fractions. During transgressions and forced regressions, waves erode and concomitantly flatten the morphology and ultimately remove a considerable part of the stratigraphic record. The rising sea level moves the high-energy shallow marine area over the shelf, resulting in a transgressive erosive or ravinement surface. Thus a crucial part in modelling wave influence on a basin scale is the capability to move the shoreline and associated wave base over the entire shelf (Fagherazzi & Overeem, 2007).

Previous modelling efforts of long-term shoreface evolution have mostly focused on the coastal profile (e.g. Niedoroda et al, 2003; Storms, 2003; Stolper et al, 2005). This approach certainly has its value, however on geological time scales the external forcing and consequent interaction with the surrounding sedimentary and possibly anthropogenic environments necessitates a dynamic linkage. Conversely, sedimentary processes in large-scale basin filling models are usually (necessarily) simplified, representing marine processes as diffusion (e.g. Granjeon & Joseph, 1999; Clevis et al., 2003, Meijer, 2002). Two notable exceptions are the Sedsim-Wave model (Tetzlaff, 2004; Martinez, 1987; Martinez & Harbaugh, 1993) and Sedflux 2.0 (Hutton et al, 2008). The former is a hydrodynamically correct representation of marine processes; it focuses on relatively small-scale features. The latter is one of the most advanced stratigraphic models currently used, and incorporates a highly abstracted version of wave induced sediment transport.

The coast forms an important interface in large-scale sedimentary models. Sands delivered by the river to the sea are reworked and –deposited as barriers along the coast, which in turn block newly created river channels from entering the marine basin. Therefore it is of utmost importance that these processes are included in our model. For now our focus lies on the influence of waves under mean and storm

conditions. We present a dynamical geomorphological and stratigraphic model, which allows direct interaction between fluvial environments, the shoreface and the open marine environment. The Dalman & Weltje (2008) model (Chapter 2, this thesis) was used for the fluvial environment. Extensions tot this model include; river plume deposition, wave resuspension and ocean currents (Chapter 3, this thesis). This paper aims to describe the theoretical and practical inner workings of wave influenced shoreface processes in a basin filling stratigraphic model. We have included crosshore sediment transport, littoral drift and coastal erosion and active progradation. Together this allows us to mimic the long-term effects of wave climate on delta and shelf development. The model cannot be described as a fully process-based in the sense that we cannot and do not wish to calculate the hydrodynamics using the Navier-Stokes equations or a simplification thereof. Yet we have attempted to base our hydro- and sediment transport dynamics on first principles as much as possible. Thus our model may be considered a hybrid behaviour orientated/process based development.

Model Description

The model described in the chapter is a modular "add-on" to the SimClast model (Dalman & Weltje, 2008/Chapter 2, 3 and 4), yet may be run and seen as a distinct and separate coastal model. The hydrodynamic part of the module is closely linked to the open marine module, but will be described when appropriate.
The coastal module is characterized by two modes of sediment transport; Crosshore sediment transport, which occurs anywhere above the wave base and may be suspended or bedload transport. Additionally longshore transport moves bedload sediment along the coast, mainly in the surf zone. The algorithm flowchart is provided in Figure 5.1

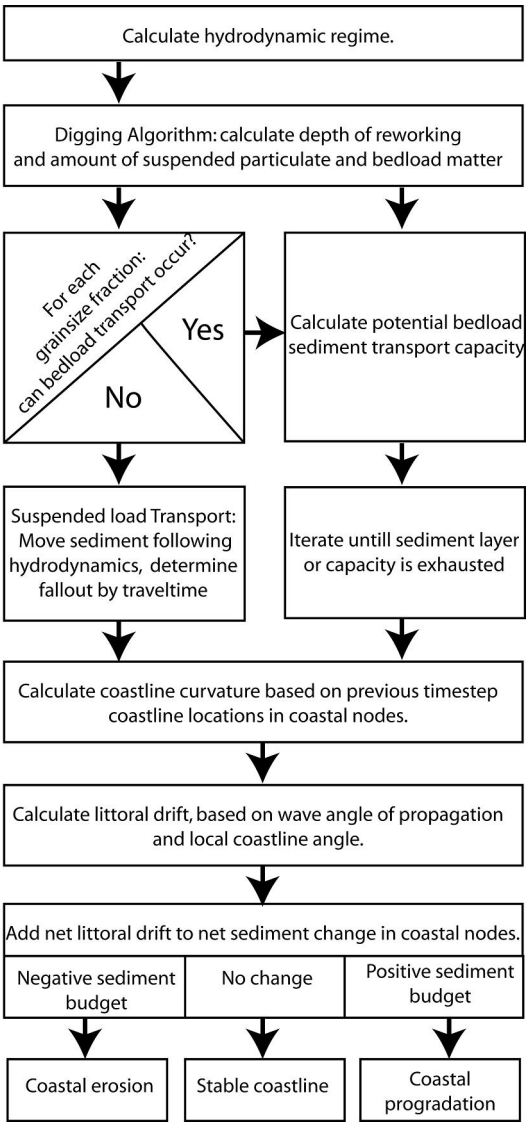

Figure 5.1; Flowchart of the marine sediment transport and accounting scheme.

Oceanic currents
The hydrodynamic flow of currents and plumes is modelled using one integrated steady-state potential flow routine. Though this technique ignores fluid viscosity, irrotational flow, compressibility and smaller scale perturbations in the hydrodynamic movement, the resultant water movement is robust, speedy and representative for geological time scales. The integration of the river plumes and the longshore currents in one hydrodynamic algorithm allows us to calculate the deposition from the plume and the longshore transport of resuspended shelf deposits. Consequently the integrated routine is not slowed by additional river plumes entering the marine domain.

Waves

Event based modelling
Crosshore profile evolution of wave-dominated coastal systems and the resulting stratigraphic record is dominated by high energy

– low frequency events (Storms, 2003; Stive & de Vriend, 1995) yet littoral drift is dominantly forced by long-term fair-weather waves. Storms (2003) developed an event based stratigraphic model that uses variable time steps to simulate individual storm events and the intermediate periods of fair weather. A similar approach is necessary to reproduce the punctuated, wave-induced sedimentary processes. As our model, presented here, is based on a linking several interacting sedimentary environments, each with their own temporal constraints, we cannot incorporate variable time steps. Accordingly our model simulates two discrete wave events per year. One short duration, high magnitude storm event that generates most crosshore sediment transport and one fair weather event. Both events are modelled as time-averaged processes, yet the inclusion of the high-frequency event allows a more realistic approach. If climatic conditions produce multiple large storms per time step, more events can be added as necessary.

The time-averaged, fair-weather wave climate is especially important for longshore sediment transport. As littoral drift is influenced much more by the high frequency, low-magnitude fair weather waves because this transport occurs in shallow areas. In a 3D modelling environment longshore transport may block river channels or provide sediment to starved areas and removing it from coastline protrusions. Thus resulting in an averaging of the coastline, and eventually a smoother stratigraphic record. Yet the small effect of fair weather waves on the deeper crosshore sediment transport allows us to minimize the extra computation necessary. Therefore only the littoral drift is calculated for the fair weather conditions.

Stochastic Storm generation

Wave influenced coastlines cannot be modelled using one season, or even several seasonal measurements. The total effect is a result of the aggregate of many different wave climates working on the system. To mimic this inherently stochastic feature we model one storm event and its associated significant wave height per time step. The significant wave height is randomly extracted from a Gaussian distribution of effective wave heights (Figure 5.2). This results in only very few large storms (i.e. the most influential ones), and many meso-scale storms. Thus approximating the low frequency of the high magnitude storms occurring in nature.

Storm duration and magnitude is very important for the sediment transport, as it determines the wave energy and consequently the ability to erode and transport sediments. Figure 5.2 illustrates the distribution of storm heights for a typical example. User data for the wave height may be used if this is available.

The direction of wind and associated wave advance are assumed constant for both storm and fair-weather events for the

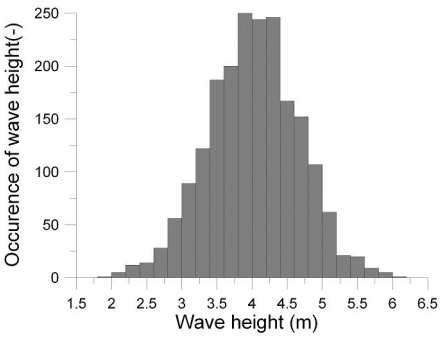

Figure 5.2; Distribution of the significant storm wave height over a 2000-year interval.

examples in this paper. Chapter 4 describes the routines used to calculate wave height from wind direction and velocity and fetch when known. This allows us to represent changes in wave climate due to climatic variations (wind direction and/or magnitude) or changes in sealevel (changes in fetch).

Deepwater waves

For purposes of sediment entrainment and determining the active layer, linear Airy Wave theory is an acceptable approximation (Komar, 1998). Wave height is calculated from the available fetch and wind velocity or provided by the user (see normal distribution of storm wave heights above). The wavelength (L) and phase velocity (C) are defined as:

$$C = \frac{gT}{2\pi}\tanh\left(\frac{2\pi h}{L}\right) \quad L = \frac{gT^2}{2\pi}\tanh\left(\frac{2\pi h}{L}\right) \qquad (1\ \&\ 2)$$

Where T (s) is the wave period and h (m) is the water depth. If the water depth is greater than half the wavelength, the phase velocity C_∞ (m/s) and wavelength L_∞ (m) in deep water approach:

$$C_\infty \approx \frac{gT}{2\pi} \qquad L_\infty \approx \frac{gT^2}{2\pi} \qquad (3\ \&\ 4)$$

Nearshore waves

As soon as waves enter depths smaller than one half their wavelength, traction slows the waves and deforms the symmetrical waves to shorter, but higher peaks and longer, shallower troughs. This wave asymmetry has profound effect on effective currents, resulting in a landwards flow at the bottom and top of the water column and a seaward flow in the middle. Moreover the onshore-directed bed shear stress is greater than the offshore directed stress, albeit of shorter duration (see the crosshore bedload sediment transport paragraph below). To effectively approximate this behaviour we use second order Stokes equations to calculate the near bed horizontal orbital velocity for the entire wave phase:

$$u = \frac{\pi H}{T}\frac{\cosh\left(k\left(z+h\right)\right)}{\sinh\left(kh\right)}\cos\left(kx+\sigma t\right)+\frac{3}{4}\left(\frac{\pi H}{L}\right)^2 C\frac{\cosh\left(2k\left(z+h\right)\right)}{\left(\sinh\left(kh\right)\right)^4}\cos\left(2\left(kx-\sigma t\right)\right)$$

(5)

Were *u* is the horizontal orbital velocity (m s^{-1}), H (m) is the wave height, k is the wave number ($2\pi/L$), σ ($2\pi/T$) is the radian frequency and t (s) is the current time. z is the current depth (m) at which the orbital velocity is to be calculated, for the purpose of

the velocity at the sediment bed we use z=-h, where z=0 at the average water depth. For any given water depth and wave period or length there is an upper limit to the height of the Stokes wave beyond which it becomes unstable and breaks. Our interest lies mainly in waves in intermediate to shallow water depths, were Miche (1944) determined the limiting steepness to be:

$$\left(\frac{H}{L}\right)_{Max} = 0.142 \tanh\left(kh\right) \qquad (6)$$

All calculated waves fall within this limit, which validates the use of Stokes wave theory for the modelling of nearshore waves.
The model does not explicitly represent broken waves, as this is far below the resolution needed for basin scale processes. Any smaller scale features are assumed to be negligible.

Coastal location "a string of nodes"

A pressing challenge in representing coastlines in a model with highly dynamic behaviour is the correct identification of the exact coastline location. It is not sufficient to map the boundary between land and sea, as the discretization is too inaccurate. We need to determine local curvature in order to accurately determine the impact of wave energy. The model has been developed to allow a continuous line of coastal cells to interface the marine and continental domains. These coastal cells not only form a "buffer zone", but also communicate directly to allow longshore sediment transport (see below). Each coastal node locally allows progradation and retrogradation, this in contrast to the other sedimentary environments where sediment may accumulate or erode only vertically.

Finding the coastline
Coastal cells are initially identified based on a continental cell that borders a marine cell. Additionally, we need the relationships between the coastal cells to allow sediment to travel longshore. A search routine starts at one edge of the model domain and follows and subsequently sorts the coastline. This creates a string of coastal nodes, which allow the direct neighbours to communicate. Eventually, this allows littoral sediment to be transported along the entire coastline. In the following time steps the coastline location is updated, but relationships between the nodes are assumed stable.

Intracellular coastal location
To determine the coastal curvature with any accuracy we cannot rely totally on the coarse discretization used in our set-up. Therefore the model uses intracellular locations of the current coastline. Niedoroda et al (2003) proposed a similar set-up in

the dedicated coastal model, CST. Notably, we allow progradation and retrogradation at the coastline while open marine and continental cells can only aggrade vertically.
To do this we calculate the current location by allowing horizontal in addition to vertical erosion and deposition. The changes in subgrid model processes are illustrated in Figure 5.3. Note that three variables must be retained for each coastline.

- The coastal depth, which determines the wave height and accommodation space during progradation.
- The cliff height, a pseudo cliff is defined which represents the amount of sediment that must be eroded to allow the coastline to backstep to a landward cell.
- The coastal width, which is the fraction of the cell that is marine. The rest of the fraction (i.e. 1-coastal width) represents the gridcell area covered by land.

As we have calculated the net sediment flux, we can define the rate of progradation. By determining the accommodation space using the coastal width and the coastal depth and comparing this with the actual sediment load. Correspondingly shoreward erosion is calculated by comparing the cliff volume, derived from the coastal width and the cliff height, to the amount of "negative sediment flux" or erosive power.

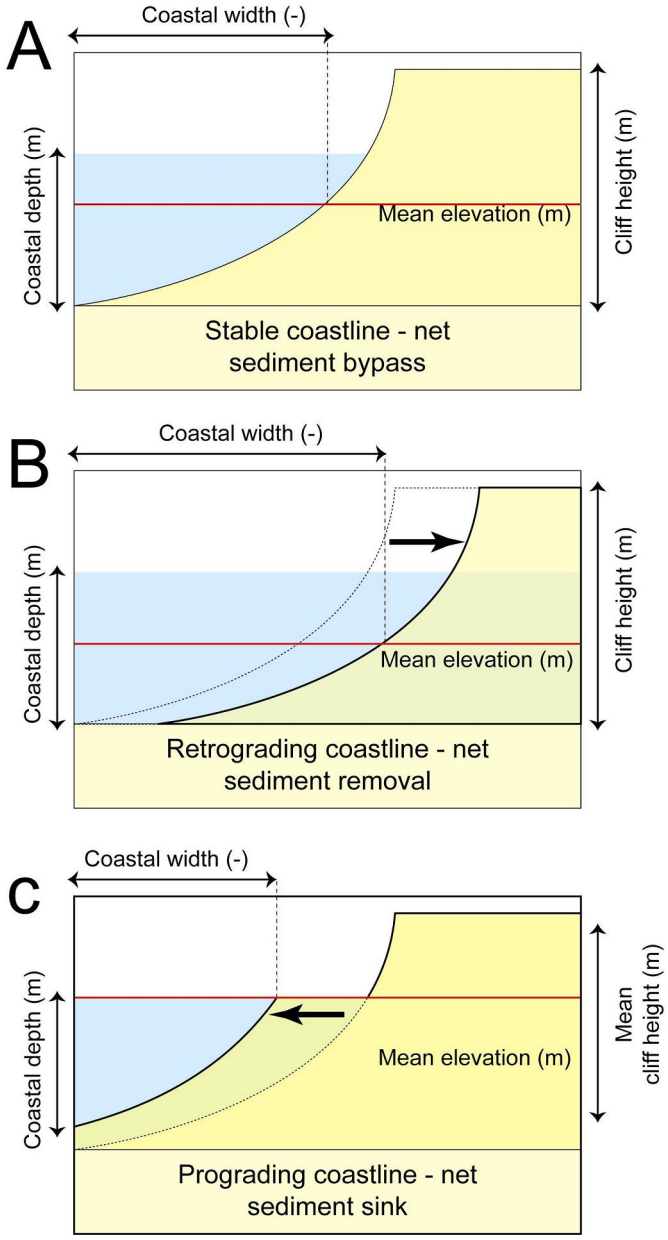

Figure 5.3; Principles of intracellular coastal movement for; (A) a stable coastline, (B) a retrograding coastline and (C) a prograding coastline.

Determining coastal curvature

Longshore sediment transport is very sensitive to the local direction of wave propagation. When using orthogonal grid cells we limit the coastal angles to multiples of 45°. This would not allow sufficiently accurate wave energy calculations; therefore

we need to use the intracellular locations. These locations are fed into a cubic spline routine (modified after Press et al, 1993; NUMERICAL RECIPES). The spline allows us to accurately determine the local angle of the coastline.

Crosshore transport

The two most important planes in the wave reworking routine are the storm wave base and the fair weather wave base. Though care must be taken in using this description of wave base, as this surface varies continuously due to changes in storm magnitude and it also different for each grainsize. Coarser grains will have a shallower wave base than finer grains, as they require a higher orbital velocity to become mobilized. Nonetheless, some generalizations may be obtained from the wave base principle.
Areas with bathymetry below the deepest storm wave base are a sink for any sediment entering it. Unconsolidated sediments between the mean and the storm wave base are only mobilized during the major storm events, resulting in the longshore and offshore drift of the suspended material and onshore migration of the coarse bedload material. Sediments above the mean wave base may be transported towards the surf zone during fair weather periods, but may be transported offshore during violent storms.
Though we use a depth-averaged approach to the hydrodynamics, we still need to parameterise the direction of sediment onshore vs. offshore sediment transport. Two mechanisms of sediment transport are modelled. Suspended load transport, which is the grain size fraction that cannot fall out of suspension under the wave and bed slope conditions. This fraction will mostly be transported offshore or alongshore if a sediment trap is present (e.g. a sheltered cove). The coarser fraction moves as bedload. Under shoaling waves this will usually result in a net shoreward transport due to the wave asymmetry. Thus the crosshore module replicates the expected behaviour of coarser grains moving nearshore and finer grains transported offshore.
Though we use the term crosshore transport throughout this paper, the sediment transport modelled is not necessarily orientated perpendicular to the coastline. The sediment is always transported parallel to the direction of wave propagation, as expected. As a result, the so-called crosshore transport may have a strong longshore transport component. The term crosshore transport describes the open marine sediment transport. The longshore transport describes the littoral/surf zone processes.

Active layer
Large storm waves have the capability to move very large quantities of sediment. Yet the water depth directly influences the wave height and related energy, therefore we cannot allow waves to dig indefinitely. This would require a continuous recalculation of the entire wave field. Instead we opt for an approach that allows capacity limited sediment transport. After the wave field has been calculated, the wave parameters are used to determine the depth of sediment mobilization (Figure 5.4A). The algorithm uses a bracketing and bisection mechanism to find the stable equilibrium surface,

where the bottom shear stress (τ_b) equals the critical shear stress. The critical shear stress (τ_{cr}) after Bagnold (1963) is defined as:

$$\tau_{cr} = 0.64\ \varrho\ W_s^2 \qquad (7)$$

Were ϱ is the sediment density (kg m) and W_s is the fall velocity (m s). We need to determine the bottom shear stress at the seabed. The maximum near bed, wave-induced orbital velocity (u_b) is given:

$$u_b = \frac{\pi H_s}{T \sinh\left[k(d - 0.5H_s)\right]} \qquad (8)$$

The bottom shear stress is calculated following Li & Amos (2001):

$$\tau_b = 0.5\ \varrho\ f_w\ u_b^2 \qquad (9)$$

Where f_w is the wave friction factor calculated following Nielsen (1979). The released finer fractions are suspended in the water column; the coarser fractions remain in the cell as the active bedload layer (Figure 5.4B). The suspended load materials may be transported by ocean currents or wave induced currents. The active bedload layer represents the maximum amount of sediment that can be moved through bedload processes in that cell. Even if no net sediment transport occurs subsequently, the newly created layer is allocated to the stratigraphic record (Figure 5.4C).

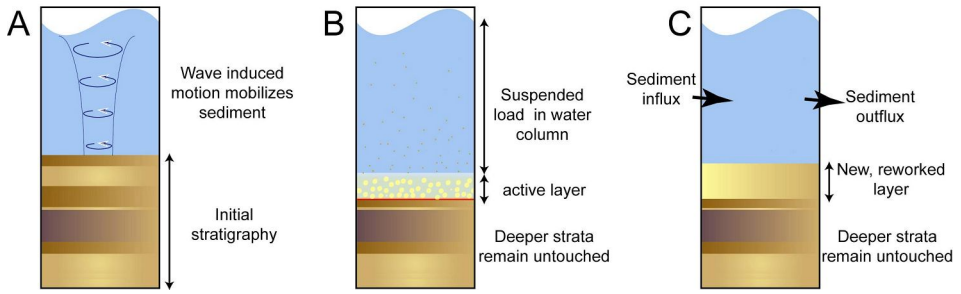

Figure 5.4; The active layer concept as used in the coastal module. The near bed horizontal orbital velocity is used to determine the depth to which the "current" wave can remobilise the sediment (A). The suspended sediment is distributed in the water column and can be transported by oceanic or longshore currents if present. The bedload active layer is the part of the volume of substratum, which can be moved by wave action (B). Finally after all sediment transport operations have been performed, the net sediment flux is used to create a new layer (C) that represents the zone of wave reworking.

Bedload sediment transport

Nearshore sediment transport equations are notoriously difficult to test, due to the complexity of the processes. In reality, waves are inherently irregular and currents and tides affect the area. In addition waves reflect and dynamically interact with the bathymetry. Most formulations are empirical in nature, being based on modifications of stream equations. We wish to realistically represent sediment motion by the asymmetric wave action; therefore we must use an instantaneous formulation that allows the sediment transport quantities to be associated with the instantaneous orbital velocities in both the onshore and offshore directions. The instantaneous sediment transport (q_b (m^2s^{-1})) is represented by the Bailard-Bagnold (Bailard, 1981; Bagnold, 1963) expression:

$$q_b = \frac{0.5\rho f_w e_b}{(\rho_s - \rho) g w_s}\left[|u_b|^3 u_b - \frac{\tan\beta}{\tan\gamma}|u_b|^3 \right] \qquad (10)$$

Where ρ (kg m^{-3}) is the water density, ρ_s (kg m^{-3}) the sediment density, f_w (-) is the friction factor based on particle diameter, e_b (-) is the efficiency factor for bedload transport, w_s (m s^{-1}) is the fall velocity of the bed grain size, β (°) is the bottom slope and γ (°) is the dynamic friction angle ($\tan\gamma = 0.6$).

The various versions of Bagnold's (1963) sediment transport relationships are the only relationships to explicitly use the beach slope β. The incorporation of the effect of gravity is important to determine the crosshore slope. Without it onshore transport would be much easier than offshore transport. As equation (10) provides only instantaneous sediment transport quantities, the net bedload sediment transport capacity under one full wave cycle is calculated by integration. Under intermediate to shallow conditions, the Stokes wave asymmetry (Figure 5.5) results in a net shoreward motion of sediment. Note the large onshore sediment transport compared to the small offshore sediment transport (effectively the model mimics the forward and backward motions experienced under shallow water waves). In order to upscale the total wave induced transport the net sediment transport capacity under one wave cycle is linearly increased to mimic the entire duration of the event.

After all sediment transport capacities between each node have been calculated, the sediment transport can start. Subsequently the sediment from the active layer is moved through the model according to the capacity calculated previously. This process continues until the active layer is exhausted (i.e. supply-limited) or the sediment transport capacity is reduced to zero (i.e. capacity-limited).

Each grain size fraction and its associated sediment transport capacities are evaluated separately. Though this procedure is not quite representative of the continuous "block of sediment" principle (Tetzlaff & Harbaugh, 1989; Martinez & Harbaugh, 1993), this does allow grain size differentiation to occur. For instance under a relatively weak wave climate, fine sand may be able to move shoreward but coarser grains will not be able to move at all, which results in a lag of coarser deposits.

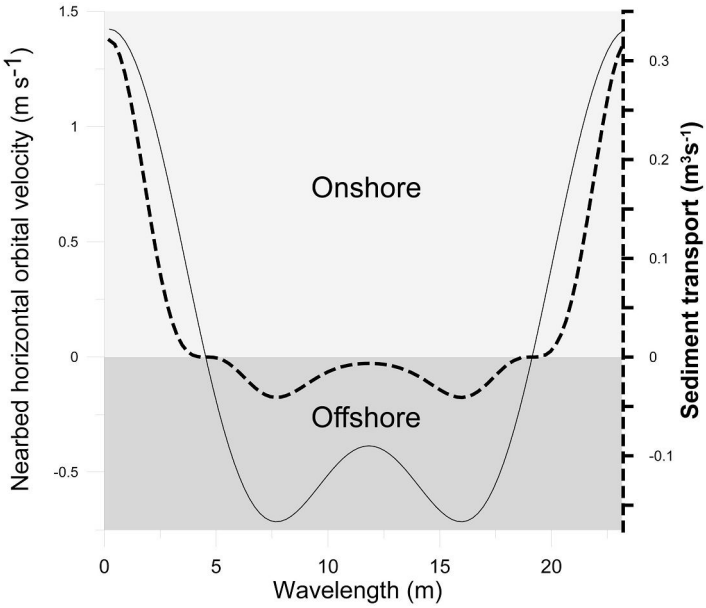

Figure 5.5; The near bed horizontal orbital velocity and associated sediment transport under one wave cycle. Under a water depth of 2.5 m and mean wave height of 1.05 m, grain size is 0.5 mm.

Suspended sediment transport

Sediment transport of the finer fraction distributed throughout the water column is considerably more complex under shoaling waves as the residual currents are quite complex. Under Stokes wave theory a net shoreward flow is present near the water surface and at the bottom. Longuet-Higgins (1953) observed that this shoreward flow is balanced by a return flow in the opposite direction at mid-depths. Therefore the direction of suspended particulate matter is dependent on the location in the water column. To model this process accurately would require a full 3D approach, which would be extremely computationally intensive. Bagnold (1963) proposed the principle of autosuspension where sediments with a fall velocity (W_s) below a certain value cannot fall out of suspension in waves of a certain magnitude conditioned to beach slope (S (-)):

$$W_s \leq \frac{\pi HS}{T} \qquad (11)$$

The modelling approach assumes that the grainsize fraction that is 'autosuspended' will not fall from suspension during the event. This entails that the net sediment transport for the autosuspended fraction is offshore, as deposition further onshore is usually not likely. Obviously tidal basins and other sheltered coastal areas can form mud traps. This is outside the scope of this model, yet does form an interesting project for future research using the subgrid parameterisation principle (analogous to

Chapter 2/Dalman & Weltje, 2008). Concluding, the autosuspended grainsize fractions move only offshore (180 degrees to the direction of wave propagation.), until the wave-induced orbital velocities decrease sufficiently to allow fallout.
Further offshore, suspended sediment may be transported by basin-scale currents using the integrated steady-state potential flow routine (See Chapter 4, this thesis). Deposition is governed by the removal rate principle introduced by Syvitski et al (1988). All suspended particulate matter is assumed to fall out of suspension or is transported out of the model domain during each event.

Littoral sediment transport
As described in the coastal location paragraphs, the coastline is modelled as a string of interconnected nodes. These nodes are located in a transitional gridcell, which is part marine and part continental. Most littoral sediment transport will occur shoreward of the breaker zone, so we assume it is located only in the coastal nodes. This assumption does somewhat limit the lower size of the gridcells as the entire surf zone must be contained within one gridcell.

Direction of transport along the string of nodes
Firstly, we need to determine the direction of transport between each gridcell based on wave direction and coastline orientation. As we only use one signification wave height and associated direction for each event, the direction of transport is always towards either one of two possible neighbours along the coastline. The direction of net transport is always oriented in the direction of the shore parallel component of the wave power vector (Figure 5.6). This relationship of transport (influx or outflux) is calculated between each neigbourpair. Subsequently the net sources and sink cells are

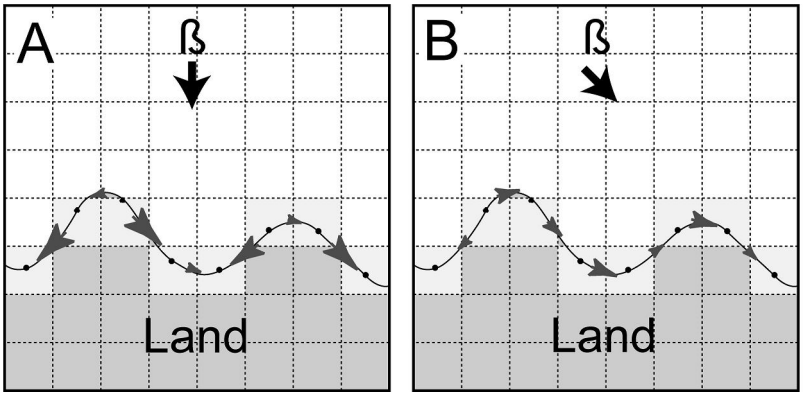

Figure 5.6; Coastal curvature as derived from the coastal locations (black dots) for a wave angle of propagation orthogonal to the mean coastline (A) and orientated 45 ° (B). The coastal cells are marked in light grey, the coastline locations as black dots. The direction and qualitative magnitude of longshore transport between coastal nodes is indicated by the direction and size of the arrows, respectively.

calculated. By using these as start and end points the potential path of littoral sediment transport can be determined.

Amount of sediment transported along the coast
The littoral sediment transport due to obliquely breaking waves is a function of wave energy and angle. Cell circulation may severely complicate this matter (Komar, 1998), but this is presumed to be below the scale and scope of this basin-scale modelling exercise. The wave energy (E) can be calculated by evaluating it in deepwater after Komar (1998):

$$E = \frac{1}{8}\rho g H^2 \qquad (12)$$

Without energy losses the energy flux in the shoaling waves remain equal to its value in deep water. The wave energy allows the calculation of the immersed weight sediment transport rate (I) at each coastal node following the Inman & Bagnold (1963) equations:

$$I = K(ECn)\sin\alpha\cos\alpha \qquad (13)$$

Where n is:

$$n = \frac{1}{2}\left[1 + \frac{2kh}{\sinh(2kh)}\right] \qquad (14)$$

Where the proportionality coefficient K is taken to be 0.70, which results in a good overall fit to measurements (Komar, 1998). The littoral drift is calculated for each coastal node. Next the sediment is transported in the coastline along the nodes from the sources towards the sinks.
Note that two sediment transport processes may operate on the coastal nodes, the crosshore sediment transport routine and this littoral sediment transport. Therefore a littoral sink or source does not necessarily mean that this gridcell is aggrading or eroding, respectively. While littoral drift may add sediment, the crosshore transport may remove it and vice versa.
The resulting total sediment fluxes are evaluated and shoreline retreat or progradation is calculated following the coastal location method described above.

Results

The results shown in this section aim to illustrate the capabilities of the shoreface module in an idealized, synthetic setting and to qualitatively assess the sensitivity to boundary and initial conditions. Several examples of relatively short-term shoreface development are shown. All model runs use a constantly sloping low angle shelf as initial surface with two grain size fractions (medium sand and clay size). Figures 5.7 and 5.8 show a strongly wave influenced delta and shelf morphology. The wave-influenced delta (Figure 5.7) shows the aggradation along the channel belts, the net erosion of the initially constant slope just offshore and deposition further offshore below the specific grain size wave base. Barriers have developed along most of the coastline, though the height varies somewhat depending on sediment supply, both from the river and the reworked substrate. The mean crosshore sedimentary history for the first 1500 years of this system is illustrated in Figure 5.9. Note that a large portion of the fine-grained fraction is removed from the subsurface and transported offshore. The total deposition shows two depocentres mainly the nearshore barrier buffer zone, consisting mostly of sandy material and the lower shoreface below the deepest storm wave base were most fines are deposited.
Without any river action the shelf develops into a fully wave dominated coastline (Figure 5.8). Note the net erosion of the initially constant slope just offshore. Barriers have developed along most of the coastline, as enough sandy material was present in the substrate. Little change occurs after several hundred years and a state of equilibrium is achieved relatively rapidly after the largest of storms have reworked the sediments. The mean crosshore development (Figure 5.10) shows a similar grainsize

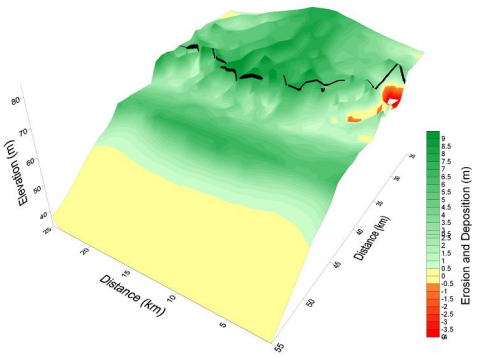

Figure 5.7: Example morphology and sedimentary/erosional history of a passive margin delta setting. The coastline is marked in blue. Wave angle of incidence is held constant orthogonal to the initial coastline. The storm wave height follows a normal distribution from 3-8 m, with the median at 5,5 m after 4000 years.

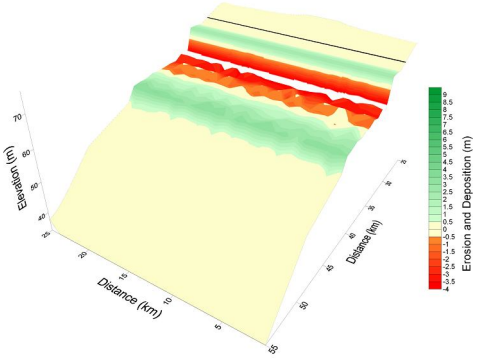

Figure 5.8: Example morphology and sedimentational/erosional history of a passive margin shelf setting. The coastline is marked in black. Wave angle of incidence is held constant orthogonal to the initial coastline. The storm wave height follows a normal distribution from 3-8 m, with the median at 5,5 m after 4000 years.

distribution as compared to the delta development (Figure 5.9), albeit without the progradation and associated extra sediment input and shift in coastline.
In order to illustrate the strong influence of wave regime on the system an example with relatively weak storm waves (median height 4 m) is shown (Figure 5.11 & 5.12). Based on the morphological development (Figure 5.12) one might conclude that weaker waves merely result in a shallower shoreface profile. The mean crosshore development (Figure 5.11) clearly illustrates the lack of wave energy. Wave reworking has removed the fine-grained deposits in the shallower parts and replaced them with sandy deposits. Yet below the wave base river plume deposition has continued relatively undisturbed. A small chain of barriers and a concave-up surface has developed (Figure 5.12).

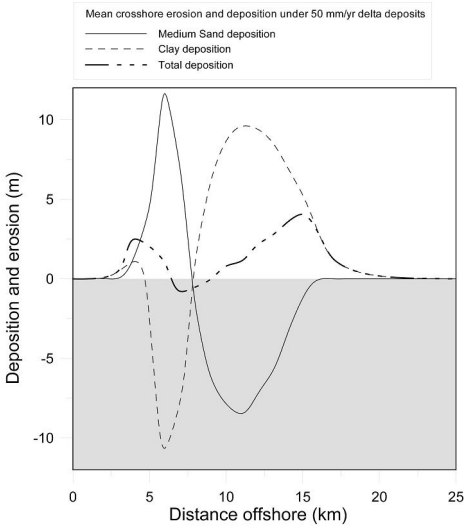

Figure 5.9; The mean crosshore sedimentation and erosion for all fractions combined, the clay fraction and the medium sand fraction. After 1500 years, under river input. Median storm wave height 6m.

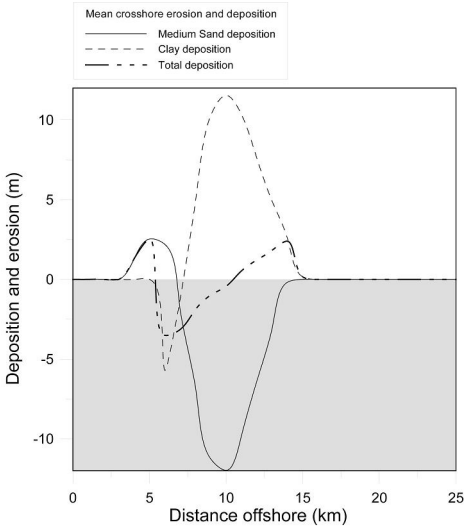

Figure 5.10; The mean crosshore sedimentation and erosion for all fractions combined, the clay fraction and the medium sand fraction. After 1500 years, no river input. Median storm wave height 6m.

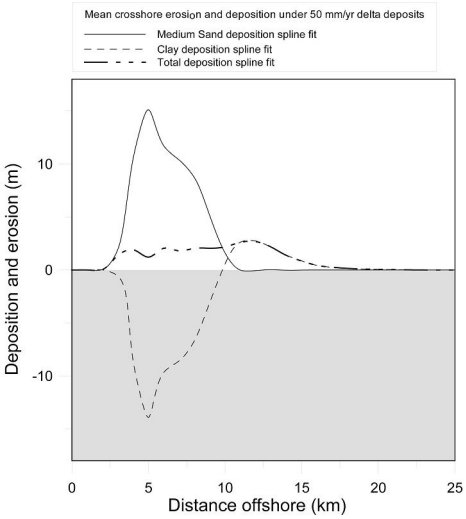

Figure 5.11; The mean crosshore sedimentation and erosion for all fractions combined, the clay fraction and the medium sand fraction. After 1500 years, river input. Median storm wave height 4 m.

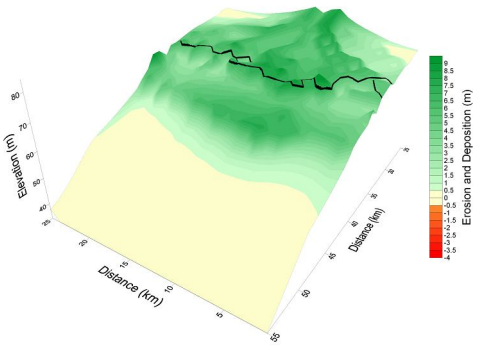

Figure 5.12; Example morphology and sedimentational/erosional history of a passive margin delta setting after 4000 year of development. The coastline is marked in blue. Wave angle of incidence is held constant orthogonal to the initial coastline. The storm wave height follows a normal distribution from 1-6 m, with the median at 4 m.

Discussion

This model creates quite realistic shoreface profiles. Under strong river and wave influence, the delta develops into a wide lobate delta with a smooth shoreline. Under lower wave regimes the delta shows (Figure 5.12) distinct lobes, which have not (yet) merged completely. Shelf developments are obviously less dynamic where no rivers are present to provide sediment. Though barriers can develop as long as the substrate provides enough coarse material. The two-dimensional, depth-averaged approach provides an obvious advantage over one-dimensional equilibrium-profile models that do not account for lateral or oblique sediment transport. The concave-up cross-shelf profile seems to stem from a distribution of grainsizes, which allow the net hydrodynamic forces to gain equilibrium. The model results illustrated in Figures 5.7 and 5.12 show a concave-up profile, yet the curvature is rather steep. This is due to only 2 grainsize classes being present, a 3rd intermediate class will "fill up" the profile and create a smoother profile.

The suspended load transport in the nearshore area is necessarily simplified, and may overestimate the offshore transport of the finer fractions somewhat. This may cause problems in filling mudtraps, such as tidal basins and other sheltered coastal areas. Refining this routine by calculating the net offshore transport might be achieved by parameterizing the sediment distribution in the water column and the net hydrodynamics due to the wave asymmetry. By integrating over the entire water

column, a net sediment transport direction and quantity can be achieved. Depending on the distribution of the suspended load, a net onshore sediment transport is possible.

Obviously some form of quantitative calibration is necessary. In any modelling exercise perhaps the most important is the estimation of the correct parameters. Future work will focus on quantifying the relationship of wave regime and river input in total volume and grainsize fraction. Ultimately we will be able to compare these results to recent and ancient systems.

A major point of discussion in long-term modelling is the morphological feedback loop. As bathymetry influences wave height (amongst others) and wave height in turn directly influences sediment transport, a change in bathymetry will in effect result in a change in sediment transport capacity during the event in question. Some small pilot tests have determined that even under large storm events the change in bed height elevation is less than 10% of the bathymetry. This should provide negligible influence on the sediment transport capacity, much smaller than the inherent variation in sediment transport equations.

Storms (2003) assumed that a net onshore transport of sediment occurs during fair weather periods, alternating with net offshore transport during storm conditions. This may apply for relatively small grainsizes, yet the large grainsizes will be preferentially moved shorewards during storms. As long as the grainsize fraction in question is transported as bedload, offshore transport is unlikely under Stokes waves as the net current at the bed is oriented shorewards.

Important applications of the model will be conducting a sensitivity analysis of the coastline change. Especially its relationship with the wave and river input forcing, as there exists a careful balance between waves removing sediment from the shoreface and rivers. By determining the conditions under which no shoreline movement occurs we can create a quantitative phase diagram of shelf response to external forcing.

Chapter 6

Autogenic controls on fluvio-deltaic architecture; Lessons from numerical modelling

Abstract

This paper uses a basin-scale 3D model, with a parameterization of fluvio-deltaic drainage network evolution and alluvial architecture, to study the relation between alluvial sedimentation and marine deltaic deposition. Avulsions take place once channel belts have reached a sufficient elevation above the floodplain. The avulsions force partial abandonment of the delta front and initiate new areas of progradation, resulting in new delta lobes. Conversely, progradation of the delta front lengthens the fluvial profile and induces aggradation upstream. The depth of the offshore bathymetry onto which the delta progrades greatly influences the alluvial aggradation. As the delta progrades into deeper water, the progradation rate decreases because more sediment is needed. This results in lower alluvial aggradation and lower avulsion rates. In a relatively low-angle coastal setting delta area increases both seawards and landwards, which causes avulsion sites to retrograde. This produces headward-shifting sequence of avulsion nodes. The entire history of progradation can be summarized as alternating long periods of initially rapid, later-slowing combined aggradation and progradation, followed by rapid shifts in location due to nodal avulsions, which may locally incise or at the very least halt aggradation upstream of the avulsion node. This hypothesis allows correlation of marine parasequences to alluvial/delta plain phases of initial incision and terrace formations and subsequent aggradation. Local incision or aggradation cannot be automatically ascribed to allocyclic controls because it may be a product of autogenic forcing. This mechanism produces an inherent range in fluvial profiles without changes in upstream or downstream control, which seems to be a logical explanation for high-frequency, incision-aggradation cycles.
Under conditions of high frequency avulsions and a low rate of progradation, a lobate rounded delta will develop. With a lower avulsion frequency and/or a higher progradation rate a bird foot type delta with elongated channels protruding from the shoreline is expected as the channels will have more time to prograde (lower avulsion frequency) or prograde faster (due to either shallower waters or increased sediment supply or both).

Introduction

Alluvial fan and delta development has mostly been researched in relation to external forcing, as this is assumed to be of greater influence on the sedimentation and erosion than intrinsic variations (Shanley and McCabe, 1993; Holbrook et al, 2006). While useful when studying the effect of large-scale allogenic perturbations, this paradigm has been extrapolated to interpret short-term and small-scale delta deposits in terms

of climatic, tectonic and eustatic change. Extreme examples of this practice include the explanation of parasequences by higher order sea-level cycles. Yet the occurrence of these sequences seems much too regular and widespread to attribute exclusively to relative sealevel and sediment supply variations. The relative influence of autogenic and allogenic forcing on deltaic development is not apparent. Many researchers have created conceptual (Emery & Myers, 1996; Shanley & McCabe, 1994; Wright & Marriott, 1993; Heller & Paola, 1996) and quantitative numerical models (Mackey & Bridge, 1995) of fluvial stacking architecture in a sequence-stratigraphic framework. These models assume a simple, relatively linear response to base-level fluctuations. Although this might be expected in a purely two-dimensional setting, it fails to take into account lateral variation and migration, which strongly influence sediment storage and release in the fluvial sequence. Mackey & Bridge (1995) were the first to take this variability into account, but their scope was limited to relatively isolated alluvial basins. Heller & Paola (1996) introduced a thorough description of channel-belt architecture using a modified Leeder (1978) model. They explicitly linked avulsion frequency to local sedimentation rate, thus greatly improving the realism of the results, although the exact forcing mechanism remained unclear.

Our paper aims to bridge the gap between these reservoir-scale fluvial models and sequence stratigraphic conceptual and numerical models. The interaction between continental and marine processes is expected to work both upstream and downstream. Before we can truly understand the processes of allogenic forcing a base case must be established to determine the autogenic processes and their associated feedback mechanism between the coupled marine and alluvial systems working the system. This should allow us to investigate the processes most relevant to correlating marine and continental deposits. Additionally, this paper aims to create a framework for fully autogenic parasequence development through delta-lobe switching and the associated relation between fluvial/delta plain and marine deposits. The proportion of distributary channel facies has been related to the type of delta, avulsion frequency, bifurcation order and channel migration (e.g. Bhattacharya; 2006, Bristow & Best, 1993; Blum & Törnqvist, 2000; Olariu & Bhattacharya, 2006). The amount and frequency in lateral shift of distributary channels strongly influence overall delta morphology and eventually stratigraphy. Most models typically allow only one single channel to avulse and migrate (Paola, 2000; Mackey & Bridge, 1995; Overeem & Weltje, 2001; Overeem et al, 2005; Olariu & Bhattacharya, 2006). Our approach allows multiple channels to develop, with decreasing downstream discharge and channel geometry influencing delta plain, delta front and prodelta deposition.

Delta-lobe switching is a dominant control on the delivery of sediments to the delta front and prodelta. Many Holocene and ancient examples have been studied, but these leave an inherently fragmented record. Many of the processes leave no deposits, or these may be eroded later. Therefore we use the Dalman & Weltje (2008) model, which includes sub-grid parameterization of alluvial processes and stratigraphy for application in a large-scale basin-filling model. A hypopycnal plume routine (Chapter 3, this thesis) allows realistic clinoform morphology to develop. Our model is the first to relate realistic avulsion processes to marine processes and capture its stratigraphic architectural signature. Our modelling exercise focuses on theoretical experiments as

purely allogenic vs. autogenic control is intrinsically difficult in real-world examples. Yet there lies the great strength of numerical modelling, as we can improve upon the understanding of these systems by focussing on the processes that form and remove the deposits. Therefore, modelling applications should focus especially on the erosional and nondepositional events as these represent the largest amount of "stratigraphic time".

Numerical model description and parameters

The architecture of the numerical model is based on Meijer (2000). A new algorithm was developed by Dalman and Weltje (2008) for the terrestrial/alluvial domain. The main features are realistic channel network development, channel stability based on dynamic calculation of the superelevation and the inclusion of small-scale subgrid channel features. Previous versions of the model included only diffusion-based mass wasting to mimic the marine clastic sediment transport. Dalman (2008, see chapter 3 this thesis) developed a fast river plume deposition routine, which allows a more realistic representation of the fine sediment fraction in marine sediment transport. The coarser grains are deposited by mass wasting, mouthbar and levee development is subgrid-scale. A short summary of the main features follows below.

Fluvial sediment dynamics

Channel network development

Initially a new channel may be created if a threshold bankfull discharge of 10 m^3s^{-1} (Van Den Berg, 1995) is exceeded. This channel will follow the path of steepest descent, until the base level is reached (the sea or a terrestrial lake). When a channel keeps receiving sufficient discharge and no or little aggradation takes place it is assumed to remain stable. River channels are inherently stable under conditions of incision (channels cannot avulse out of a canyon).

The dimensions of grid cells (4 by 4 km) used in our basin-scale stratigraphic model are required to be much larger than the widths of most channel belts. Aggradation of the alluvial ridge and overbank deposition is modelled by redistributing the sediment in one cell using a one dimensional diffusion equation (Pizzuto, 1987). By continuously updating the subgrid-scale deposition after each time step, we evaluate the channel stability over time, as the superelevation of the channel vs. the floodplain is known implicitly. Crevasses are modelled by stochastically instigating potential crevasses by means of uniform random deviates. Each cell containing one or more channels is a candidate at every time step. The probability of a crevasse occurring is set to 0.5. We assume that the new configuration will reach equilibrium within one time step. The equilibrium crevasse channel is calculated iteratively, using bracketing and bisection. We start with an initial guess for the crevasse depth. The water above the level of the crevasse is redistributed over the old channel and the new crevasse channel according to the algorithm of Freeman (1991). The cross-valley gradient is calculated by subtracting the crevasse depth from the amount of alluvial ridge aggradation. Crevasse stability is determined by evaluating the ratio of sediment load to transport capacity. The sediment transport capacity is compared to the sediment load received from the main channel. The avulsion process is self-stabilising, as the increase in transport capacity due to a steeper slope is balanced by a decrease in sediment load delivered from the main channel and vice versa.

If the discharge of the equilibrium crevasse channel does not exceed the threshold discharge defined above, the avulsion has failed. A partial avulsion (bifurcation) occurs when both the newly created crevasse channel and the old channel each receive more discharge than the threshold discharge. Discharge at bifurcations is distributed according to the Freeman (1991) method, which is dependent on downstream channel

gradient. A full avulsion occurs if the discharge received by the old channel does not exceed the threshold discharge. If the avulsion has partially or fully succeeded, the new channel follows the path of steepest descent of the inter-gridcell gradients.

Hydrodynamics and alluvial deposition

Channel style and dimensions are parameterised using empirical relationships (Leopold & Maddock, 1953; Van Den Berg, 1995; Boogaart et al, 2003). The sediment transport capacities are calculated using the modified Bagnold bedload transport equation (Bridge & Dominic, 1984). Net erosion or aggradation is calculated by comparing the sediment transport capacity to the actual sediment load. Deposition occurs when the load exceeds capacity, whereas erosion occurs if the opposite holds true.

The vertical distribution of suspended sediment load over the water column is approximated using the logarithmic Rouse equation (Rouse, 1937). This is necessary to calculate the amount of material a newly created crevasse receives. In our model we assume that the crevasse stabilizes within one time step (i.e. one year), permitting a stable bifurcation to form. In such a case, sediment is distributed over the channels in proportion to the sediment transport capacities of the downstream channel segments. This may result in a slight overestimation of bifurcation stability, but viable alternative solutions (cf Ikeda et al, 1981) are considered too complex to be incorporated in the model.

Marine sediment dynamics

Hypopycnal plume hydrodynamics

River plumes entering the marine domain are dynamically integrated by automatically assigning an inflow point with water velocity, direction of flow and sediment load derived from the fluvial routine. The flow is modelled using one integrated steady-state potential flow routine (See Chapter 3). The river plumes are used as inflow points and the resulting velocity potentials at each grid node are used to calculate the component vectors and consequently the resulting flow direction and velocity. Our model somewhat simplifies the spreading of the 2D jet (vs. Albertson, 1950; Syvitski et al 1998), though the discrepancies are negligible compared to the natural variability on spatial and temporal scales used in our experiments. In a smaller scale model this might result in a somewhat diffuse plume. Yet when using gridcell sizes of 4 km, the results are quite acceptable and computationally very efficient, while allowing an infinite number of distributaries to enter the marine basin. No waves are imposed on the model runs used in this paper. Therefore the potential (re-) distribution of sediments due to wave action is not discussed. For more information on this see chapter 3 and 4.

Sediment deposition from plumes

The coarse-grained sediment fraction is dumped in front of the river mouth by bedload dumping. Oversteepening of these deposits may allow mass wasting to occur, which is represented by linear diffusion. Suspended particulate matter can be transported a significant distance from the river mouth by the hypopycnal plumes.

This is modelled by transporting the sediment according to the flow velocities and directions calculated with the potential flow routine. The sediment fallout rate is calculated using a first-order rate law approximation after Syvitski (1988). Thus the amount of suspended sediment decreases exponentially away from the river mouth. The coarser fractions, transported as bedload, are dumped at the river mouth, to form amalgamations of channel-levee complexes and mouthbar deposits.

Stratigraphy

The net sediment deposited as well as nondepositional and erosional surfaces are written every time step and subsequently compressed to represent 10 time steps in one stratigraphic layer. Each layer records the thickness, grainsize fractions and age of the sediments.

Results

Several scenarios of time-invariant delta development are presented in this section. Table 6.1 provides the quantification of the parameters used in each experiment.

Laterally confined, high-angle shelf, run 1

Figure 6.1 illustrates the geomorphological development of a high angle shelf run 1 under time invariant conditions. Initially a small elongate channel-levee complex develops as a single channel and associated levee, which progrades into the sea and over its mouthbar and plume deposits. Several upstream and nodal avulsions occur as the feeder channel has aggraded sufficiently and allow a more lobate delta to develop. After 6 kyr the lobate delta has widened sufficiently for the delta to become constrained by the edges of the model, which forces the delta to prograde. The stratigraphy correspondingly shows the result of these processes. A small initial delta develops and rapidly progrades (Figure 6.2A) forming a complex sigmoid-oblique clinoform that widens into a mounded lens shape (Figures 6.2B and C). After 6 kyr the central lobe is abandoned and the outer parts of the delta are widened by vertical and lateral stacking. The central lobe acts as a "point source" for lobe stacking, though there is considerable variability in stacking pattern and timing. The morphology of each lobe depends on location and direction of the feeder channel, which is highly variable. The spikes present in cross sections (particularly visible in Figure 6.2C) are a result of the relatively coarse gridding used in the model, as each spike represents an

Parameter	Run 1 Laterally confined, high-angle shelf	Run 2; Laterally unconfined, low-angle shelf	Run 3; Laterally unconfined, no imposed shelf
Discharge (m3/s)	3000	2500	2500
Sandy sediment load (km3/year) 200 μ	0.0608	0.025	0.025
Mud sediment load (km3/year) 5 μ	0.2433	0.075	0.075
Shelf slope (-)	$7.5 * 10^{-4}$	$2 * 10^{-4}$	Subaqueous: $7.5 * 10^{-4}$
Shelf width (km)	100	200	200

Table 6.1; An overview of all parameters used in all model runs

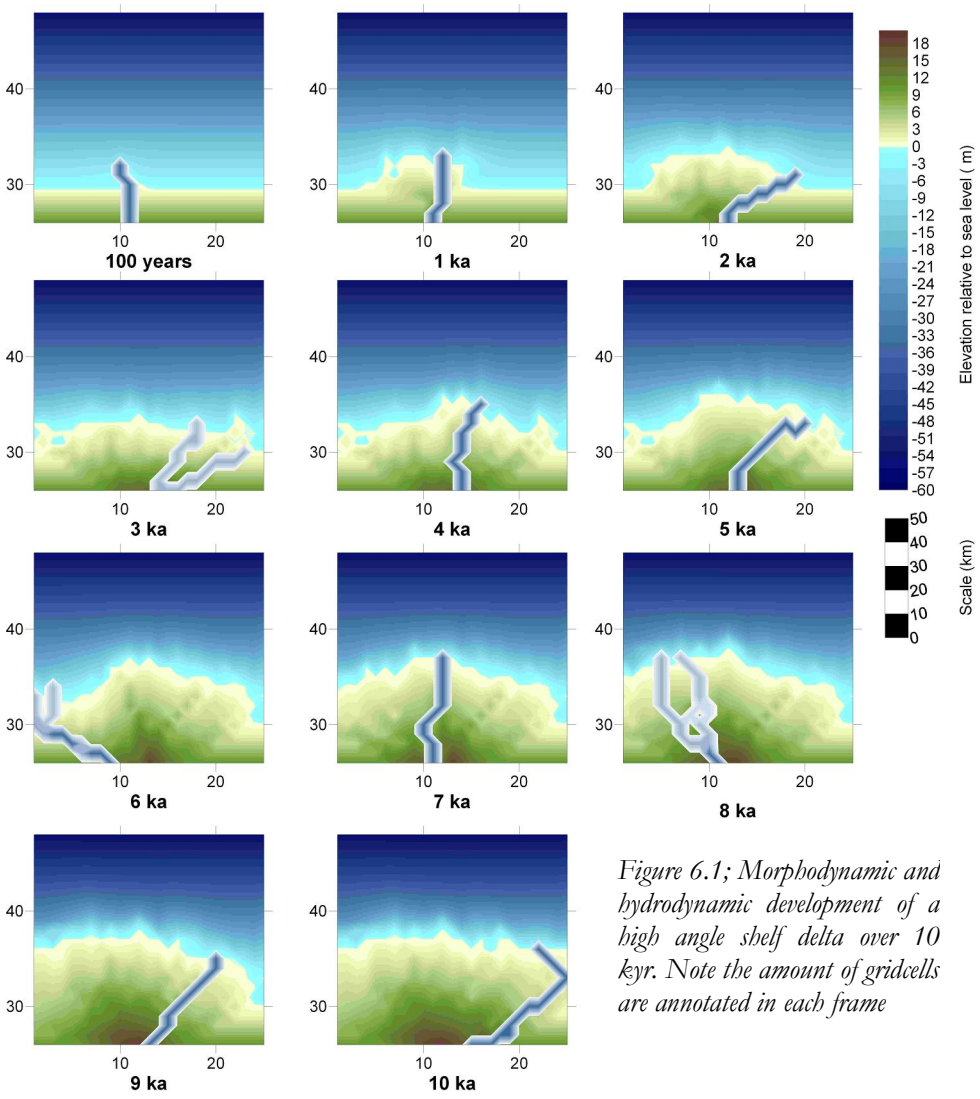

Figure 6.1; Morphodynamic and hydrodynamic development of a high angle shelf delta over 10 kyr. Note the amount of gridcells are annotated in each frame

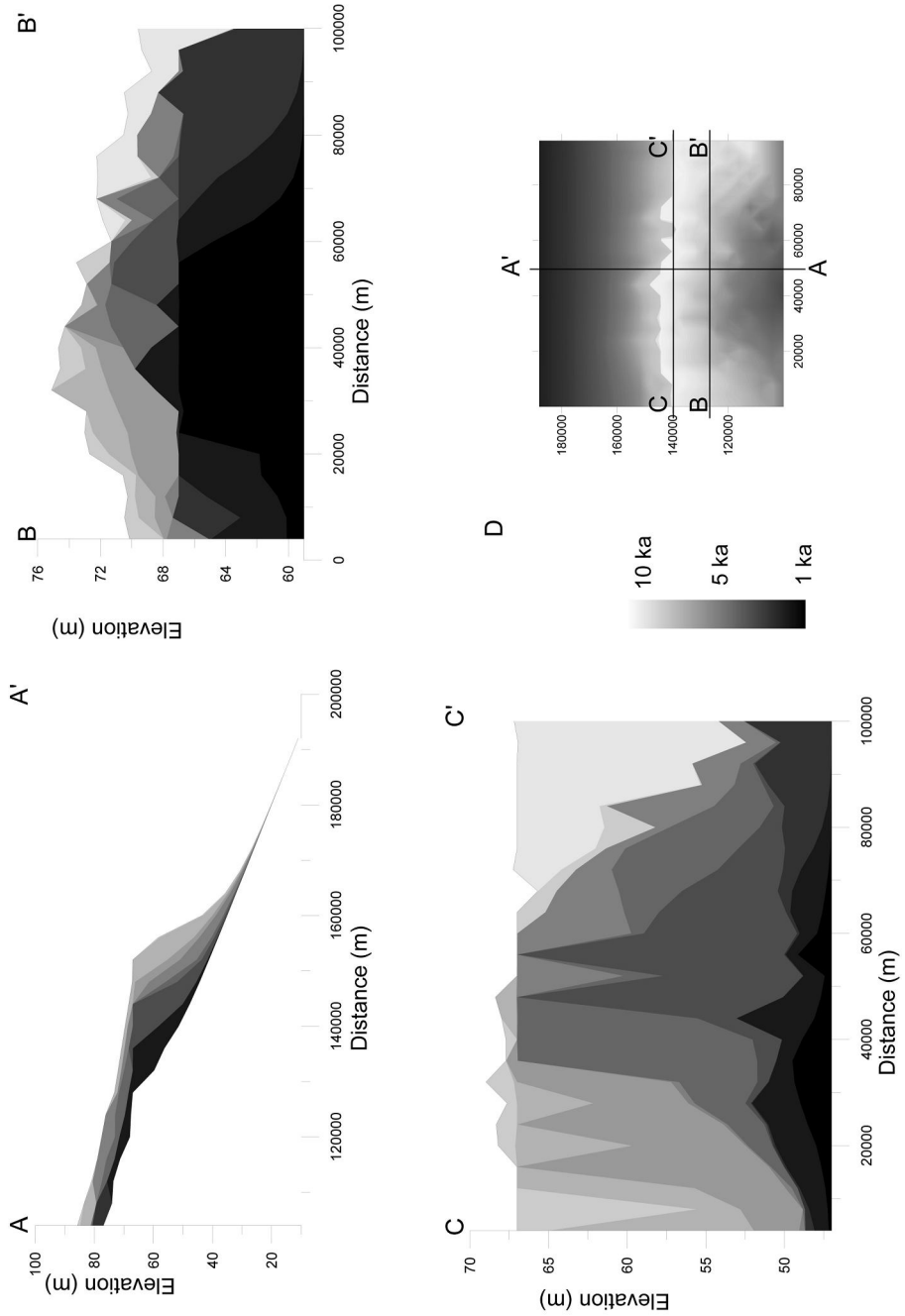

Figure 6.2; Chronostratigraphy of a high angle shelf delta. The complex sigmoid-oblique clinoforms (A), two cross sections, indicating clearly the offset stacking nature of the delta lobe deposits (B & C). The location of the cross sections are

area of 4 km in width. These spikes should be understood as channel-levee complexes (mostly bedload deposition in mouthbars and levees) prograding over the mounded prodelta deposits (mostly diffuse plume deposition).
The most proximal deposits show lower-angle foresets (Figure 6.2B) as compared to the more distal delta (Figure 6.2C), probably due to the larger accommodation space in the distal part. This is a direct result of hypopycnal plume deposition
Patterns of erosion and deposition are illustrated by a Wheeler diagram (Figure 6.3). Initially, one single channel feeds the delta and avulsions can develop only after this channel has aggraded sufficiently to permit successful avulsions. Continuation of this process results in a large increase in delta-plain area, both through progradation and onlap (backstepping). The delta apex migrates upstream as the area of the delta plain increases, effectively shortening the fluvial valley. Each nodal avulsion bypasses the old channel and allows a new delta lobe to start developing next to the previous lobes. Repeated nodal avulsions result in a depositional pattern similar to an "inverted Christmas tree" (Figure 6.3), produced by the repeated parallel progradation events of each delta lobe. Marine deposition by plumes is strongly dependent on the outflow velocity and direction of the distributaries. This is clearly visibly in the Wheeler diagram (Figure 6.3), where spikes of plume deposition are present in the marine domain, albeit clearly linked to delta plain and fluvial processes.

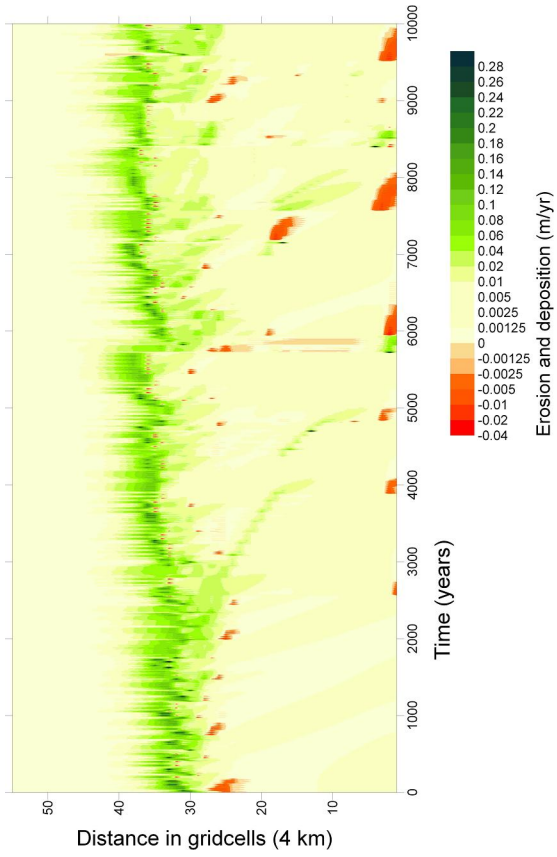

Figure 6.3; Wheeler diagram of all sediment dynamics summed along the downstream axis.

Influential nodal avulsions are created by storage of sediment in the fluvial valley as the river attempts to attain a graded profile. This local aggradation starves the downstream area of the basin of sediment and decreases the rate of delta-front progradation. Additionally, the avulsions induce severe erosion, starting at the point of avulsion where the gradient is high. These local knick points (note the red points in Figure 6.3) may retreat and erode further upstream depending on stream power, sediment supply and slope.

Low angle, unconfined shelf run 2

The morphological and hydrodynamic development on a less confined and low angle shelf is illustrated with run 2. The geomorphological and hydrodynamic development over the 20 kyr modelled is presented in Figure 6.4. The smooth initial surface and time-invariant forcing allow a highly symmetrical delta to form. A major difference between the high-angle Run 1 and Run 2 is the relatively discontinuous delta front morphology of the latter. Avulsion frequency is relatively low and the shallow marine basin allows rapid progradation, which favours the development of long single-channel feeder system (bird-foot type deltas) instead of a rapidly avulsing multi-distributary system. Additionally, the low-angle coastal plain allows the delta apex to migrate upstream synchronously with the increase in active delta-plain area (Figure 6.6). The symmetrical development of Run 2 is illustrated by the stratigraphic cross section (Figure 6.5B). Initial deposition is progradational in the centre section (Figure 6.5A) and the en-echelon stacking of later delta lobes results in a mounded lens shape (Figure 6.5A). Yet the subsequent aggradation and apex migration have an unforeseen effect, as the superelevation necessary for an avulsion results in a local knick point. This will inherently result in local deposition (just downstream of the new crevasse) and erosion (upstream of the crevasse) as the channel attempts to attain grade. These features are visible in the Wheeler diagrams (Figure 6.6 and 6.3), where simultaneous erosion (upstream) and deposition (downstream) occur cyclically. As total aggradation on the delta plain is limited in run 2, these avulsion scours severely erode older deposits (Figure 6.5A). These features might easily be interpreted as changes in stream power due to floods or changes in base level. Yet these features of self-organisation are a completely independent of external perturbations.

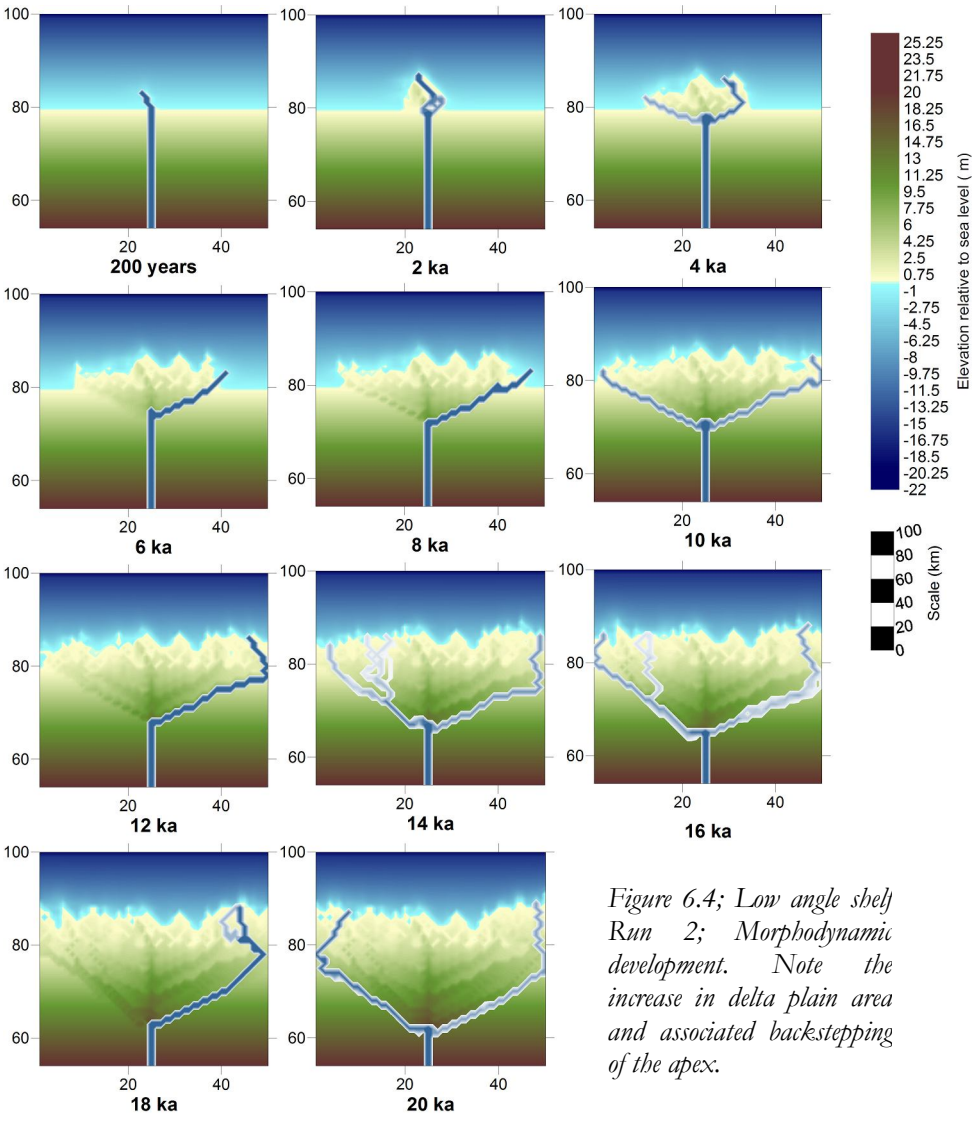

Figure 6.4; Low angle shelf Run 2; Morphodynamic development. Note the increase in delta plain area and associated backstepping of the apex.

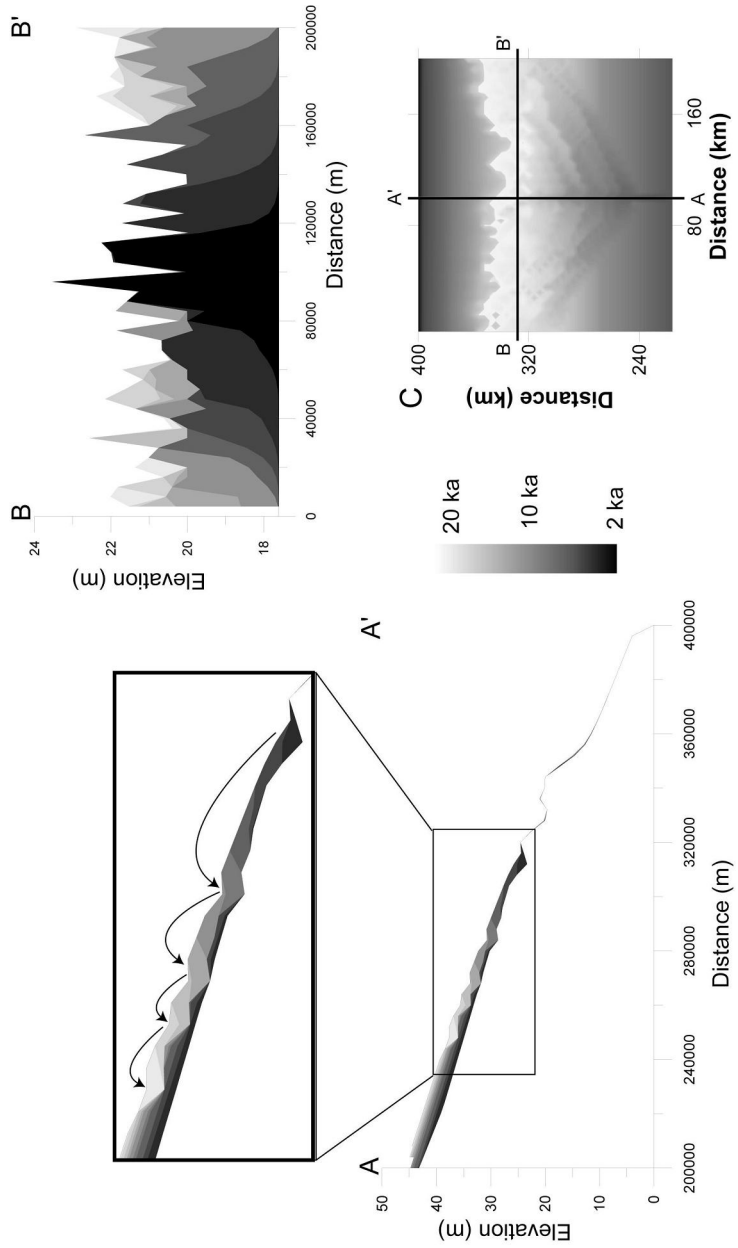

Figure 6.5; Stratigraphic cross sections of the low-angle run 2. The middle section is enlarged (A) to illustrate the backstepping of the nodal point and associated scouring of older deposits after each major avulsion. The lateral cross section illustrates the symmetrical offset stacking of the delta lobes (B). The locations of the cross sections are provided (C), for legend of the morphology, see Figure 4.

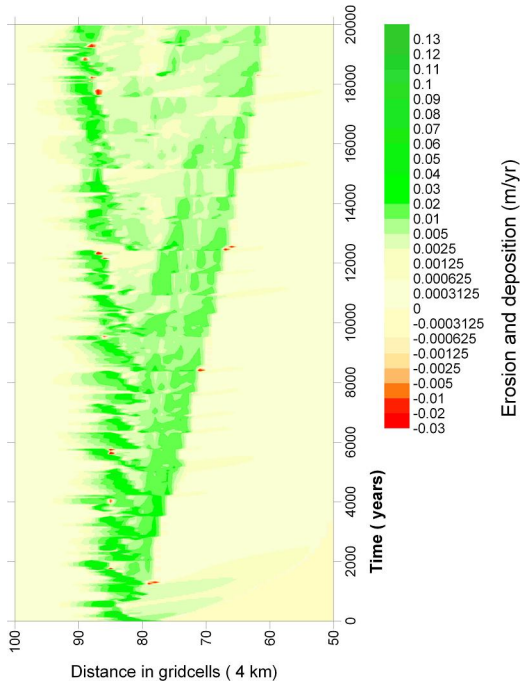

Figure 6.6; Wheeler diagram summed along the downstream axis for Run 2. Note the controlling nodal point avulsions, which instantaneously controls the downstream deposition.

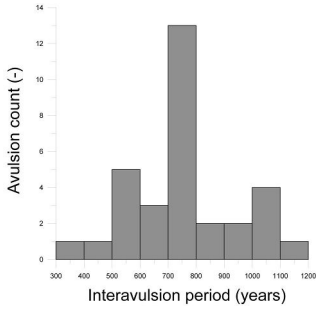

Figure 6.7; Interavulsion period histogram for Run 2. Note the strong peak around 700-800 years.

No imposed angle, laterally confined basin

All previous examples have been influenced, to a certain extent by inherited morphology, as is expected for most if not all real-world system. To illustrate the "natural development" of a delta, Figure 6.8 shows the chronostratigraphic events of a delta growing in standing water with no pre-existing fluvial channel present. Effectively, the system is allowed to create its own equilibrium surface. Initially each individual channel lobe progrades and this period of progradation is punctuated by nodal point avulsions, which move the river mouth to a point along the shore from the previous lobe. Note that the location of avulsions shifts basinwards as the area of the initial deposits reaches a state of equilibrium.

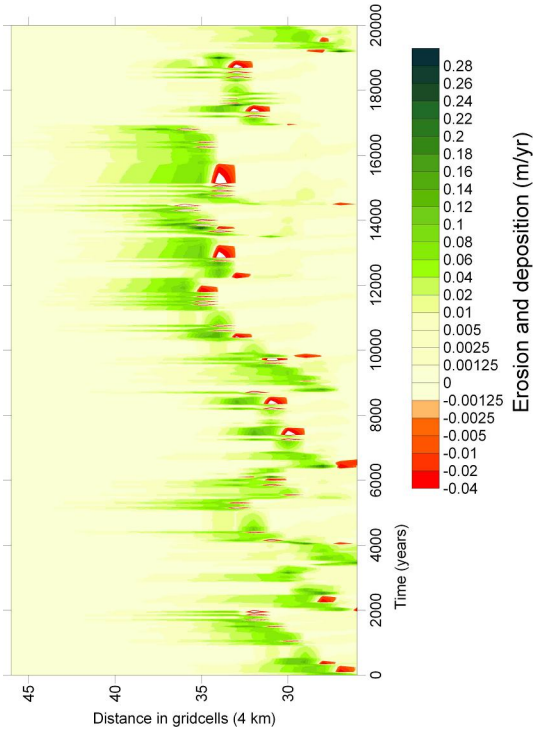

Figure 6.8; Wheeler diagram for delta Run 3. Note the Backwards and forwards translation of avulsion points (indicated by the erosive avulsion scours).

Discussion

Large-scale morphology

Delta morphology and stacking architecture

Depending on the stability of distributaries a bird-foot type or a lobate delta may develop. In deepwater settings, progradation will be slow due to the large accommodation, inhibiting bird-foot type deltas to develop and favouring a rapidly-avulsing rounded lobate delta. The type of fluvial-dominated system that develops depends on the ratio between avulsion frequency and rate of progradation. Under conditions of high-frequency avulsions and a low rate of progradation, a lobate, relatively smooth delta front will develop. With a lower avulsion frequency and/or a higher progradation rate a bird foot type delta with elongated channels protruding from the shoreline is expected as the channels will have more time to prograde (lower avulsion frequency) or prograde faster (due to shallower waters, increased sediment supply or both). Delta front morphology is therefore not as dependent on water depth as previously assumed (Fisk, 1961; Fisher, 1969). Even the most famous bird-foot type deepwater delta, the Mississippi, has been artificially stabilised for decades

(Bhattacharya, 2006) thus allowing the current overextended channel to develop. Dependence on progradation rate is illustrated in Figure 6.1 and 6.4. Figure 6. 1 shows a high-angle shelf that sufficiently slows progradation rate to allow a smooth delta to develop. The low-angle delta (Figure 6.4) allows a much more punctuated delta front to occur due to the high progradation rates in the shallow basin.
The morphology of the clinoforms created by the model (Figure 6.2A and 6.5A) is typical for a hypopycnal plume dominated system. Clinoforms have been modelled in many 2D and 3D models, but the most difficult pattern in stratigraphic reconstructions are lateral cross-sections. Although our model runs have used a simplified set of input parameters, the cross sections in Figure 6.2C and 6.5B unmistakeably indicate the offset/ en echelon stacking of the delta lobes. Compared to seismic profiles of the Natashquan River Deltas (Hart and Long, 1996) the only major difference is the absence of a ravinement surface in the stratigraphy. This is to be expected, as we have not modelled a relative sealevel rise or subsidence, which allows a transgressive erosive surface to cut off the shallow deposits. The delta obviously strives to fill the entire basin equally, yet the truncated nature of avulsions allows these discrete lobes to form in an offset stacking pattern.

Change in avulsion frequency during avulsion cycles
Mackey & Bridge (1995) suggest that avulsion frequency will decrease over time, as their model shows that channel belts downstream of avulsions will not be able to aggrade sufficiently. Yet their approach uses an imposed aggradation rate dependent on downstream distance, as opposed to our dynamic sedimentation calculation, which is influenced by changes in slope, sediment influx and discharge. Thus, channel belts can only aggrade when the local slope is sufficiently low to decrease the sediment-transport capacity below the sediment influx. Our model indicates that the self-stabilising effect of local avulsion scouring directly upstream of the avulsion node and concomitant deposition just downstream stabilises the system. Concluding, under time-invariant forcing and a constant slope, avulsion frequency will not change significantly if the profile is not lengthened substantially by progradation. Figure 6.7 shows the frequency distribution of major interavulsion periods, with a clear clustering around 700 to 800 years, with a standard deviation of 240 years. The interavulsion period is influenced mainly by liquid and solid discharge regimes and initial slopes. Note that little progradation occurs in Run 2 after 6000 years, as the delta reaches deeper waters and the increased delta-plain size sequesters more sediment by effectively lowering and lengthening the down channel slope. Stouthamer & Berendsen (2001) calculated an interavulsion period of 945 years for the Rhine and Meuse Rivers, which is of the same magnitude, although they attributed the change in frequency over the Holocene to changes in relative sealevel.
An increase or decrease in frequency of autogenic avulsions depends mostly on progradation rate and initial morphology (i.e. is the channel under or over grade). The backwards and forwards motion of the downstream avulsion nodes (illustrated in Figure 6.8) clearly indicates the natural variability of avulsion location. Mackey and Bridge (1995) interpreted avulsion sequences from their pioneering modelling work, yet the decrease in interavulsion period seems to be an artefact of their imposed

channel belt aggradation rate. In a delta setting, or a similar continental setting with a dynamic base level, the aggradation rate is strongly dependent on the distance from baselevel and therefore upon the initial topography and bathymetry. In a shallow setting, progradation will be very rapid and therefore induce rapid aggradation and increased avulsion rates. In a sloping bathymetry, as used in this paper, the initial progradation rate is rapid yet decreases as the delta front reaches deeper waters. This does induce a decreasing rate of aggradation and associated avulsion frequency. Thus, the shelf gradient controls the (average) rate of progradation, which in turn controls avulsion frequency.

Marine-continental correlation

Downstream influence of sealevel on fluvial grade is strongest near the shore. Further from the shore, upstream controls are more important (Blum, 1993; Shanley & McCabe, 1994; Guccione, 1994; Törnqvist, 1998; Blum & Törnqvist, 2000). Shanley & McCabe (1994) introduced a conceptual model for channel stacking architecture. Their model explores one possible example in a range of possibilities, since they assume an incised valley will develop under lowstand conditions. Incision is inherently dependent on the angle of the exposed shelf; typically an incised canyon will only develop when sea level falls below the shelf edge. Hence relative sealevel fall may induce aggradation on sufficiently low-angle shelves (e.g. Ridente & Trincardi, 2005). The Shanley & McCabe and related Wright & Marriott (1993) models may be seen as two possible examples of alluvial architectural response to base level changes, Emery & Myers (1996) illustrate variations on these possible end members. Real-world settings will show a rich variety of responses depending mostly on the relationship between rate of creation of accommodation space (forced by relic topography) and sediment supply, which can be assessed using numerical models such as those used in this paper.

Most alluvial architecture research focuses on continental deposition, where little or no change in graded profile is expected from baselevel changes (either autogenic or allogenic). Sedimentation is assumed to be directly linked to local subsidence, with only minimal baselevel disturbance. Our modelling exercise attempts to link nearshore alluvial architecture to inherent changes in prograding and aggrading delta systems. Obviously the aggradation is coupled to progradation which lengthens the fluvial profile, this provides the link between new channel deposits and delta lobe formation.

The effects of nodal-point avulsions on clinoform stratigraphy (Figure 6.2A) are sufficient to explain deltaic parasequences. Each phase of delta-lobe progradation has the typical coarsening-upward and progradational features. The version of the model used in these exercises does not incorporate compaction due to loading and its associated subsidence. Note that we do not observe any actual drowning surface as expected at the bounding surface of a parasequence, but instead a phase of abandonment indicates a locally condensed sequence. By incorporating self-induced subsidence we would obtain a classic parasequence capped by a flooding surface. Our model results even show a clear shallowing upward sequence (Figure 6.2C); thin beds of distal, fine-grained continuous prodelta deposits are present at the base of the sequence. Above this, thick proximal mounded prodelta deposits are present, over

which coarse-grained steep sided mouthbar and channel-levee complexes prograde. If aggradation is sufficient (as in Run 1 see Figure 6.2), we can even have fluvial channel and overbank deposits on top of this sequence.

Dalman & Weltje (2008) (Chapter 2, this thesis) proposed a relationship between channel-network pattern and fluvial sediment storage and release. Under conditions of high avulsion frequency, this may influence the sediment capture of the delta plain. Under the lower avulsion frequencies in the examples provided in this paper, little influence of channel network on sedimentation is discernable. Most of this friction increase-decrease cycle is obscured by avulsion scouring and deposition. Under relatively stable, near-equilibrium conditions we expect channel network architecture to create sufficiently strong storage-and-release events to have a measurable effect on stratigraphy.

The main reason why rivers avulse is, as in most processes clastic, gravitational advantage. Yet the rivers maintain their stability for a longer time than expected from purely diffusive transport. An increase in active channel length due to progradation results in a consequent increase in sedimentation on the delta plain relative to the delta front and prodelta. After an avulsion much sediment is sequestered in the channel path just downstream of the avulsion because the slope is very low (Figure 6.9). Conversely, severe scouring may occur upstream of the avulsion point (Figure 6.5A). Karssenberg & Bridge (2008) observed a similar model response to avulsion in a purely alluvial setting, which confirms this process as being a robust feature of fluvial channel dynamics. This phenomenon will be strongest in areas were channels are very stable, i.e. high-gradient deltas with strong vegetation and limited flood peaks. In low-gradient areas with easily erodible banks, high frequency avulsions will most likely obscure any sediment sequestration events.

Post-avulsion erosion in the upstream fluvial channels may thus induce terrace formation, which in turn allows localized downstream fluvial aggradation and slow progradation rate of the newly created prograding delta lobe due to sediment starvation. These model results indicate phases of subgrid-scale, upstream terrace

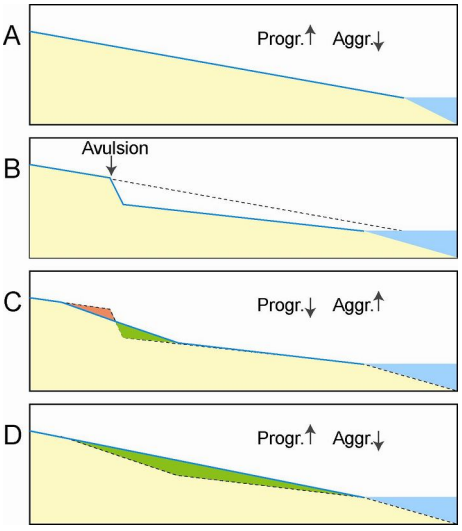

Figure 6.9; Aggradation and progradation influenced by avulsions. In a hypothetical fluvial channel at grade (A), aggradation is minimal all sediment is available for progradation at the delta front. After an avulsion (B) a new channel path is created which is clearly out of equilibrium. Initial channel behaviour (C) will locally erode just upstream of the avulsion node and aggrade downstream. The net behaviour is strongly aggradational, resulting in a very low progradation rate at the new delta front. Only after the new distributary nears equilibrium (D) will the progradation rate increase again.

formation by channel incision. Real-world examples of this process might give interesting insights into this complex response to delta-lobe switching. This inherent sedimentary feedback mechanism provides a method to correlate fluvial processes to marine deposition. High resolution dating will be necessary to substantiate this, but the implications are significant. One marine parasequence is linked to one phase of delta lobe progradation, which in turn is linked to a phase of local scouring upstream of the avulsion and sediment sequestration just downstream. From this hypothesis we might speculate on an increase in sedimentation rate at the delta front during the deposition of one parasequence, as sediment sequestration on the delta plain will be highest at the start and lowest at the end of one phase of lobe progradation.

Our model provides information on channel stacking associated with marine processes, which allows us to assess the likelihood of marine phases of progradational parasequences being linked to alluvial/delta plain phases of initial incision and subsequent aggradation. Visualization of channel belt architecture will allow us to directly test the conceptual models (i.e. Emery & Myers, 1996; Shanley & McCabe, 1994; Wright & Marriott, 1993; Heller & Paola, 1996) of sedimentary response to base level change.

The entire history of a large progradational event can be summarized as an alternating cycle of long periods of initially rapid, and subsequently slowing aggradation in the alluvial environment and progradation in the marine environment. This is followed by rapid shifts in location of the delta lobe due to nodal avulsions, which may locally provoke incision or at the very least halt aggradation upstream of the avulsion node. Downstream of the avulsion knick point the river is below grade, which allows simultaneous aggradation. Combined, the effects of continuous progradation lengthen the fluvial profiles, which induces the avulsions, which in turn affect the distributaries (Figure 6.9), resulting in a complex and counterintuitive response. Avulsions in the fluvial channels induce terrace formation, which allows downstream aggradation, and initially slow the progradation rate of the delta front. This hypothesis allows correlation of marine phases of progradational parasequences to alluvial/delta plain phases of initial incision and subsequent aggradational in ancient delta deposits. However, the complexity of the response in this relatively simple set-up makes it likely that real-world deltas with associated complications, such as allogenic forcing and/or a heterogeneous subsurface etc. will have even more complex sedimentary histories. Our hypothesis based on the simulations reported in this paper cannot be directly applied to ancient fluvial and deltaic deposits. Whether fluvial aggradation can be linked to initiation of parasequences due to nodal point avulsions depends strongly on the response time of the system.

Yet the outcome does increase possible explanations for sedimentary features in ancient deposits. Local incision or aggradation cannot be automatically ascribed to allocyclic controls because it may be a product of autogenic forcing. This mechanism produces an inherent range in fluvial profiles without changes in upstream or downstream control, which seems to be a logical explanation for high-frequency incision-aggradation cycles (cf Van Dijk et al, 2008; Kim et al, 2007; Holbrook et al, 2006).

Conclusions

Under conditions of high frequency avulsions and a low rate of progradation, a lobate rounded delta will develop. With a lower avulsion frequency and/or a higher progradation rate a bird foot type delta with elongated channels protruding from the shoreline is expected as the channels will have more time to prograde (lower avulsion frequency) or prograde faster (due to either shallower waters or increased sediment supply or both). Under time-invariant forcing and a constant slope, avulsion frequency will not change significantly if the profile is not lengthened substantially by progradation.

Avulsions in fluvial channels induce terrace formation and concomitant downstream aggradation, which initially slows the progradation rate at the delta-front. This hypothesis allows correlation of marine deltaic parasequences to alluvial/delta plain phases of initial incision and terrace formation and subsequent aggradation. These effects of nodal-point avulsions on clinoform stratigraphy (Figure 6.2A) are sufficient to explain deltaic parasequences.

The most important factor in delta and fluvial development, on time scales where little allocyclic forcing occurs, is the geologically inherited surface. Low-angle surfaces will induce rapid aggradation and increase avulsion frequencies, whereas high-angle surfaces will favour less aggradation and subsequently decrease avulsion frequency. The shelf gradient controls the (average) rate of progradation, which in turn controls avulsion frequency. Avulsion frequency will remain constant, assuming all other factors are stable, if the progradation rate is sufficiently high to induce constant upstream aggradation.

Chapter 7
Sequence-stratigraphic implications of compound clinoform decoupling during sea-level cycles

Abstract

This paper aims to investigate the variability in morphodynamic and stratigraphic response of wave influenced deltas and coastlines under different scenarios of sea level and sediment supply. Additionally the link between the subaerial and subaqueous delta couplets in associated compound clinoforms is studied. The main focus is on morphodynamics, coastline curvature and implications for sequence stratigraphy. A 3D stratigraphic model is used, comprising fluvial network processes, plume dynamics, wave-induced bed load transport and marine suspended load dispersal.
Numerical experiments indicate that relative sea level rise increases local coastline curvature due to the increased discrepancy between eroding coastal sections and sections receiving direct sediment input. Wave erosion provides considerable amounts of sediment to the subaqueous foresets, allowing rapid progradation. This mechanism increases the subaqueous topset length of the compound clinoform as coastal erosion is increased and this material is deposited on the subaqueous foresets. The considerable amounts of sediment transported to the subaqueous delta front effectively decouples the subaerial delta front development from the subaqueous rollover point. Thus a wave ravinement surface can be associated with synchronous subaqueous delta progradation, resulting in a proportional increase of subaqueous clinoform topset length. During sea level rise, regression of the coastline may correspond with aggradation and/or non-deposition of the subaqueous topset. The decoupling of the behaviour of compound clinoform segments necessitates further studies and a subclassification of sequence stratigraphic terminology.
The correlation between rollover points and sealevel is a tenuous one. For direct correspondence only the coastal rollover point should be used. Relative sealevel rises will be underrepresented when using the subaqueous rollover point. Long-lived, wave-influenced delta deposits most likely contain fewer subaerial unconformities than fluvial dominated delta systems. Only under very large glacio-eustatic cycles do large-scale incision and lowstand systems occur.

Introduction

Coastal processes are focused on a relatively narrow band of the passive margins. Yet these processes have a profound effect on grainsize distribution, stratal geometry and stacking patterns of coastal deposits. Under the influence of sea level changes, sediment supply and wave regime the narrow band can move over the shelf and rework a large area of the shelf. The influence of wave power on delta development is

expected to vary significantly during sea level cycles. This can be determined by measuring coastal erosion/progradation rates and coastal curvature.

Three dimensional coastal, sedimentary architecture

Most models that mimic wave-influenced coastal sedimentary architecture are purely one-dimensional and depth-averaged, with two-dimensional output (e.g.: Swenson et al, 2005, Storms, 2004, Cowell et al, 1995, Niedoroda at al, 1995). Such models do not account for out-of-plane variations in sediment supply, subsidence or wave regime. Niedoroda et al (2003) linked a set of two-dimensional transect models to create a three-dimensional model of the Coastal Systems Tract. Their focus was mainly on the morphodynamic response to short-term, low amplitude sea level cycles. The model presented in this paper is a fully 2-D, depth-averaged approximation with 3-D output. This allows the complex interaction between fluvial and wave influences on deltaic and shoreface development to be studied. The strength of numerical modelling is that it allows us to improve upon the understanding of sedimentary systems by focussing on the processes that form and remove the deposits. Therefore modelling applications should focus especially on the erosional and nondepositional events as these probably represent the greatest amount of "stratigraphic time" and cannot be observed.

Compound clinoforms are common in many delta systems (e.g. Nittrouer et al, 1996). The oceanic/marine processes by which sediment is moved to the subaqueous foreset varies, in our model we use wave-induced currents but the results will be similar to current influenced shelf settings. Nittrouer et al (1996) observed that the Amazon subaerial and subaqueous deltas prograde at different rates. Swenson et al (2005) developed an analytical model to determine downdip influence of these complex stratal patterns. Their work indicated a strong dependence on grainsize and the dispersive marine influence (i.e. storm frequency and intensity). While valuable for determining preliminary, theoretical boundaries, the linear nature of the model does not allow much natural variability, nor does it account for spatial variability (out-of-plane) in fluvial channel dynamics and sea level cycles. This paper aims to expand on this work and study the response of wave-influenced deltas in three dimensions and under complex forcing mechanisms.

Coastline curvature through time is not constant (Kim et al 2006). The numerical experiments presented in this chapter, are aimed at providing some generalizations on coastal and shoreface architecture and morphology under various scenarios of sea level change, river input and substrate grainsize distribution. Specifically we try to link variation in coastline curvature and stratigraphic expression of compound clinoform development to sea level cycles, grainsize and sediment supply fluctuations.

Numerical model description and parameters

The architecture of the numerical model is based on Meijer (2000). A new algorithm was developed by Dalman and Weltje (2008) for the alluvial (subaerial) domain. The continental clastic sedimentary system is represented by two algorithms, a diffusive and an advective one. A two-dimensional diffusion algorithm characterizes hill slope denudation. Fluvial processes and stratigraphy are represented by sub-grid parameterisation for application in the large-scale basin-filling model. Sub-grid sediment transport and channelisation are derived from physical equations, capable of producing convergent and divergent drainage networks, trunk channels and most importantly, detailed representations of avulsions and bifurcations. The channel network model allows realistic input and more importantly spatial and temporal changes of the liquid and solid discharge entering the marine domain.

The marine module mimics wave resuspension and advective transport. The marine part is implicitly linked to the fluvial module, thus permitting the study of feedback and interactions between marine and continental sedimentary environments. This approach allows us to quantify the stratigraphic response to external and intrinsic forcing under the influence of waves and currents. The hydrodynamic flow of currents and plumes is modelled using one integrated steady-state potential flow routine (see Chapter 4, this thesis). Though this technique ignores fluid viscosity, irrotational flow, compressibility and smaller scale perturbations in the hydrodynamic movement, the resultant calculation of water movement is robust, speedy and representative for geological time scales. The integration of river plumes and longshore currents in one hydrodynamic algorithm allows us to calculate the combined effects of deposition from plumes and longshore transport of resuspended shelf deposits.

The near shore coastal module (see Chapter 5, this thesis) is characterized by two modes of sediment transport: crosshore suspended and/or bedload sediment transport, occurring anywhere above the (variable) wave base, and longshore transport, which moves bed load sediment along the coast, mainly in the surf zone.

Storm generation and wave propagation

To mimic the inherently stochastic nature of storm frequency and magnitude we model one storm event and its associated significant wave height per time step. The significant wave height for each storm event is randomly extracted from a Gaussian distribution of effective wave heights. This results in only very few large storms (i.e. the most influential ones), and many meso-scale storms. The mean (fair weather) wave height is assumed to be constant. This routine determines the significant height of the deepwater wave, which is deformed by traction as the bathymetry shallows. To approximate this behaviour, the model uses a second order-solution of the Stokes equations to incrementally calculate the near-bed horizontal orbital velocity during one entire wave phase. The near-bed, horizontal orbital velocity under the wave crest is relatively strong and directed onshore, whereas under the wave trough the velocity is relatively weak and directed offshore.

Bed mobilization and sediment transport

The waves are assumed to dig to the depth where the bottom shear stress equals the critical shear stress. Even though a certain amount of sediment has been mobilized by digging, sediment transport is not necessary. Rather this depth represents the zone that has been reworked by waves and represents the datum level of wave reworking. Sediment transport is subdivided into bed load and suspended load transport. The suspended load fraction is defined as those grains with sufficiently low density and/or small size to be entrained or suspended during the event in question. This fraction is assumed to move offshore, effectively following the net water motion under shoaling waves. The bed load fraction is influenced only by the near-bed velocities, of which the strongest are oriented onshore. Therefore the net motion of the coarser grain fractions is onshore, barring the very largest storms that can suspend these fractions. The bed load transport is calculated incrementally over one wave phase using the Bailard-Bagnold transport equation and linearly upscaled over the entire duration of the event.

Littoral sediment transport and coastline stability.

Coastal cells are processed independently; they are first identified based on the boundary between marine and land gridcells. The location of the coastline is calculated on a smaller scale than the grid discretization, as this allows us to accurately calculate littoral transport and to balance the sediment budget precisely. The intra-cell location of the coastal nodes is used to calculate a cubic spline to determine the coastline curvature. The curvature is necessary to accurately determine the angle between wave incidence and coastal orientation, which in turn determines littoral drift.

The coastal cells are run by a separate routine to model littoral drift using the relationship by Inman & Bagnold (1963), which effectively smoothes the coastline by moving sediment to adjacent coastal cells if necessary, depending on shoreline curvature. Littoral transport occurs during the entire time step; therefore one coastal cell may receive sediment during the fair-weather time-step and have a sediment deficit during the storm event, or vice versa. After both processes have been calculated the net sediment input is used to determine whether a) the coastline remains in place (no net sediment transport), b) the coastline progrades (net sediment input) or c) the coastline erodes (net sediment deficit).

Experimental design

Choice of parameters

Sea level is seldom constant over several thousand years, fluctuations severely influence delta morphology and architecture. In fluvial-dominated settings this will mostly result in a shift in coast location and local subaerial incision during lowered sealevels. In wave-influenced settings the erosive power of the waves will produce erosive surfaces and redistribute this sediment in reaction to changes in sealevel. In order to quantify this mechanism and its influence on deltaic morphology and sedimentary architecture we model several cyclic sea-level fluctuations. Sea-level cycles are often associated with glacio-eustasy, which in turn is caused by changes in climatic conditions. The effect of changing climatic conditions and simultaneous sealevel cycles is modelled by varying the sediment supply, thereby mimic climatic influence on delta behaviour.

Scenarios

The relative influence of wave and river processes on delta development was examined by using five scenarios. The reference scenario (scenario 1) is a system with constant sea level over 10,000 time steps of one year. The other scenarios are forced by 8 m cyclic sea-level cycles, with a relatively muddy (scenario 2) and sandy (scenario 3) sediment input (0.2 and 0.4 sand/mud ratio, respectively). In order to estimate the effect of climate-induced changes in sediment load related to sea-level fluctuations the last two scenarios incorporate a sinusoid variation in sediment load in phase (scenario 4) and out of phase (scenario 5) with the sea level curve (Figure 7.1). All parameters distinguishing the scenarios are provided in table 7.1.

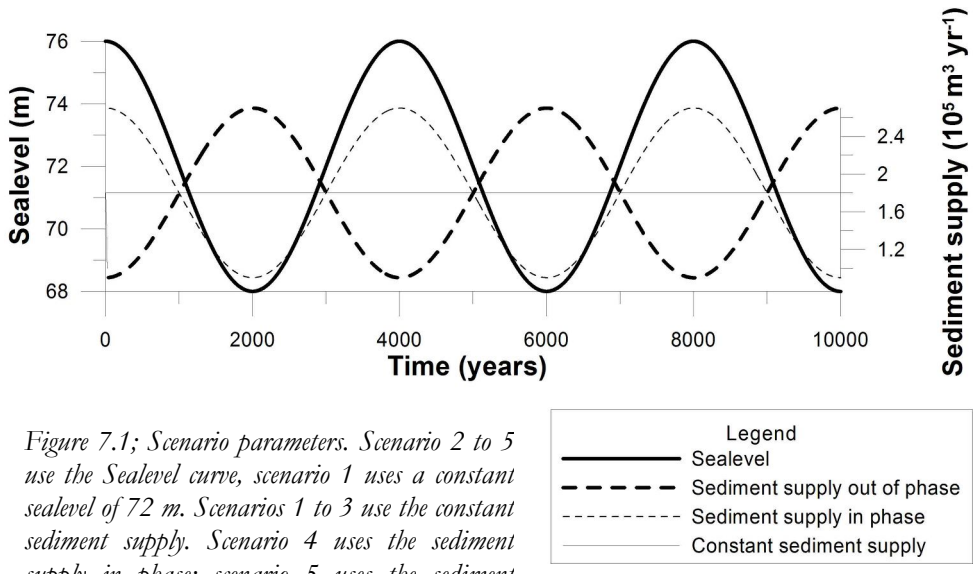

Figure 7.1; Scenario parameters. Scenario 2 to 5 use the Sealevel curve, scenario 1 uses a constant sealevel of 72 m. Scenarios 1 to 3 use the constant sediment supply. Scenario 4 uses the sediment supply in phase; scenario 5 uses the sediment supply out of phase.

Scenario number	Scenario description	Sea level change (m)	River discharge (m3/s)	Storm Wave distribution	Median Storm Wave Height	Clay fraction suspended load (m3/year)	Sand fraction suspended load (m3/year)
1	Static Sea level Mud Rich	0	2000	3.9-5.9	4.9	$8*10^5$	$2*10^5$
2	SL fluctuating Mud Rich	8 m, 2000 year phase	2000	3.9-5.9	4.9	$8*10^5$	$2*10^5$
3	SL fluctuating Sand Rich	8 m, 2000 year phase	2000	3.9-5.9	4.9	$6*10^5$	$4*10^5$
4	In-phase	8 m, 2000 year phase	1000-3000	3.9-5.9	4.9	$4*10^5$ - $12*10^5$	$1*10^5$ - $3*10^5$
5	Out-of-phase	8 m, 2000 year phase	1000-3000	3.9-5.9	4.9	$4*10^5$ - $12*10^5$	$1*10^5$ - $3*10^5$

Table 7.1; the parameters used in each scenario.

Reference scenario (1)
The base case, scenario 1, is not influenced by any external forcing factors in order to provide a comparative measure for other more complex scenarios. The median, deepwater storm wave height is 4.9 m, 95% of the storms fall in the range of 3.9 to 5.9 m.

Sea level fluctuating scenarios (2, 3)
Both scenarios with a fluctuating sea level forcing use the same sea level curve (Figure 7.1). The first is the SL fluctuating Mud-rich scenario (scenario 2), in which the mud is only 80% of the sediment load. A higher mud fraction will result in a system with no upper shoreface bed load activity and only progradation at the subaqueous rollover point. The SL fluctuating Sand-rich scenario (scenario 3) is distinguished by an increased sand/mud ratio of 0.4 to assess the relative effect of sand on coastal trajectory. The sand/mud ratios are the same for the fluvial sediment supply and the initial substrate.

Sea level and Supply fluctuating scenarios (4, 5)
Two scenarios with supply variation are discussed; the total sediment load over the entire runtime is not changed compared to the other scenarios but varies from 50% to

150% of the standard sediment input (Figure 7.1) in a sinusoid. The sand/mud ratio is kept at 0.2.
The in-phase scenario (4) is indicative of a location of the environment in which the sediment supply decreases simultaneously with the sea level. This can be interpreted as a shift from arid to semi-arid climate during warming (Langbein & Schumm, 1958). This could occur in cases of rerouting of large-scale monsoons, or due to shifts in the arid bands between 30 and 60 degrees latitude. This could also occur as a change from polar desert/tundra conditions in the catchment area during glacial periods to more temperate and humid climate zones. The out-of-phase scenario (5) is a representation of locations at latitudes where sediment supply increases as sea level drops. As the climate becomes colder and sea level drops, the sediment supply increases. This might be caused by a decrease in vegetation during glacial, and more arid periods, which will induce sediment erosion by decreasing the stabilising effects of vegetation. This could occur as a change from tropical, humid conditions in the catchment area during interglacial periods to more arid, subtropical climates during glacial periods.

Shoreline morphology
Shoreline protuberances are measured as a deviation from the mean. The mean standard deviation of each coastal node is plotted relative to the entire coastline. This gives us a general measure about the entire coastline morphology, as the standard deviation will become large as local progradation occurs. But it does not give us much information on local changes; I wish to quantify the development of delta lobes, which are on a smaller scale than the entire delta. The curvature of the coastline is calculated by determining the second derivative of the coastline for each coastal segment using a cubic spline routine. The mean curvature gives a measure of the smoothness of the entire coastline.

Results

Shoreline evolution

In order to illustrate the shoreline evolution, the model is run with constant sea level, sediment and discharge input for 3000 years (using the same input as scenario 1). After this time, the model is run for another 3000 years with the sediment and discharge input turned off, to mimic a major upstream avulsion. Figure 7.2 shows the curvature of the shoreline over the entire 6000-year time series. The delta formation shows a stepwise growth, with a rapid increase in curvature when a new delta lobe is created. As progradation slows due to increasing water depth and increased subaerial sediment sequestration the littoral drift becomes more influential and curvature decreases exponentially. This feature is similar to the decreasing curvature after the river is turned off after 3000 years.

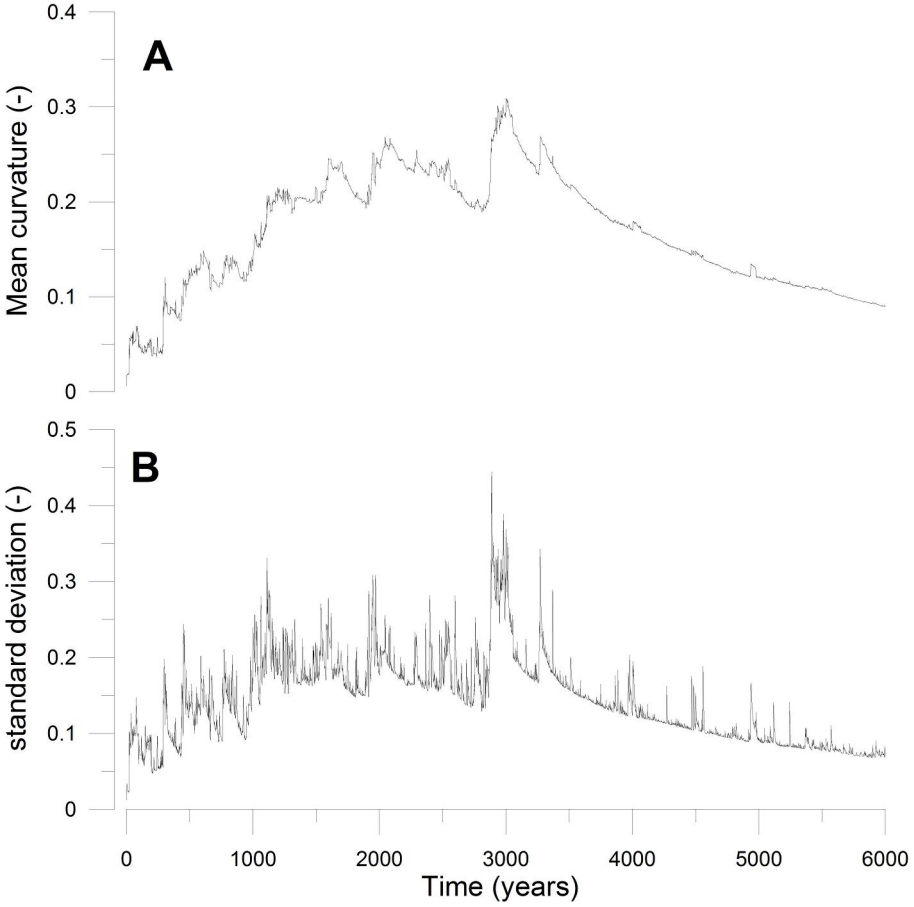

Figure 7.2; Mean curvature of the coastline over 6000 years (A). At 3000 years the river input ceases. Note the rapid changes during progradation related to delta lobe switching. After river input ceases, the coastline curvature decreases exponentially. The mean standard deviation (B) shows a similar signal.

Scenario 1; Static Mud-Mud Rich

The net result is a relatively constant progradation rate of the subaqueous delta front/rollover point. The coastal progradation is mainly dominated by the location of influx of a tributary (Figure 7.3) . When the river reaches the sea the great amount of sediment results in local progradation, with some removal by the longshore transport and a wave-influenced delta lobe progrades. When an avulsion removes the influx of sediment locally, the delta lobe is rapidly reworked and smoothed due to the excess sediment transport capacity of the wave-induced longshore transport. Thus the local foci of coastal progradation are mainly controlled by the avulsion rate. The subaqueous delta front is less sensitive to this process because of the dispersive nature of the finer sediments delivered there.

The curvature (Figure 7.4A), standard deviation (Figure 7.4B) and the distribution of curvature indicates a general trend of overall increase of curvature. A smooth delta front is created as delta size increases. Over shorter time scales the effect of autogenic sediment pulses can be observed, produced by shifts in alluvial sediment sequestration after major nodal avulsions. These pulses (cf Chapter 6, this thesis; Kim et al, 2006) allow rapid, local progradation (the spikes), but consistent reworking by waves results in a smoothly decreasing curvature of the coastline

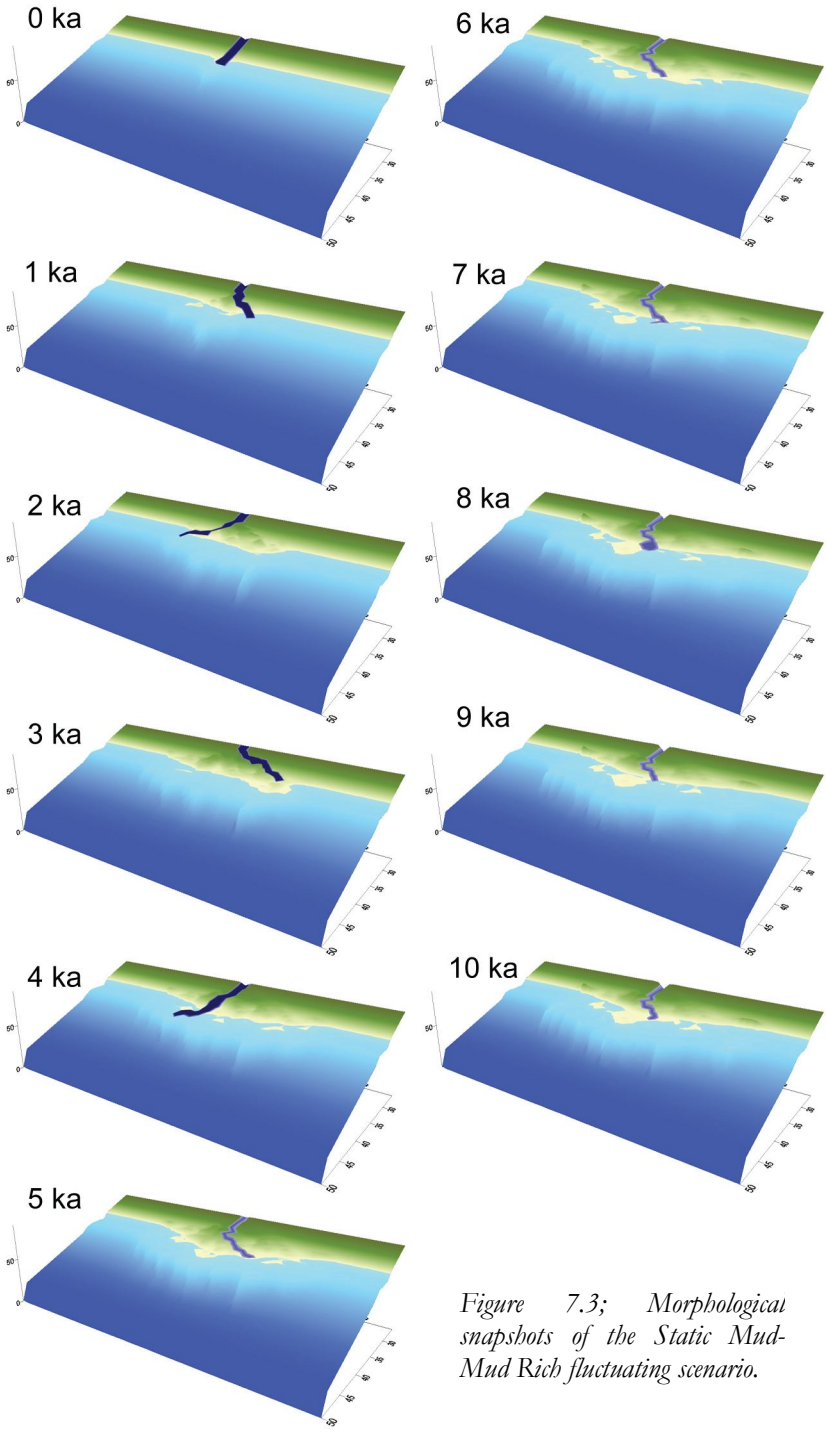

Figure 7.3; Morphological snapshots of the Static Mud-Mud Rich fluctuating scenario.

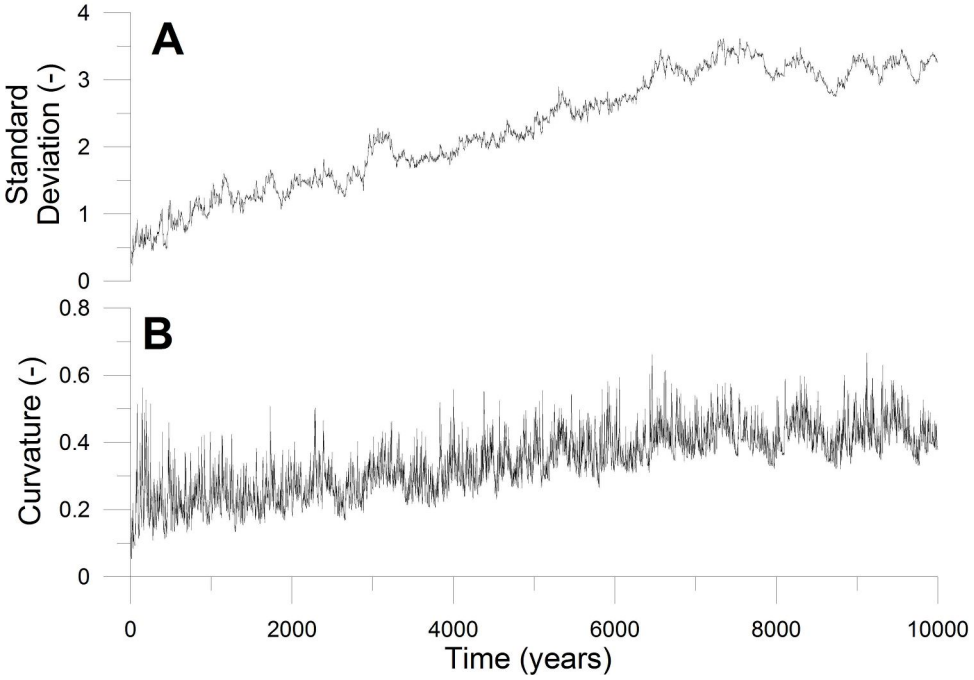

Figure 7.4; Coastline curvature of the Mud rich, Static Sealevel scenario. (A) The standara deviation as compared to the initial straight coastline, (B) The curvature shows the local raggedness of the coastline.

Scenario 2; SL fluctuating Mud-rich scenario

The rapid sea level lowering induces a forced regression and an associated translation of the shoreline and the subaqueous rollover (Figure 7.5). During the sea level rise a significant part of the topset and coast is eroded and transported offshore, facilitating continued progradation of the subaqueous rollover.

The overall coastline shows a pseudocyclic increase and decrease forced by sea level fluctuations (Figure 7.6A), whereas the overall trend shows an increase in curvature over time. The coastline is significantly more rugged during sea level rise (Figure 7.6B), as coastal erosion is limited to those regions not receiving fluvial sediment input. Thus the local progradation at the distributary mouths and erosion along the rest of the shoreline result in a considerable increase in curvature.

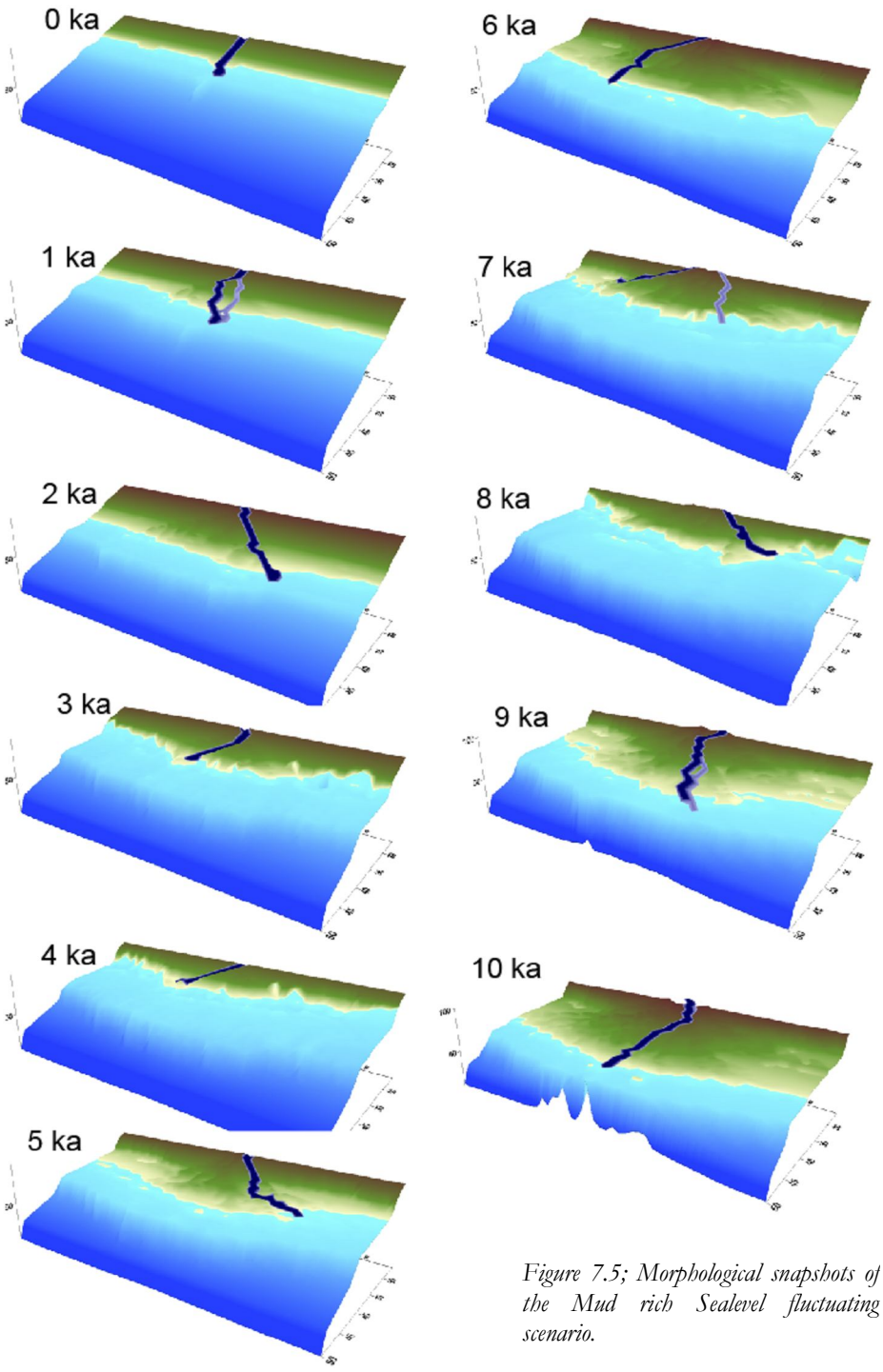

Figure 7.5; Morphological snapshots of the Mud rich Sealevel fluctuating scenario.

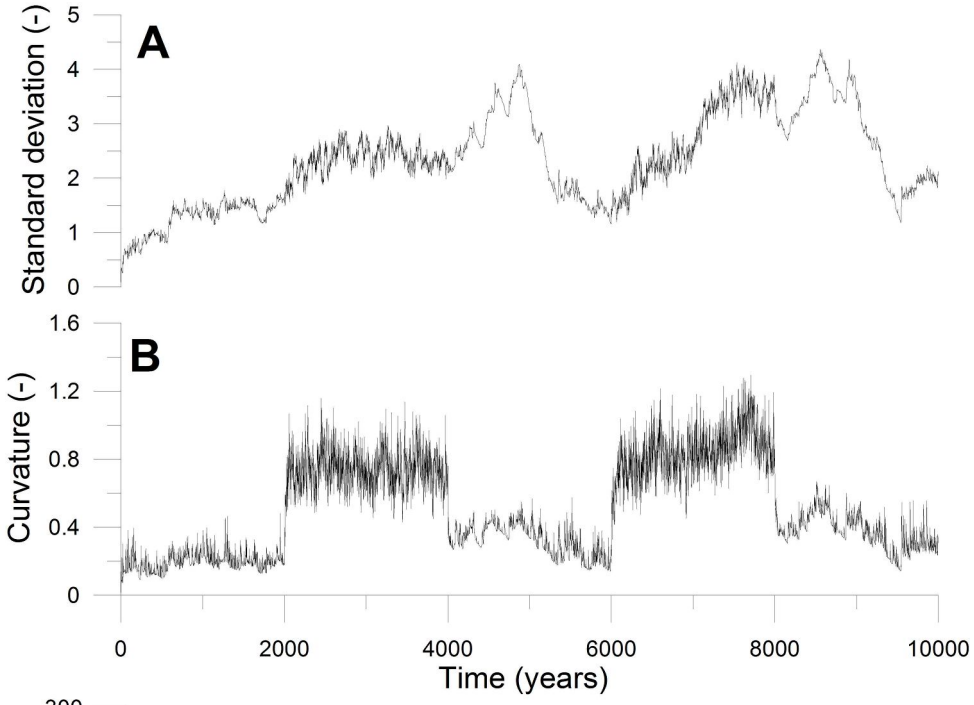

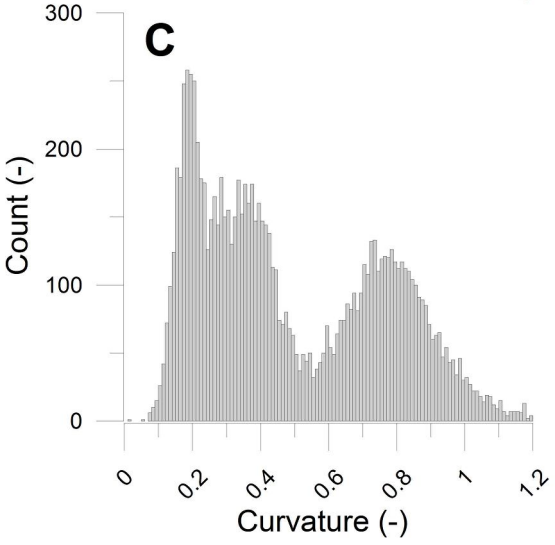

Figure 7.6; Coastline curvature of the Mud rich, Sealevel fluctuating scenario. (A) The standard deviation as compared to the initial straight coastline, note the increase of the standard deviation during sealevel rise and highstand is associated with an increase in total curvature and progradation. During sealevel fall, the areas with no or little direct sediment supply are drowned much faster. (B) The absolute curvature shows the local raggedness of the coastline, notable during sealevel fall the coastline is much smoother than during sealevel rise. Probably due to localised coastal erosion. The histogram of the curvature distribution (C) shows the bimodal distribution due to the difference in response of coastline curvature to the regressive and transgressive settings.

Scenario 3; SL fluctuating Sand-rich scenario

This scenario allows considerably more sandy barriers to develop (Figure 7.7). Associated with the higher sand input is the decreased net coastal erosion. Because of the diminished sediment supply, provided by wave erosion, the net progradation of the subaqueous rollover point is less than the mud-rich scenario 2. Additionally the compound-clinoform, subaqueous topset is shorter, as there is less sediment available for diffusive transport. The coastline progrades faster due to the larger amount of sand available for upper shoreface deposition.

The coastline standard deviation (Figure 7.8A) and curvature (Figure 7.8B) shows a similar response to the scenario 2, except for the distribution of the curvature (Figure 7.8C). The first peak of the bimodal distribution is associated with the regressive coastlines and is much narrower than the mud rich (cf Figure 7.6C). This narrow band of curvatures is associated with the larger amount of sand present, which allows littoral drift to become more dominant. Mud cannot (usually) be transported by this process.

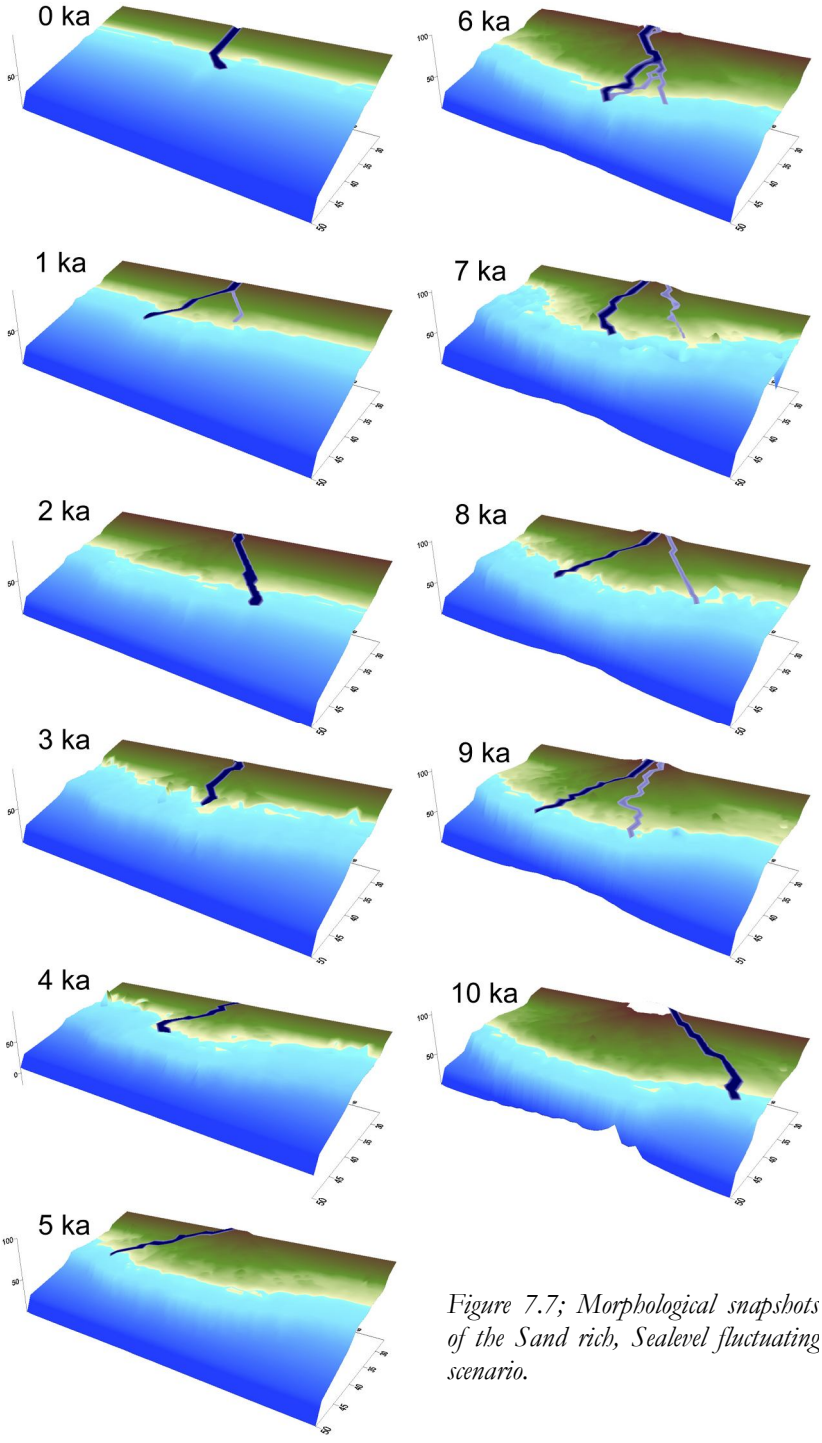

Figure 7.7; Morphological snapshots of the Sand rich, Sealevel fluctuating scenario.

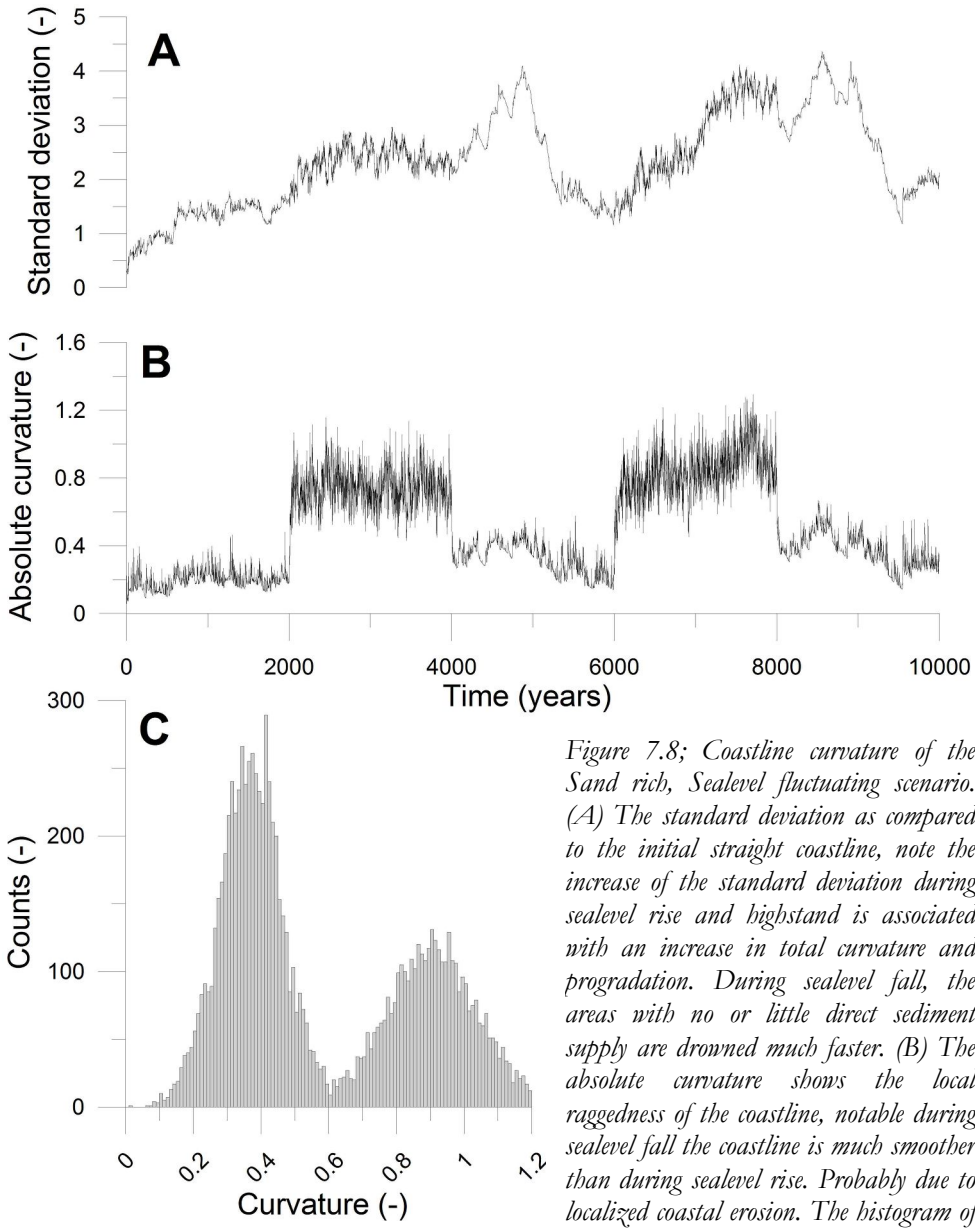

Figure 7.8; Coastline curvature of the Sand rich, Sealevel fluctuating scenario. (A) The standard deviation as compared to the initial straight coastline, note the increase of the standard deviation during sealevel rise and highstand is associated with an increase in total curvature and progradation. During sealevel fall, the areas with no or little direct sediment supply are drowned much faster. (B) The absolute curvature shows the local raggedness of the coastline, notable during sealevel fall the coastline is much smoother than during sealevel rise. Probably due to localized coastal erosion. The histogram of the curvature distribution (C) shows the bimodal distribution due to the difference in response of coastline curvature to the regressive and transgressive settings.

Scenario 4; Sea level cycles with in-phase sediment supply variations, Mud-rich scenario

The geomorphological response (Figure 7.9) to this scenario is similar to scenario 2, which shares the same mud-sand ratio. The relative input of fluvial sediment to the sea is somewhat mitigated due to the in-phase link of sediment supply and relative sea level. As sea level drops, the increase in gradient and length of the subaerial topset usually results in a net increase of sediment input to the sea. As this is decreased in scenario 4, this effect is smaller than usual. The bimodal distribution of coastline curvature (Figure 7.10B and 7.10C) is less pronounced than scenario 2. The increase in shoreline protrusion during sea level fall (Figure 7.10A) is much clearer than scenario 2, due to the initially high sediment input during the first phase of sea level lowering.

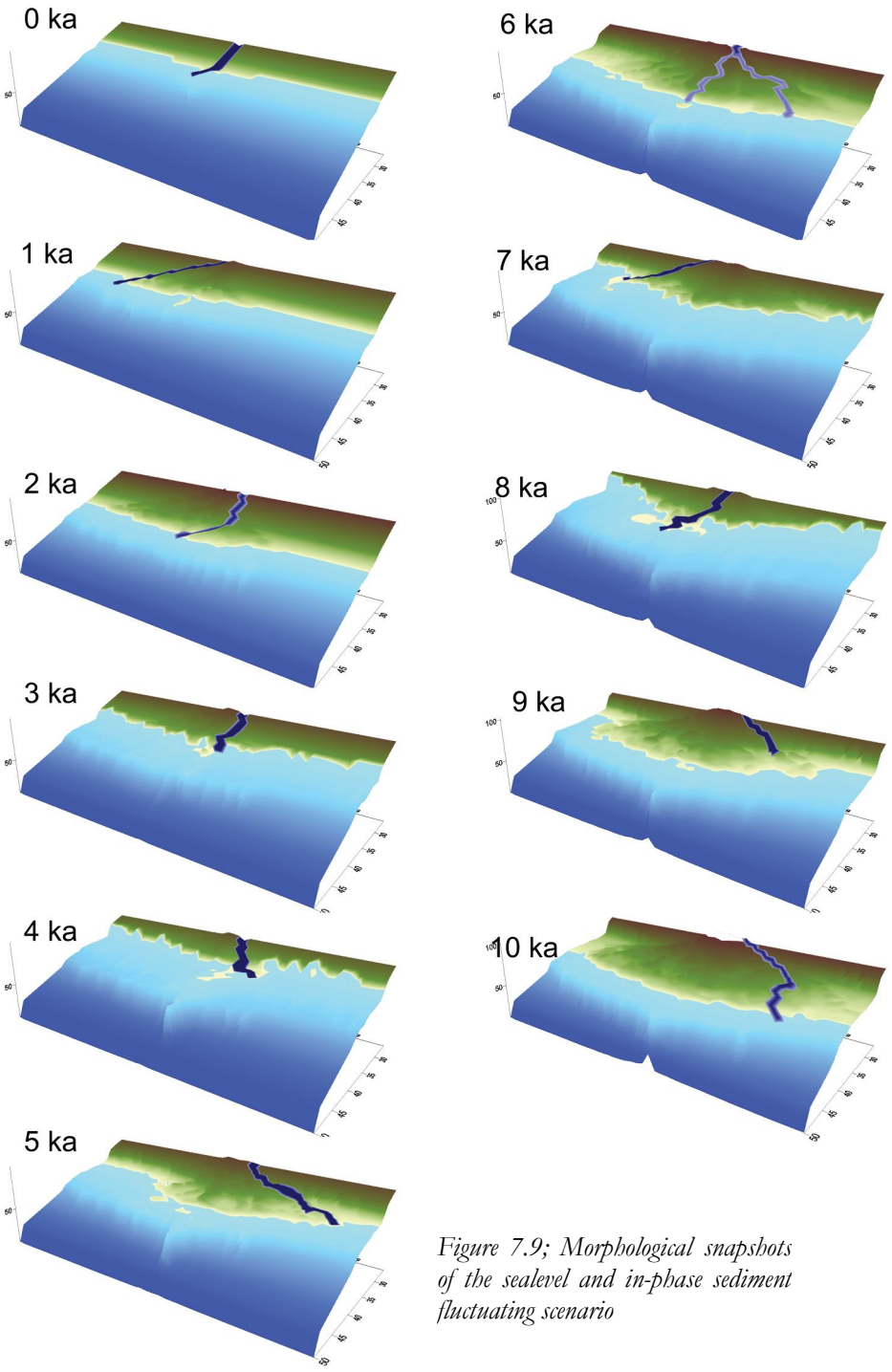

Figure 7.9; Morphological snapshots of the sealevel and in-phase sediment fluctuating scenario

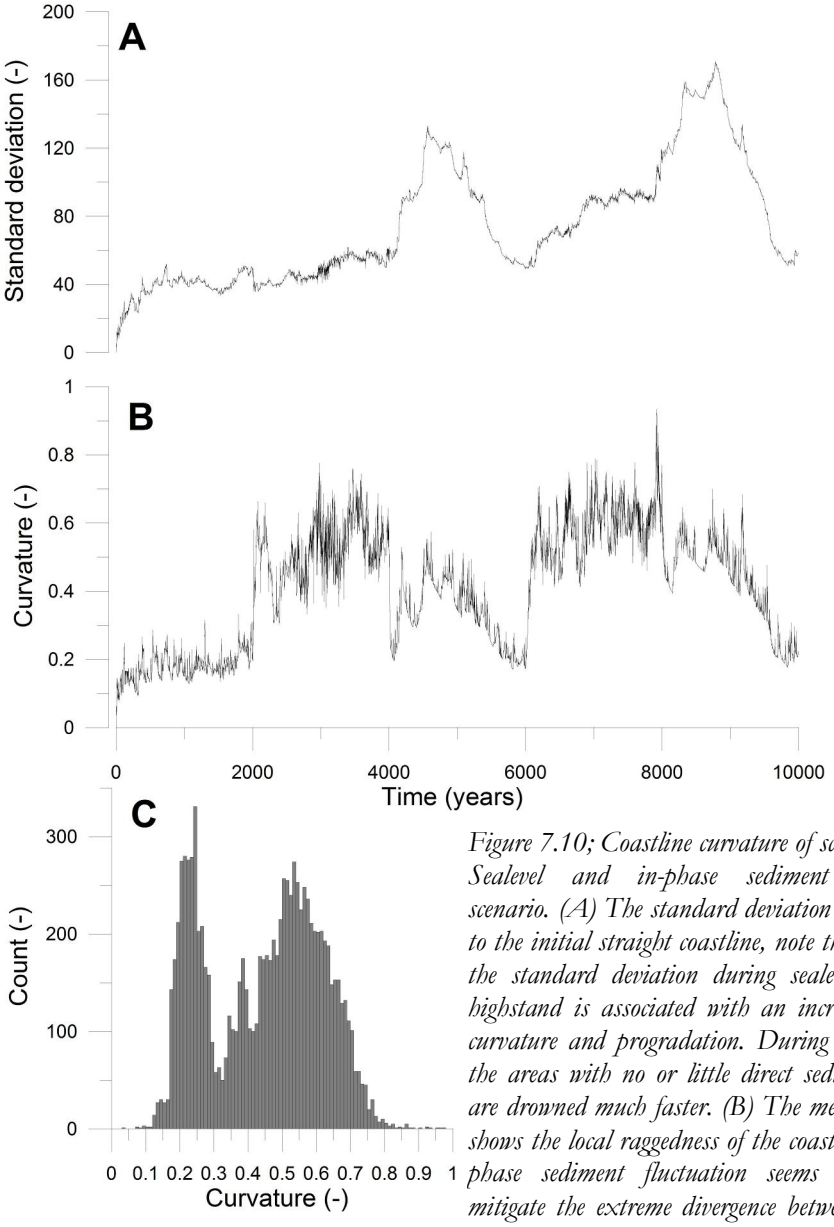

Figure 7.10; Coastline curvature of scenario 4; the Sealevel and in-phase sediment fluctuating scenario. (A) The standard deviation as compared to the initial straight coastline, note the increase of the standard deviation during sealevel rise and highstand is associated with an increase in total curvature and progradation. During sealevel fall, the areas with no or little direct sediment supply are drowned much faster. (B) The mean curvature shows the local raggedness of the coastline. The in-phase sediment fluctuation seems to partially mitigate the extreme divergence between regressive and transgressive curvature observed in scenarios 2 and 3. The histogram of the curvature distribution (C) shows the bimodal distribution due to the difference in response of coastline curvature to the regressive and transgressive settings. The transgressive distribution is much narrower than the regressive distribution.

Scenario 5; Sea level cycles with out-of-phase sediment supply variations, Mud-rich scenario

The geomorphological response (Figure 7.11) to this scenario is somewhat similar to scenario 2, which shares the same mud-sand ratio. The relative input of fluvial sediment to the sea is increased due to the out-of-phase fluctuation of sediment supply and relative sea level. As sea level drops, the increase in gradient and length of the subaerial topset usually results in a net increase of sediment input to the sea. As the sediment input is decreased during sea level lowstands, this effect is larger than usual. This has a strong effect on lobe distribution; during highstands the sediment supply is relatively low, which slows topset aggradation and concomitantly inhibits nodal avulsions. In several cases the channel is incised to the side of an old channel belt complex and remains fixed on one side of the delta. This results in a strongly asymmetric delta development until aggradation catches up and allows the feeder channels to migrate freely across the delta.

The distribution of the coastline curvature (Figure 7.12B and 7.12C) is still partitioned into two modes, yet the bimodality is severely obscured due to the wide distribution of possible curvatures during transgression or regressions. The coastline protuberance is again greatest during sea level lowering, which hints at the large differentiation in lateral coastal migration during forced regressive systems tracts.

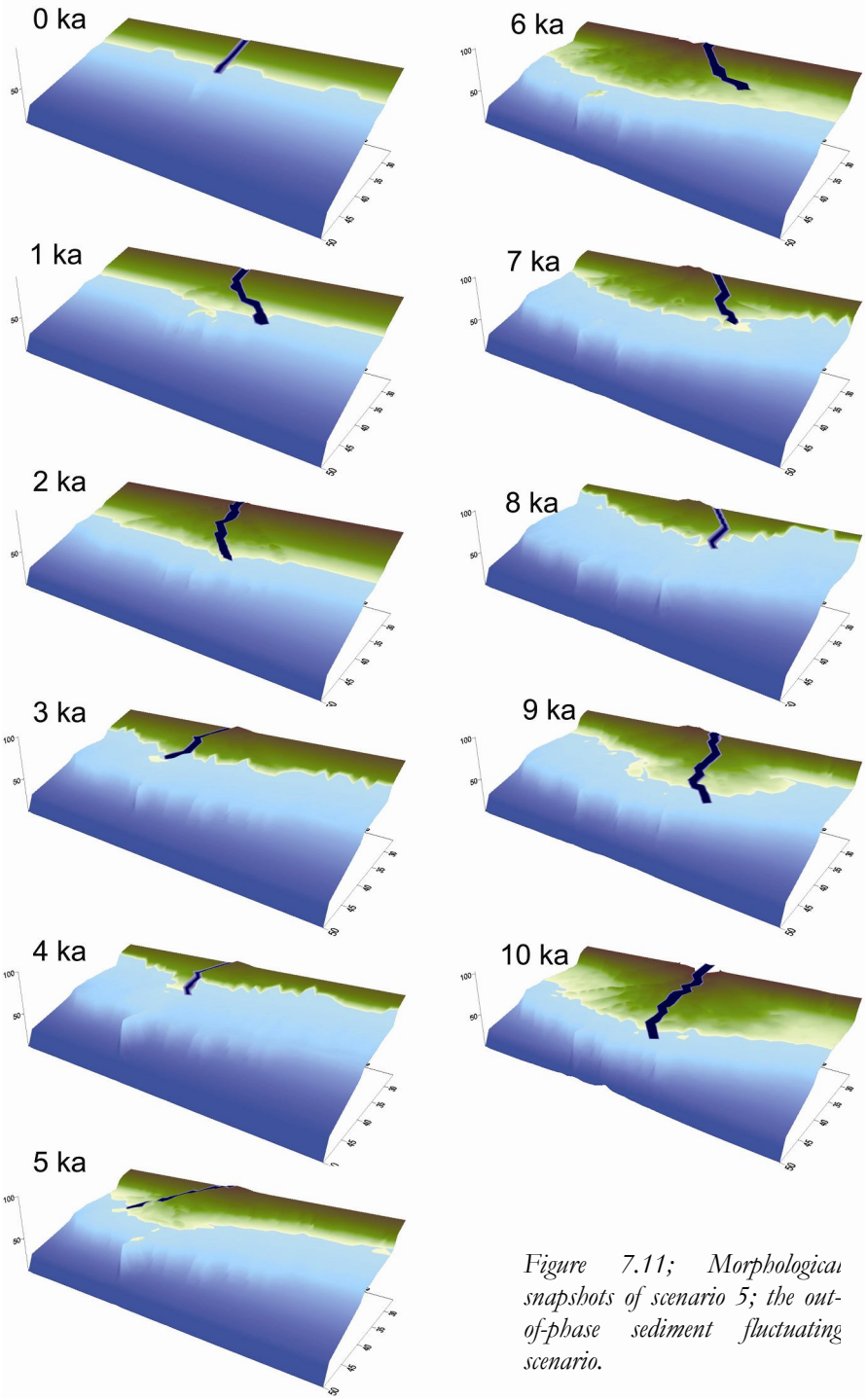

Figure 7.11; Morphological snapshots of scenario 5; the out-of-phase sediment fluctuating scenario.

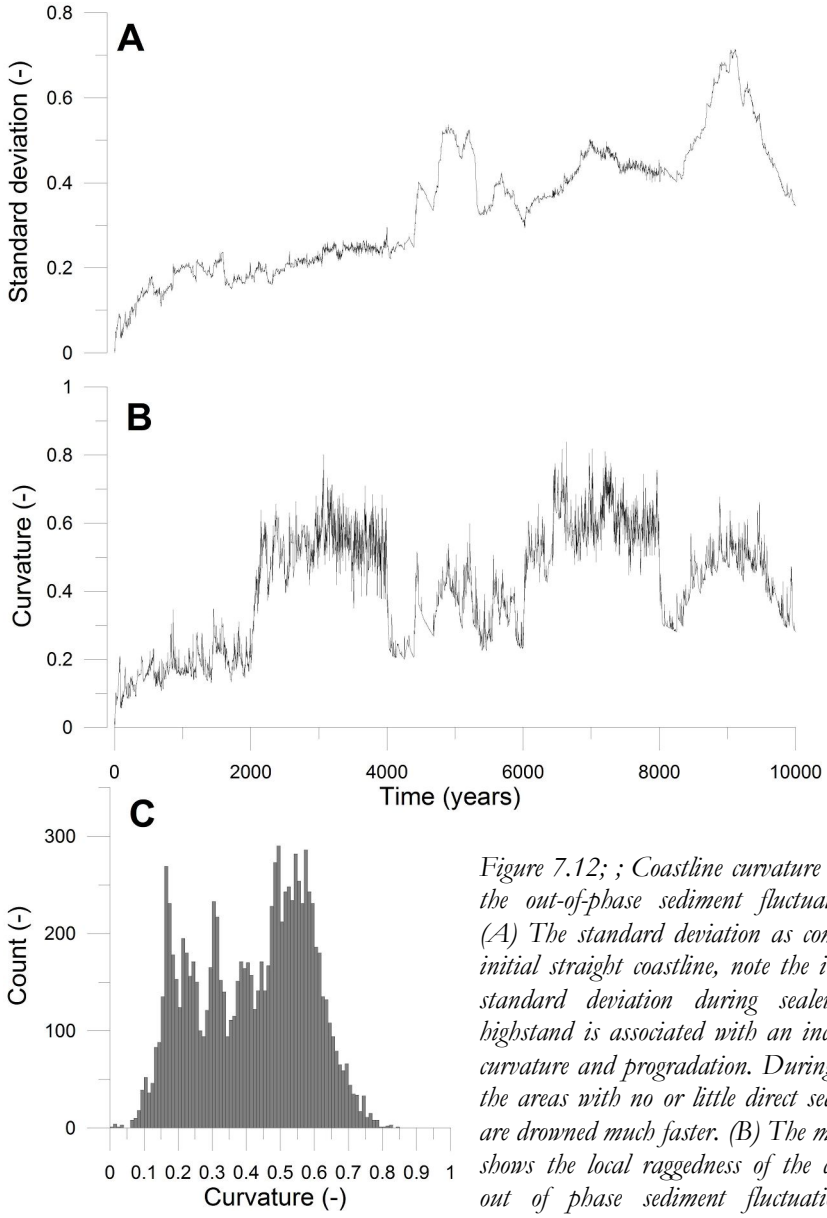

Figure 7.12; ; Coastline curvature of scenario 5; the out-of-phase sediment fluctuating scenario. (A) The standard deviation as compared to the initial straight coastline, note the increase of the standard deviation during sealevel rise and highstand is associated with an increase in total curvature and progradation. During sealevel fall, the areas with no or little direct sediment supply are drowned much faster. (B) The mean curvature shows the local raggedness of the coastline. The out of phase sediment fluctuation seems to partially mitigate the extreme divergence between regressive and transgressive curvature observed in scenarios 2 and 3. The histogram of the curvature distribution (C) shows the distribution due to the difference in response of coastline curvature to the regressive and transgressive settings. The distribution shows a much less distinct bimodal distribution than other distributions.

Discussion

Increased net progradation due to sediment reworking by wave ravinement.

The main difference between the static and fluctuating sea level scenarios is the large increase in net progradation at the end of the model run (compare Figure 7.3 to Figure 7.5 at 10 ka). Fluvial incision during sea level lowering and lowstands will have provided some extra sediment, but the net effect will be minimal as the fluvially incised valleys are quickly filled in during transgression and highstand. The only source of sediment is the substrate, which is reworked during transgressions and highstands. The mud fraction of this reworked sediment is pumped towards the subaqueous foreset and lost to the shallow system. Effectively the subaqueous rollover point progrades continuously during any sea level cycle, though it will slow severely during highstands as much of the fine sediment is deposited temporarily on the shallow marine topset of the compound clinoform. During the early highstand, sediment will be sequestered on the subaerial and subaqueous topsets as the river attempts to reach grade and the marine topset aggrades to the hypothetical wave base. During relative sea level fall much of this material will be eroded rapidly and transported offshore, thus facilitating an increased progradation rate of the forced regressive wedge. The initial topography of the grid is of some importance, especially for the purely fluvial part of the model domain. But the formidable power of the waves is sufficient for the system to create its own bathymetry. The bathymetry does influence the rate of subaqueous rollover point progradation, as the toe of the clinoform becomes deeper the net progradation rate of the subaqueous delta front decreases (see Figure 7.13, scenario 1).

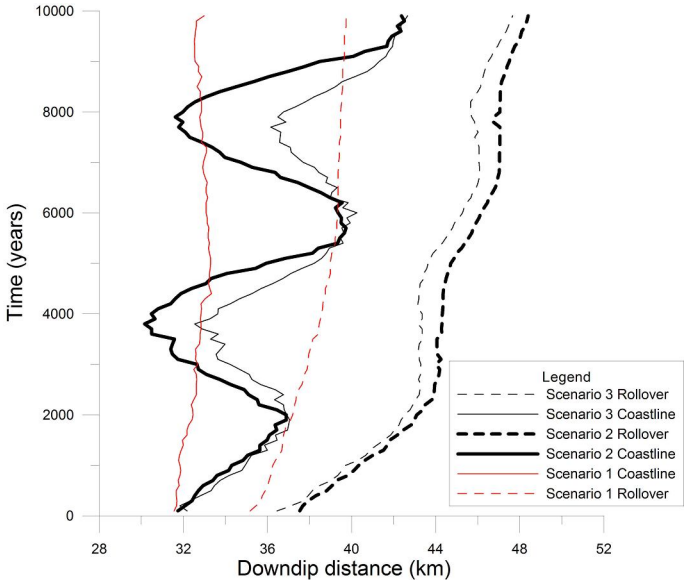

Figure 7.13; the downdip migration of the averaged coastline (continuous lines) and the averaged subaqueous rollover point (dashed lines) for scenarios 1 to 3.

Nittrouer et al (1996) observed the difference in progradation rate between the subaqueous delta front and the shoreline deposits on compound clinoforms. This difference is observed in our base case scenario (figure 7.13) and can be explained by differences in the bathymetry of foreset toe (deeper waters results in slower progradation) and the water depth near the coastline, the sediment transport capacity of the mechanism of subaqueous topset process (be it waves, currents or other shallow marine hydrodynamic processes), grainsize distribution and sediment partitioning between the subaqueous and the coastal foresets.
During transgressions the amount of material supplied by coastal erosion is moved to the subaqueous topset, which creates transgressive, aggradational deposits on the shelf. These deposits are stable as the effective wave base rises with sealevel. Figure 7.13 clearly shows that the rollover point does not retreat during transgressions, as there is no mechanism to remove the sediments there. But instead the subaqueous topset increases in length and aggrades rapidly. Even under relatively low-amplitude sea level cycles, wave erosion provides significant amounts of sediment to the subaqueous delta front and effectively decouples the subaerial delta front development from the subaqueous rollover point. There is a significant time lag in subaqueous migration; the progradation of the subaqueous rollover point continues for a significant amount of time during early transgression (Figure 7.13 after 2000 and 6000 years). Large amounts of sediment are pumped to the foresets due to wave erosion during the creation of the wave ravinement surface.
The mean development of the systems (Figure 7.14) is dominated by the erosive power of waves under sealevel fluctuations. Effectively, wave erosion and reworking completely overprints even the significant fluctuations of sediment supply introduced in scenarios 4 and 5. The sediment fluctuation is noticeable, but most deposits are reworked during transgressions and regressions effectively masking the original input variations. Additionally the system filters the sediment input to the coast and subaqueous rollover point by sediment sequestration in the alluvial domain. The rollover point migration paths are averaged over the entire coastline. Local variation in fluvial sediment supply will produce lateral differences alongshore, as can be observed in Figure 7.11 where fluvial incision allows an asymmetrical profile to develop.

Stratigraphic results of wave induced sediment redistribution
Figure 7.13 illustrates the coastline and subaqueous rollover point migration through time for scenarios 1 to 3. The clear lack of sediment input provided by the wave ravinement during sea level cycles is clearly illustrated by the decoupling between the coastline and rollover points in the sea level cycling scenarios and the static scenario. The rollover point never actually retreats during sea level cycles, as this does not undergo erosion. Figure 7.14 shows the coastline and subaqueous rollover point migration through time for scenarios 2, 4 and 5. The effect of the sediment supply seems minimal, although some local variation occurs.
As the sea level does not fall below the shelf-edge and the river is kept above grade no erosion takes place and the normal regressive and forced regressive sequences are separated by a correlative conformity (sensu Posamentier & Allen, 1999). The systems shows a clear forced regressive wedge of the subaerial delta deposits developing on

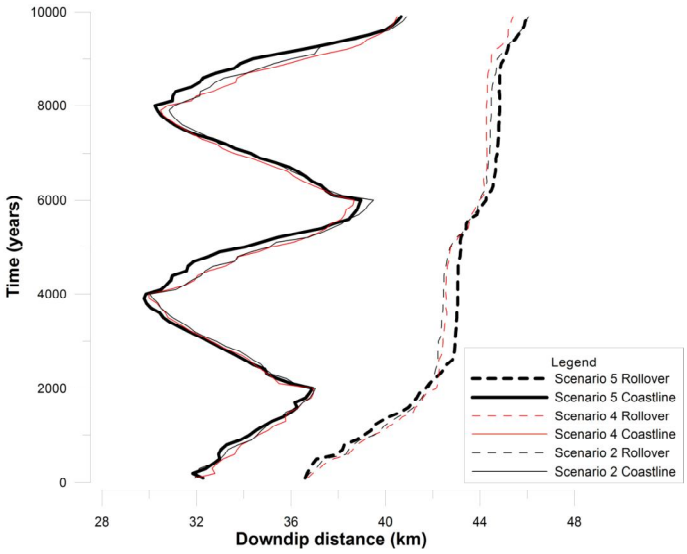

Figure 7.14; the downdip migration of the averaged coastline (continuous lines) and the averaged subaqueous rollover point (dashed lines) for scenarios 2, 4 and 5.

the shelf as sea level is lowered, indicative of a low angle shelf system. Note that the nomenclature used here is approximate, as the forced regression is only felt strongly on the subaerial part of the clinoform. The subaqueous clinoform foresets continue prograding during the subaerial delta front progradation, as the subaqueous topset is either eroded during sealevel lowering, resulting in a regressive surface of marine erosion or accommodation space decreases to nil by lowering of the effective wave base.

The wave ravinement surface

Over sea level cycles the coastline seems to stay much smoother during sea level fall than during sea level rise. Its effect on preservation potential is immense. The transgressive erosive surface is often described as an unstoppable force rolling over and reworking the entire shelf. Obviously this is the case for areas with little sediment input, yet the numerical experiments clearly show that in areas with a large sediment input erosion can be halted or slowed, depending on wave climate, rate of sea level rise, substrate cohesion and sediment supply. Fine-grained sediments will be immediately dispersed to deeper waters and will have little influence; only coarse-grained sediments will remain in place. Thus the spatial variability of the effective reworking associated with a wave ravinement surface is highly dependent on local sediment supply.

Climatic experiments

The mean development of the systems (Figure 7.14) is dominated by the erosive power of waves under sealevel fluctuations. Effectively, wave erosion and reworking completely overprints even the significant fluctuations of sediment supply introduced in scenarios 4 and 5. Additionally the system filters the sediment input to the coast and subaqueous rollover point by sediment sequestration in the alluvial domain. The rollover point migration paths are averaged over the entire coastline. Local variation in fluvial sediment supply will produce lateral differences alongshore, as can be observed in Figure 7.11 where fluvial incision allows an asymmetrical profile to develop.

Wave-influenced sequence boundaries

The response of a fluvio-deltaic system to a fall in base level is largely dependant on the emerged profile (Emery & Myers, 1996). If the profile is at a lower angle than the equilibrium profile a forced regression will allow aggradation on the emerged surface. If the emerged surface is at a higher angle than the equilibrium profile, a subaerial unconformity will develop.

As sea level does not fall below the shelf and subsequently keeps the river above grade the deposits of the sea level cycles are not truncated but separated by a correlative nonconformity. The systems show a clear aggradation on the shelf, as sea level is lowered, indicative of a low-angle shelf system. This low-angle morphology is not inherited by ancient systems, but rather inherently produced by the continued wave reworking, which effectively creates its own low-angle shelf system. After several sea level cycles the strong wave influence has created a platform due to continuous wave reworking. This low-angle shelf allows rapid progradation of the subaerial delta platform during relative sealevel highstands and falls. Only where sea level falls below the subaqueous rollover point will fluvial incision occur and an erosional, subaerial unconformity will form. Only under very large glacio-eustatic cycles can large-scale incision and lowstand systems occur. This contrasts starkly with fluvially dominated systems where the system creates a high-angle shelf. A lowering of base level will therefore more likely induce a subaerial unconformity than in wave-dominated system would. These results suggest that long-lived, wave-influenced delta systems most likely contain fewer subaerial unconformities than fluvial dominated delta systems.

Coastline curvature

During sea level rise sediment sequestration by alluvial aggradation will decrease sediment supply to the coastline. Only small amounts of sediment are available to compensate localized coastal erosion by littoral drift. Wave action cannot respond fast enough to compensate for the large lateral discrepancies. Littoral drift is insufficiently powerful to transport enough sediment from the prograding delta lobes to the localized eroded areas. Under conditions of sea level rise the fluvial component controls delta development more than during sea level fall. In a smaller-scale exercise Niedoroda et al (2003) found a similar change to a jagged coastline during highstands vs. lowstands. The shoreline protuberance, measured using the proxy of standard deviation (Figure 7.6A and 7.8A) shows a much slower response to sealevel change.

The most marked change is the increase during sealevel fall as the forced regressive wedge progrades rapidly where fluvial input is concentrated (compare Figures 7.5 and 7.7). The areas receiving only indirect sediment input (through littoral drift) prograde much slower, yet without the marked increase in curvature observed during sealevel rise.

Fluvial influence on the shoreface

Fluvially generated autogenic sediment pulses can be observed (Figure 7.5) in the coastline development. These pulses (cf Chapter 6, this thesis; Kim et al, 2006) allow rapid progradation (the spikes), but are consistently reworked by the waves resulting in a smoothly decreasing curvature of the coastline. Thus the net effect is relatively small. Fluvial influence on shoreface evolution is greatest during sea level rise when the decoupling between prograding delta lobes and drowning and/or eroding coastal segments is greatest. Areas receiving more sediment will suffer less from wave reworking.

Conversely the influence of wave action on fluvial aggradation and stability is indirect. Wave removal of sediments from the shoreface through either resuspension events or gradual longshore transport will do not allow the fluvial channels to aggrade, effectively reducing avulsion frequency and stabilising the system. In real-world systems, aeolian action will create high dunes on the coastal barrier, which will block outflow paths. For now, the model used here cannot recreate this sediment transport mechanism, though will be an important addition to determine barrier and fluvial stability.

Coastline trajectory

The migration through time and space in a cross-section for the Mud rich Fluctuating Sea level scenario coastline and rollover point is illustrated in Figure 7.15. The coastline trajectories (Figure 7.15) indicate a very low angle of turnaround. Løseth et al (2006) correlated low angles of turnaround with a short pinchout distance (effectively

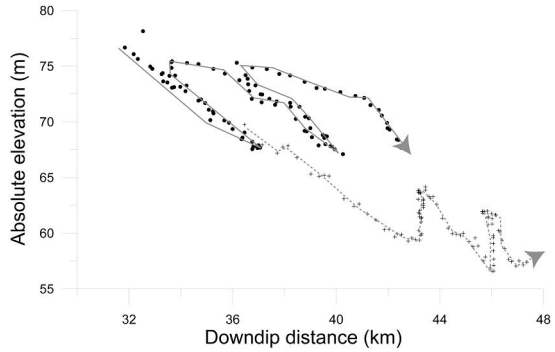

Figure 7.15; the vertical and horizontal mean migration of the coastline (black dots) and the subaqueous rollover points (crosses) for the Mud rich Fluctuating SL scenario. The lines with arrows indicate the time path. Note the highs in each graph correspond to the highstands at 0, 4000 and 8000 years and the lows to the lowstands at 2000 and 6000 years.

the horizontal distance between marine muddy deposits and continental to brackish deposits). The exact correlative mechanism and internal pinchout architecture may be determined using similar techniques described in this paper. This will give us a heightened insight into sedimentary architecture of wave-influenced systems under sealevel cycles.

Rollover points have been used to determine onlap/offlap charts, resulting in generalized sealevel curves (Haq et al, 1987). The decoupling between the coastal and subaqueous rollover points indicates a rather tenuous relationship between subaqueous rollover points and sealevel. Catuneanu et al (2009) also indicated a decoupling between shoreline and shelf-edge trajectory in the Pelotas Basin, southern Brazil, but only during transgressive systems tract and highstand normal regressive systems. Consequently, care must be taken in assuming a linear relationship between rollover point and sealevel. As the subaerial delta front has a much lower preservation potential than the subaqueous rollover points, most rollover points observed in seismics will be subaqueous shelf breaks. This point cannot be used as a direct proxy for sealevel as relative sealevel rises will be underrepresented when using the subaqueous rollover point.

Conclusions

Wave ravinement, even under low-amplitude sea level fluctuations, will provide considerable amounts of sediment to the subaqueous foresets, allowing rapid progradation. This mechanism increases the subaqueous topset length of the compound clinoform as coastal erosion is increased and this material is deposited on the subaqueous foresets.

The numerical experiments show that in areas with a large sediment input, erosion by wave ravinement can be halted or slowed, depending on wave climate, rate of sea level rise, substrate cohesion and sediment supply

During sea level rise, regression of the coastline may correspond with aggradation and/or non-deposition of the subaqueous topset. The correlation between rollover points and sealevel is a tenuous one, for direct correspondence only the coastal rollover point should be used as relative sealevel rises will be underrepresented when using the subaqueous rollover point. These results suggest that long-lived, wave-influenced delta systems most likely contain fewer subaerial unconformities than fluvial dominated delta systems. Only under very large glacio-eustatic cycles do large-scale subaerial unconformities occur.

Chapter 8
General discussion

Aggregated modelling

Sedimentary environments are always open to influences from other environments. The only exception might be deep marine, mass-transport deposits which will mostly be influenced by upstream controls only. The most complex features occur at the boundaries between sedimentary environments where different processes fight for control. So as to be able to study these feedback mechanisms SimClast aggregates various processes in continental and marine environments. This has allowed us to study the upstream and downstream feedback mechanisms under the influence and absence of allogenic forcing. Although the research presented in this thesis is a useful tool for explaining fluvial and delta behaviour, the ultimate goal of fully source-to-sink modelling is still quite far away. This will require coupling of different models for sediment production in the drainage basin and the inclusion of subaqueous gravity flows.

The next paragraphs synthesise the most important findings of the modelling exercises in this thesis.

Channel network development

Our study on the development of river-dominated low-angle shelf deltas clearly shows an initial increase in the number of distributaries. Yet, the number of distributaries may decrease during progradation of the delta, notably after major nodal point avulsions. On the scale of the entire delta (i.e. several delta lobes), a quasi-cyclic autogenic increase and decrease of distributaries is expected and indeed observed in model output.

Marine-continental correlation

The main reason why rivers avulse is, as in most processes clastic, gravitational advantage. Yet rivers maintain their stability for a longer time than expected from purely diffusive transport. An increase in active channel length due to progradation results in a consequent increase in sedimentation on the delta plain relative to the delta front and prodelta. After an avulsion much sediment is sequestered in the channel path just downstream of the avulsion because the slope is very low. Conversely, headward erosion may occur upstream of the avulsion point. This phenomenon will be strongest in areas were channels are very stable, i.e. high-gradient deltas with strong vegetation and limited flood peaks. In low-gradient areas with easily erodible banks, high frequency avulsions will most likely obscure any sediment sequestration events.

Post-avulsion erosion in the upstream fluvial channels may thus induce terrace formation, which, in turn, allows localized downstream fluvial aggradation and slows the progradation rate of the newly created prograding delta lobe due to sediment starvation. These model results indicate phases of subgrid-scale, upstream terrace formation by channel incision. Real-world examples of this process might give

interesting insights into this complex response (cf Bull, 1991) to delta-lobe switching. This inherent sedimentary feedback mechanism provides a method to correlate fluvial processes to marine deposition.
Yet the outcome does increase possible explanations for sedimentary features in ancient deposits. Incision or aggradation cannot be automatically ascribed to allocyclic controls because it may be a product of autogenic forcing. This mechanism produces an inherent range in fluvial profiles without changes in upstream or downstream control, which seems to be a logical explanation for high-frequency incision-aggradation cycles observed in the geological record.

Clinoform behaviour under influence of a strong wave climate
In wave-influenced systems the erosive power of the waves will produce erosive surfaces and consequently redistribute this sediment in reaction to changes in sealevel. In order to assess this mechanism and its influence on deltaic morphology and sedimentary architecture we model several cyclic sealevel fluctuations. Relative sea level rise increases local coastline curvature due to the increased discrepancy between eroding coastal sections and sections receiving direct sediment input. Wave ravinement, even under low-amplitude sea level fluctuations, provides considerable amounts of sediment to the subaqueous foresets, allowing rapid progradation. This mechanism increases the subaqueous topset length of the compound clinoform as coastal erosion is increased and this material is deposited on the subaqueous foresets.
Numerical experiments indicate that even under relatively low-amplitude sea level cycles, wave erosion provides considerable amounts of sediment to the subaqueous delta front and effectively decouples the subaerial delta front development from the subaqueous rollover point. Thus the initiation of the wave ravinement surface can be associated with synchronous subaqueous delta progradation, and in a proportional increase of subaqueous clinoform topset length. The decoupling of the behaviour of compound clinoform segments necessitates further studies and an enhancement of sequence stratigraphic terminology. During sea level rise, regression of the coastline may correspond with aggradation or non-deposition of the subaqueous topset. Hence, the correlation between rollover points and sealevel is a tenuous one. For direct correspondence only the coastal rollover point (the shoreline) should be used. Relative sealevel rises will be underrepresented when using the subaqueous rollover point.
Wave-influenced deltas create a platform due to continuous wave reworking. This low-angle shelf allows rapid progradation of the subaerial delta platform during relative sealevel highstands and falls. Only where sea level falls below the subaqueous rollover point will fluvial incision occur and an erosional, subaerial unconformity will form. Only under large glacio-eustatic cycles do large-scale incision and lowstand systems occur. This contrasts starkly with fluvially dominated systems where the system creates a higher angle shelf. A lowering of base level will therefore induce a subaerial unconformity more easily than in a wave-dominated system. These results suggest that long-lived, wave-influenced deltas most likely contain fewer subaerial unconformities than fluvial dominated deltas.

Future model development

Ideally, all simplified representations of sedimentary and stratigraphic systems would become obsolete and would be modelled using a full 3D representation of water flow and sediment transport. Although hydrodynamics can be modelled quite accurately, the main problems herein are the large discrepancies in the sediment transport equation, which require extensive calibration not possible on geological time scales. Also, the highly detailed initial and boundary conditions for these advanced model types are, even in recent Quaternary systems, unknown. Therefore these must be represented stochastically, thereby at least partially negating the detailed process representation.

The following section illustrates some ideas towards future model applications.

The relative influence of autogenic processes under allogenic forcing

Obviously the active delta area increases in time, though not all areas receive water and sediment simultaneously. Effectively, this prograding in two dimensions results in a net lengthening of the river channel due to progradation and by forcing the river to take the "long way around". As the shortest path has been filled in resulting in insufficient gravitational advantage. In two-dimensional experiments Muto et al (2007) showed that this increase in delta plain size is sufficiently large to cause auto-retreat of the shoreline under constant sealevel rise, without any change in sediment supply. Future experiments will focus on delta behaviour under allocyclic control to determine the effects of any "out-of-plane" variations. Figure 8.1 shows the stratigraphic realisations of a shelf edge delta, under influence of a rapid rise in sea level. Little autogenically induced delta lobe switches are observable during the rapid sealevel rise,

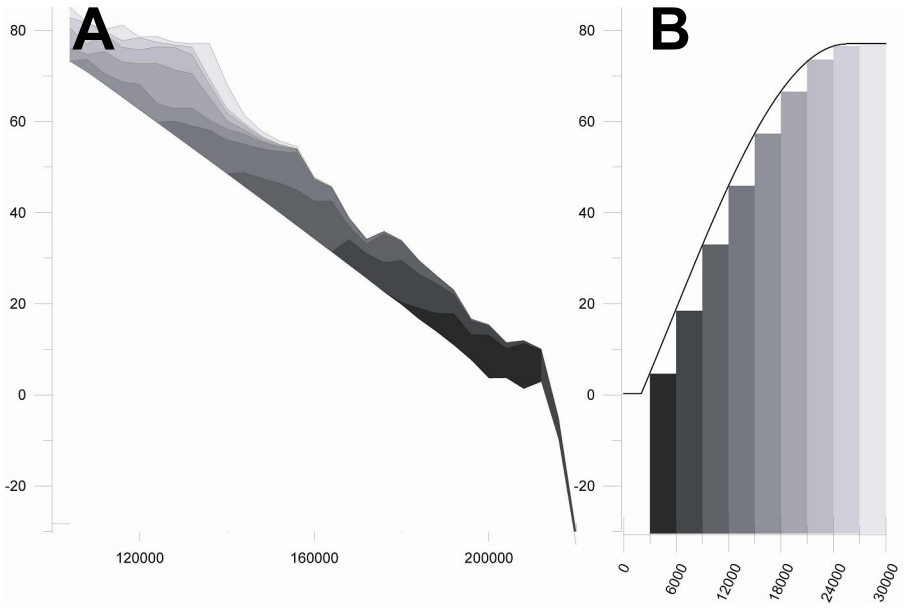

Figure 8.1. Transgressive and highstand systems tract Cross section through time (A) and the associated sea level curve (B)

in these 2000-year interval deposits. Yet these are probably present on a slightly smaller scale. Especially as aggradation will be rapid under conditions of rising base level, thus inducing many more avulsions.
Under strong allogenic forcing, the effect of the autogenic processes observed in these time invariant experiments will be somewhat limited. Yet under conditions where the hypothetical A/S is around or near unity, rapid aggradation on the delta plain will allow the avulsion rate to increase dramatically. Effectively resulting in similar results as the time-invariant examples, but at a much higher frequency.
SimClast may be used to quantitatively determine the relative influence of autogenic processes under similar allogenic controls. This distinction is impossible to make in field studies, making quantitative numerical models the only choice for this subject.

Towards a solution of the inverse problem
Current approaches to geological modelling of complex fluvial reservoirs rely heavily on spatial statistical models designed to simulate fields of continuous stochastic variables or spatial arrangements of specific objects (e.g. sand bodies or shale lenses). Although such techniques are potentially capable of creating realistic-looking models, they provide limited opportunities to directly incorporate knowledge of the physical laws that govern basin-filling processes. This is mirrored in the fact that current geological reservoir models typically suffer from a high degree of non-uniqueness, which seems at least partly attributable to the fact that alluvial architecture is stochastically generated without regard for the basin-scale geological scenario. The integration of basin and reservoir-scale geological information in such models is likely to narrow down the range of possible scenarios (realizations) at an early stage, which should result in more efficient optimisation of candidate models.
To contribute towards solution of this problem, SimClast incorporates a reservoir-scale alluvial architecture module nested within a basin-scale sequence-stratigraphic model. We propose a new optimisation strategy, in which the model is run with the intent to approximate large-scale basin-fill properties (based on geological background information about sea level, sediment supply, subsidence, and so forth). Subsequently it may be stochastically optimised to mimic the sub-grid (reservoir-scale) properties of selected parts of the basin fill. This approach promises a simultaneous increase in the geological credibility of stochastically simulated fluvial reservoir models and a significant reduction of the time needed to attain an acceptable level of fit to observations.

Real-world applications
SimClast was created to simulate both theoretical and real-world settings. Up until now, no real calibration to field-scale areas has been done. Yet, the wide variety of processes and scales in the model does make it usable in many settings.

Current work using field data is ongoing on several projects:
At Kiel University, Germany, SimClast is being used to model the transgressive and highstand infill of the Mekong delta, Vietnam. This project focuses on the large-scale

stratigraphic patterns, especially the infill of the incised valleys during sealevel rise and subsequent delta progradation during sealevel highstand.
At the Delft University of Technology modelling work is being done on the sediment (re-) distribution of prodelta-deposits in the Adriatic Sea from the Last Glacial Maximum to the present. This project focuses on the distribution of the muddy clinoforms, which have been strongly influenced by thermo-haline currents. The muddy clinoform project may be extended to understand the stacking architecture of these poorly understood clinoforms in other basins.
Ongoing research on the Holocene development of the Mahakam Delta, Indonesia, at the Delft University of Technology will form an interesting and challenging modelling exercise due to the strong influence of tidal forces and tropical vegetation. Correct modelling of this system will require the addition of vegetation. Biogeomorphological processes on decadal time scales influence many longer time scale processes. Our peatland model, albeit simplistic, is a first-order, approximation towards this coupling. Future additions might include several vegetation types, which differ in their sediment capture and bed stabilising features. This will require a dependence of vegetation type on climate and careful calibration of local groundwater table to the growth rate of vegetation. Tidal currents strongly influence the Mahakam Delta and will also need to be incorporated. This will allow the modelling of the entire range of the Galloway delta classification. The potential flow routine is a first step towards this, but will need to be expanded to include complexities such as tidal flow through restrictions, change in tidal amplitude and subgrid-scale tidal channels.

References

Albertson, M. L., Dai, Y. B., Jensen, R.A. & Hunter, R., 1950. Diffusion of submerged jets. *American Society of Civil Engineers Transactions, v. 115,* p. 639-697.

Asselen, van S., Stouthamer, E. & Ash, van T., W.J., 2009. Effects of peat compaction on delta evolution: A review on processes, responses, measuring and modelling. *Earth Science Reviews, v. 92*, p. 35-51.

Athy, L.F., 1930. Density, porosity and compaction of sedimentary rocks. AAPG Bulletin 14, 1 24.

Bagnold, R.A., 1963. Mechanics of marine sedimentation. *In: Hill, M.N. (ed.), The sea: Wiley-Interscience, New York, v.3*, p. 507-527.

Bahr, D.B., Hutton, E.W.H., Syvitski, J.P.M., Pratson, L.F., 2001. Exponential approximations to compacted sediment porosity profiles. Computers & Geosciences 27, 691-700.

Bailard, J.A., 1981. An energetics total load sediment transport model for a plane sloping beach. *Journal of Geophysical Research, v. 86*, p. 10938-10954.

Berendsen, H.J.A. and Stouthamer, E., 2000. Late Weichselian and Holocene palaeography of the Rhine-Meuse delta, The Netherlands. Palaeography, Palaeoclimatology, Palaeoecology 161, 311-335.

Bhattacharaya, J.P. & Giosan, L., 2003. Wave-influenced deltas: geomorphological implications for facies reconstruction. *Sedimentology, v. 50-1*, p. 187-210.

Bhattacharya. J.P, 2007. Deltas. *In: Facies Models Revisited. SEPM Special Publication,* No. 84.

Bierkens, M.F.P. and Te Stroet, C.B.M., 2007. Modelling non-linear water table dynamics and specific discharge through landscape analysis. Journal of Hydrology 332, 412-426.

Blum, M.D., 1993. Genesis and architecture of incised valley fill sequences: a late Quaternary example from the Colorado River, Gulf coastal plain of Texas, *in: Weimer, P. & Posamentier, H.W., eds., Siliciclastic Sequence Stratigraphy: Recent developments and Applications: American Association of Petroleum Geologists, Memoir 58*, p. 259-283.

Blum, M.D. & Tornqvist, T.E., 2000. Fluvial responses to climate and sea-level change: a review and look forward: *Sedimentology, v.* 87, p. 2-48.

Boogaart, P.W., Tucker, G.E. & de Vries, J.J., 2003. Channel network morphology and sediment dynamics under alternating periglacial and temperate regimes: a numerical simulation study. *Geomorphology* 54, 257-277.

Bowman, S.A. & Vail, P.R., 1999. Interpreting the stratigraphy of the Baltimore Canyon section, offshore New Jersey with PHIL, a stratigraphic simulator. In *Numerical Experiments in Stratigraphy: Recent advances in Stratigraphic and Sedimentologic Computer Simulations,* ed. JW Harbaugh, WL Watney, EC Rankey, R. Slingerland, RH Goldstein, EK Franseen, SEPM Spec. Publ. 62, p. 117-138. Tulsa, OK: SEPM.

Bull, W.B., 1991. Geomorphic Responses to Climatic Change, 326 pp, Oxford, Univ. Press, New York, 1991.

Bridge, J.S, & Dominic, D.F., 1984. Bed load grain velocities and sediment transport rates. *Water Resources Research* 20-4, 476-490.

Bridge, J.S., 2003. Rivers and Floodplains; Forms, Processes and Sedimentary Record. Blackwell Publishing, Oxford, UK, 491 pp.

Bristow, C.S. & Best, J.L., 1993. Braided rivers: perspectives and problems, *In: Best, J.L. and Bristow, C.S., eds., Braided Rivers: Geological Society of London, Special Publication 75,* p. 1-11.

Cattaneo, A., Trincardi, F., Asioli, A. & Correggairi, A., 2007. The Western Adriatic shelf clinoform: energy-limited bottomset. *Continental Shelf Research, v. 27*, p. 506-525.

Catuneanu, O., Abreu, V., Bhattacharaya, J.P., Blum, M.D., Dalrymple, R.W., Eriksson, P.G., Fielding, C.R., Fisher, W.L., Galloway, W.E., Gibling, M.R., Giles, K.A., Holbrook, J.M., Jordan, R., Kendall, C.G.S.C., Macurda, B., Martinsen, O.J., Miall, A.D., Neal, J.E., Nummedal, D., Pomar, L., Posamentier, H.W., Pratt, B.R., Sarg, J.F., Shanley, K.W., Steel, R.J., Strasser, A., Tucker, M.E. & Winker, C., 2009. Towards the standardization of sequence stratigraphy. *Earth Science Reviews, v. 92*, p. 1-33.

CERC, 1984. Shore Protection Manual (2 volumes). Coastal Engineering Research Centre, Waterway, Experiment Station, Corps of Engineers.

Christieblick, N. & Driscoll, N.W., 1995. Sequence stratigraphy. *Annu. Rev. Earth. Planet. Sci, v. 23*, p. 451-478.

Clevis, Q., De Boer, P.L., & Wachter. M., 2003. Numerical modelling of drainage basin evolution and three-dimensional alluvial fan stratigraphy. *Sedimentary Geology* 163, 85-110.

Cowell, P.J., Roy, P.S. & Jones, R.A., 1995. Simulation of large-scale coastal change using a morphological behaviour model. *Marine Geology, v. 126*, p. 45-61.

Dalman, R.A.F. & Weltje, G.J., 2008. Subgrid parameterisation of fluvio-deltaic stratigraphy. *Computers & Geosciences Special Publication. Computers & Geosciences, v.* 34-10, p. 1370-1380.

Desbarats, A.J., Logan, C.E., Hinton, M.J., Sharpe, D.R., 2002. On the kriging of water table elevations using collateral information from a digital elevation model. Journal of Hydrology 255, 25-38.

Einstein, H.A., 1950. The bedload function for sediment transportation in open channel flows. *U.S. Department of Agriculture Technical Bulletin* 1026, 1-78.

Emery, D., and K.J. Myers, 1996, Sequence stratigraphy: Oxford, Blackwell Science, 297 p

Fagherazzi, S., Howard, A.D. & Wiberg, P.L., 2004. Modelling fluvial erosion and deposition on continental shelves during sea level cycles. *Journal of Geophysical Research* 109, 1-16.

Fagherazzi, S, & Overeem, I., 2007. Models of Deltaic and Inner Continental Shelf Landform Evolution. *Annu. Rev. Earth Planet, Sci, v. 35*, p. 685-715.

Fisher, W.L., Brown, L.F., Scott, A.J. and McGowen, J.H., 1969. Delta systems in the exploration for oil and gas, a research colloquium: Austin, Texas, Texas Bureau of Economic Geology, 204 p.

Fisk, H.N., 1961. Bar finger sands of the Mississippi delta, *in* Peterson, J.A. & Osmond, J.C., eds., Geometry of Sandstone Bodies – A Symposium : Tulsa, American Association of Petroleum Geologists, p. 29-52.

Flemings, P.B. & Grotzinger, J.P., 1996. STRATA: freeware for analysing stratigraphic problems. *GSA Today, v. 12*, p. 1-7.

Freeman, G.T., 1991. Calculating catchment area with divergent flow based on a regular grid. *Computers & Geosciences* 17-3, 413-422.

Gibbs, R.J., Mathews, M.D. & Link, D.A., 1971. The relationship between sphere size and settling velocity. *Journal of Sedimentary Petrology, v. 92*, p. 8244-8264

Gouw. M.J.P. and Berendsen, H.J.A, 2007. Variability of channel-belt dimensions and the consequences for alluvial architecture: observations from the Holocene Rhine-Meuse delta (The Netherlands) and Lower Mississippi Valley (U.S.A.) Journal of Sedimentary Research 77, 124-138.

Granjeon, D. & Joseph, P., 1999. Concepts and applications of a 3-D multiple lithology, diffusive model in stratigraphic modelling. In: J.W. Harbaugh, W.L. Watney, E.C. Rankey, R. Slingerland, R.H. Goldstein & E.K. Franseen (Eds.), Numerical Experiments in Stratigraphy: Recent Advances in Stratigraphic and Sedimentologic Computer Simulations *SEPM Special Publication* 62, 197-210.

Guccione, M.J., 1994. Indirect response of the Peace River, Florida, to episodic sealevel change. *Journal of Coastal Research, v. 11*, p. 637-650.

Harbaugh, J.W. & Bonham-Carter, G., 1970. Computer simulation in geology. P. 575.

Harris, C.K. & Wiberg, P.L., 2001. A two-dimensional, time-dependent model of suspended sediment transport and bed reworking for continental shelves. *Computers & Geosciences, v. 27*, p. 675-690.

Hart, B.S. & Long, B.F., 1996. Forced regressions and lowstand deltas: Holocene Canadian examples: Journal of Sedimentary Research, v. 66, p. 273-298.

Haq, B.U., Hardenbol, J. & Vail, P.R., 1987. Chronology of fluctuating sea level since the Triassic (250 million years to present). *Science 235*, pp. 1156-1167.

Heller, P.L. & Paola, C., 1996. Dowstream changes in alluvial architecture: An exploration of controls on channel stacking patterns. *Journal of Sedimentary Research, v. 666-2,* p. 297-306.

Hilbert, D.W., Roulet, N., Moore, T., 2000. Modelling and analysis of peatlands as dynamical systems. Journal of Ecology 88, 230-242.

Holbrook, J., Scott, R.W. & Oboh-Ikuenobe, F.E., 2006. Base-level buffers and butresses: A model for upstream versus downstream control on fluvial geometry and architecture within sequences. *Journal of Sedimentary Research, v. 76*, p. 162-174.

Horikawa, K. K., C.T. (1966). "A Study of Wave Transformation Inside the Surf Zone." Proceedings of the 10th Coastal Engineering Conference: 217-233.

Howard, A.D., 1994. A detachment-limited model of drainage basin evolution. *Water Resources Research* 30-7, 2261-2285.

Hutton, E.W.H. & Syvitski, J.P.M., 2007. Sedflux 2.0: an advanced process-response model that generates three-dimensional stratigraphy. *Computers & Geosciences*, v. 34-10, pp. 1319-1337.

Ikeda, S., Parker, G. & Sawai, K., 1981. Bend theory of river meanders, part 1, Linear development, *Journal of Fluid Mechanics*, 112, 363-367.

Jerolmack, D.J. & Mohrig, D., 2007. Conditions for branching in depositional rivers. *Geology, v. 35-5*, p. 463-466.

Jerolmack, D.J. & Paola, C., 2007. Complexity in a cellular model of river avulsion. *Geomorphology, v. 91*, p. 259-270.

Jones, L.S. & Schumm, A., 1999. Causes of avulsion: an overview. *Special Publications International Association of Sedimentology* 28, 171-178.

Karim, F., 1998. Bed material discharge predicition for nonuniform bed sediments. *Journal of Hydraulic Engineering, v. 124-6*, p. 597-604.

Karssenberg, D.J., Törnqvist, T., Bridge, J.S., 2001. Conditioning a process-based model of sedimentary architecture to well data. *Journal of Sedimentary Research* 71, 868-879.

Karssenberg, D.J. & Bridge, J.S., 2008. A three-dimensional numerical model of sediment transport, erosion and deposition within a network of channel belts, floodplain and hill slope: extrinsic and intrinsic controls on floodplain dynamics and alluvial architecture. *Sedimentology, v. 55-6*, p. 1717-1745.

Kehew, A.E., 2006. Geology for engineers and environmental scientists (3rd ed.). Pearson Prentice Hall, pp. 395-449.

Kim, W., Paola, C., Swenson, J.B. & Voller, V.R., 2006. Shoreline response to autogenic processes of sediment storage and release in the fluvial system. *Journal of Geophysical Research – Earth Surface, v. 111-F4*.

King, F.H., 1899. Principles and conditions of the movements of groundwater. US Geol. Survey 19th Ann. Rep. Part 2, 59-294.

Knighton, D. 1998. Fluvial Forms and Processes – A New Perspective. Edward Arnold, London, 383 pp.

Kleinhans, M. & Stouthamer, E., 2005. Remarkable bifurcation stability in the Holocene Rhine delta. In: Abstracts, 8th International Conference on Fluvial Sedimentology, Delft, The Netherlands.

Komar, P.D., 1998. Beach processes and sedimentation.

Langbein, W.B. & Schumm, S.A. 1958. Yield of sediment in relation to mean annual precipitation. *Transactions of the American Geophysical Union, v. 39*, p. 1076-1084.

Leeder, M.R., 1978. A quantitative stratigraphic model for alluvium, with special reference to channel deposit density and interconnectedness. In: A.D. Miall (Ed.) Fluvial Sedimentology, *Canadian Society of Petroleum Geology Memoirs* 5, pp. 587-596.

Leopold, L.B. & Maddock, Jr.T., 1953. The hydraulic geometry of stream channels and some physiographic implications. *U.S. Geological Survey Professional Paper* 252, 57.

Li, M.Z., & Amos, C.L., 2001. SEDTRANS96: the upgraded and better calibrated sediment transport model for continental shelves. *Computers & Geosciences, v. 27*, p. 619-645.

Løseth, T.M., Steel, R.J., Crabaugh, J.P. & Schellpeer, M., 2006. Interplay between shoreline migration paths, architecture and pinchout distance for siliciclastic shoreline tongues: evidence from the rock record. *Sedimentology, v. 53*, p. 735-767.

Mackey, S.D., Bridge, J.S., 1995. Three-dimensional model of alluvial stratigraphy; theory and applications. *Journal of Sedimentary Research* 65-1, 7-31.

Martinez, P.A., 1987. WAVE: Program for simulating onshore-offshore sediment transport in two dimensions. *Computers & Geosciensces, v. 13-5*, p. 513-532.

Martinez, P.A. & Harbaugh, J.W., 1993. Simulating nearshore environments. Pergamon Press, Oxford, UK.

Muto, T., Steel, R.J. & Swenson, J.B., 2007. Autostratigraphy; a framework norm for genetic stratigraphy. Journal of Sedimentary Research, v. 77-1, p. 2-12.

McCave, I.N., 1972. Transport and escape of fine-grained sediment from shelf areas. In: Swift, D.J.P., Duane, D.B., Pilkey, O.H. (Eds.), Shelf Sediment Transport: Process and Pattern. Von Nostrand Reinhold, New York, pp. 225-248.

Meijer, X.D., 2002. Modelling the drainage evolution of a river-shelf system forced by Quaternary glacio-eustasy. *Basin Research* 14-3, 361-377.

Miche, R., 1944. Undulatory movement of the Sea in Constant and Decreasing Depth. *Ann. de Ponts et Chaussees* (May-June, July-August), pp. 25-78, 131-164, 270-292, 369-406.

Michels, K.H., Kudrass, H.R., Hubscher, C., Suckow, A. & Wiedicke, M., 1998. The submarine delta of the Ganges-Brahmaputra; cyclone dominated sedimentation patterns. *Marine Geology, v. 149*, p. 133-154.

Nanson, G.C. & Huang, 1999. Anabranching rivers; divided efficiency leading to fluvial diversity. In: A.J. Miller & G. Avijit (eds). Varieties of fluvial form, Geomorphology publication 7, 477-494.

Niedoroda, A.W., Reed, C.W., Swift, D.J., Arato, H. & Hoyanagi, K., 1995. Modelling shore-normal large-scale coastal evolution. *Marine Geology, v. 126*, p. 181-199

Niedoroda, A. W., C. W. Reed, H. Das, J. Koch, J. Donoghue, Z. B. Wang and M. J. F.
Stive. 2003.Modeling Large-scale Morphodynamics of Complex Coastal Systems. *Coastal Sediments '03, ASCE, Proceedings 5th International Symposium on Coastal Engineering and Science of Coastal Sediment Processes,* Clearwater, Florida, 14 pps.

Nielsen, P., 1979. Some basic concepts of wave sediment transport. Institute for Hydrodynamics and Hydraulic Engineering, Technical University of Denmark, Serie Paper 20, 160 pp.

Nitttrouer, C.A., Kuehl, S.A., Figueiredo, A.G., Mead, A.A., Sommerfield, C.K., Rine, J.M., Faria, E.C. & Silveira, O.M., 1996. The geological record preserved by Amazon shelf sedimentation. *Continental Shelf Research, v. 16-5/6*, p. 817-841.

Olariu, C. & Bhattacharya, J.P., 2006. Terminal distributary channels and delta front architecture of river-dominated delta systems. *Journal of Sedimentary Research* 76, 212-233.

Oreskes, N., Shrader-Frechette, K. & Belitz, K., 1994. Verification, validation and confirmation of numerical models in earth sciences. *Science, v. 263,* p. 641-646.

Overeem, I. & Weltje, G.J., 2001. Conditioning channel switching for a 3-D fluvio-deltaic process model. In: IAMG 2001, Proceedings of the 6th Annual Conference of the International Association for Mathematical Geology, Cancun, Mexico, 6-12 September 2001; www.kgs.ku.edu/Conferences/IAMG/Sessions/H/Papers/overeem.pdf

Overeem, I., Syvitski, J.P.M. & Hutton, E.W.H., 2005. Three-dimensional numerical modelling of deltas. *In: Giosan, L. & Bhattacharya, J.P., eds., River Deltas – Concepts, Models, and Examples: SEPM Special Publication 83,* p. 13-30.

Paola, C., Heller, P.L. & Angevine, C.L., 1992. The large scale dynamics of grain-size variation in alluvial basins, 1: Theory. *Basin Research* 4, 73-90.

Paola, C., 2000. Quantitative models of sedimentary basin filling. *Sedimentology* 47 (Suppl.1), 121-178.

Posamentier, H.W. & Allen, G.P., 1999. Siliciclastic Sequence Stratigraphy: concepts and applications. *Concepts in Sedimentology and Paleontology, v. 7*, Society of Economic Paleontologists and Mineralogists (SEPM), 210 pp.

Press, W.H., Flannery, B.P., Teukolsky, S.A. & Vetterling, W.T., 1989. Numerical Recipes – The Art of Scientific Computing (FORTRAN version). Cambridge University Press, Cambridge, UK.

Roelvink, J.A. and Van Banning G.K.F.M., 1994, Design and Development of DELFT3D and application to coastal morphodynamics*, Proceedings of Hydroinformatics 1994,* Verwey, Minns, abovic and Maksimovic eds., A.A. Balkema Publishers, Rotterdam, 451-456.

Pizzuto, J.E., 1987. Sediment diffusion during overbank flows. *Sedimentology, v 34*, p. 301-317.

Ridente, D. & Trincardi, F., 2005. Pleistocene "muddy" forced-regression deposits on the Adriatic shelf: A comparison with prodelta deposits of the late Holocene highstand mud wedge. *Marine Geology,* doi:10.1016/j.margeo.2005.06.042

Rouse, H., 1937. Modern conceptions of mechanics of fluid turbulence. *Transactions, ASCE,* 102, 436-505.

Schumm, S.A., 1977. The fluvial system. John Wiley & Sons, New York, 338 pp.

Sclater, J.G. and Christie, P.A.F., 1980. Continental stretching: An explanation of post-mid-Cretaceous subsidence of the central North Sea basin. Journal of Geophysical Research 85, 3711-3939.

Sheldon N.D. and Retallack G.J., 2001. Equation for compaction of paleosols due to burial. Geology 29, 247-250.

Shanley, K.W. & McCabe, P.J., 1993. Alluvial architecture in a sequence stratigraphic framework: a case history from the Upper Cretaceous of southern Utah, USA. In: S.S. Flint & I.D. Bryant (Eds.), The Geological Modelling of Hydrocarbon Reservoirs and Outcrop Analogues*, Special Publication of the International Association of Sedimentologists* 15, pp. 21-56.

Slingerland, R.H., Harbaugh, J.W. & Furlong, K.P., 1994. Simulating clastic sedimentary basins. Prentice Hall publishers, Eaglewood Cliffs, USA, 220 pp.

Slingerland, R.H. & Smith, N.D., 1998. Necessary conditions for a meandering-river avulsion. *Geology* 26-5, 435-438.

Stive, M.J.F. & De Vriend, H.J., 1995. Modelling shoreface profile evolution. *Marine Geology, v. 126,* p. 235-248.

Stolper, D., List, J.H & Thieler, R.E., 2005. Simulating the evolution of coastal morphology and stratigraphy with a new morphological-behaviour model (GEOMBEST). *Marine Geology, v. 1-4, p. 17-36*.

Storms, J.E.A., 2003. Event-based stratigraphic simulation of wave-dominated shallow-marine environments. *Marine Geology, v. 199*, p. 83-100.

Storms, JEA, Geleynse, N, Stive, MJF & Walstra, DJR (2008). Forward stratigraphic modelling of progrding deltas using a process model. In R Dalrymple, G Hampson, S Kuehl, D Mohrig & J Swenson (Eds.), *SEPM field conference proceeding* (pp. 1). Tulsa, OK, USA: SEPM.

Stouthamer, E. and Berendsen, H.J.A., 2000. Factors controlling the Holocene avulsion history of the Rhine-Meuse delta (the Netherlands). Journal of Sedimentary Research 70, 1051-1064.

Stouthamer, E. & Berendsen, H.J.A., 2001. Avulsion Frequency, Avulsion Duration and Interavulsion period of Holocene channelt belts in the Rhine-Meuse Delta, The Netherlands. Journal of Sedimentary Research, v. 71-4, p. 589-598.

Swenson, J.B., Paola, C., Pratson, L., Voller, V.R. & Murray, A.B., 2005. Fluvial and marine controls on combined subaerial and subaqueous delta progradation: Morphodynamic modelling of compound-clinoform development. *Journal of Geophysical Research – Earth Surface, v. 110-F02013*.

Syvitski, J.P., Skene, K.I., Nicholson, M.K. & Morehead, M.D., 1998. Plume 1.1: Deposition of sediment from a fluvial plume. *Computers & Geosciences, v. 24-2,* p. 159-171.

Tetzlaff, D.M. & Harbaugh, J.W., 1989. Simulating Clastic Sedimentation; Computer Methods in the Geosciences, Van Nostrand Reinhold, New York, p. 202.

Törnqvist, T.E., 1998. Longitudinal profile evolution of the Quaternary Rhine-Meuse river system during the last deglaciation: Interplay of climate change and glacio-eustasy? *Terra Nova, v. 10,* p. 11-15.

Van Den Berg, J.H., 1995. Prediction of alluvial channel pattern of perennial rivers. *Geomorphology* 12, 259-279.

Van Dijk, M., Postma, G. & Kleinhans, M.G. Autogenic cycles of sheet and channelised flow on fluvial-fan deltas. *In; River, Coastal and Estuarine Morphodynamics,* Eds. Dohmen-Janssen, C.M. & Hulscher, S.J.M.H., 2008, Taylor and Francis Group, London, UK.

Wright, V. P. & Marriott, S.B., 1993. The sequence stratigraphy of fluvial depositional systems: the role of floodplain sediment storage. *Sedimentary geology,* , v. 86-3-4, p. 203-210

Yu, Z., Campbell, I.D., Vitt, D.H., Apps, M.J., 2001. Modelling long-term peatland dynamics. I. Concepts, review, and proposed design. Ecological Modelling 145, 197-210.

Samenvatting

In het algemeen is het doel van stratigrafische modelleren om de onderliggende regels en wetmatigheden die de complexe interactie tussen processen besturen te ontdekken. Er is in het algemeen enige zelforganisatie, aangezien het uiteindelijke resultaat van deze processen in een voorspelbaar en herkenbaar eindproduct culmineren. Door de expertise te gebruiken die in korte termijn (10-tallen jaren) modelleerwerk en morphologisch onderzoek is gedaan, is het nu mogelijk om deze korte-termijn processes te extrapoleren en een beter stratigrafisch model te bouwen met morphodynamische eigenschappen. De ontwikkelingen in numeriek modelleren hebben nu het punt bereikt waarop simulatie van de evolutie van continentale marges over lange termijnen mogelijk is met een goede representatie van sedimentaire processen. De huidige generatie van numeriek modellen zijn in staat om realistische strata en sedimentaire architectuur te produceren in een reeks sedimentaire milieus van fluvio-deltaisch tot diepzeebekkens. Echter, veel van deze modellen beperken zicht tot een enkel milieu en zijn inherent twee dimensionaal (doorsnede). De volgende logische stap is om deze modellen te koppelen en uit te breiden om een volledig, holistisch drie dimensionaal model van de continentale marge te maken.
Het doel van dit proefschrift is om te illustreren hoe een overkoepelend sedimentair systeem over verschillende sedimentaire milieus kan worden nagebootst in een dynamisch model. Het uiteindelijke doel van het onderzoek naar de dynamiek in sedimentaire systeen is om het systeem van bron tot eindpunt volledig weer te geven. In dit proefschrift worden de eerste stappen tot dit doel genomen, en worden een reeks verschillende model onderdelen besproken alsmede enkele, theoretische, toepassingen. Uiteindelijk kan door het koppelen van modellen van sediment productie in het drainage gebied en diepzee sediment transport, een grotere schaal bestudeerd worden. Echter, dit zal in de toekomst verder moeten worden uitgewerkt.

Geaggrageerd modelleren
Sedimentaire milieus staan altijd open voor invloeden van andere milieus. De enige uitzondering hierop zijn diepmariene, massa-transport afzettingen die grotendeels door bovenstroomse invloeden beinvloed worden. Door de continue interactie tussen de milieus ontstaan de meeste complexe fenomenen op de grenzen, waar de verschillende processen vechten om de controle op de afzettingen. Om deze interessante terugkopplings-mechanismen te besturen, aggregeert SimClast verschillende processen in contintentale en marine omgevingen. Deze impliciete koppeling van processen in het model heeft ons vrij gelaten om deze mechanismen in boven- en benedenstroomse richting te bestuderen, zonder allogene sturing. De volgende paragrafen geven een samenvatting van de modelbeschrijving en de belangrijkste bevindingen uit onze numerike experimenten welke te lezen zijn in dit proefschrift.

Modelbeschrijving (Hoofdstukken 2, 3, 4, & 5)
Simclast is een 3D stratigrafisch model op de schaal van sedimentaire bekkens, dit staat het interacteren van verschillende sedimentaire milieus toe. Wij hebben het van 2004 tot 2008 ontwikkeld aan de Technische Universiteit Delft and gebruikten hiervoor een deel van de Meijer (2002) code voor de boekhoudkundige, laad- en wegschrijf-algoritmes. SimClast modelleert de hydrodynamica en het bijbehorende sediment transport in 2D, verticale-stroming is gemiddeld. Deze simplificatie staat ons toe om de complexe interactie tussen fluviatiele en golf invloeden op deltaische en kustprocessen te bestuderen. De modeltoepassingen focussen vooral op de erosieve en nondepositie gebeurtenissen, aangezien daar waarschijnlijk het grootste deel van de stratigrafische tijd is.
Korte-termijn, hoge-resolutie processen zijn gekoppeld met het lange-termijn stratigrafisch model, door het nesten van geparameteriseerde versies van de hoge-resolutie processen. Wij extrapoleren fysische en empirische relaties van de geomorphologidsche ontwikkeling en implementeren deze in het model. Een noodzakelijke restrictie in lange-termijn modelleren op bekken-schaal is het gebruik van relatief grove gridcel discretizaties (in de orde van kilometers), aangezien het te modelleren gebied op de schaal van continentale marges is en de tijdsduur in de orde van vele millenia. Gebieden van groot belang worden gesimuleerd door het implementeren van sub-grid schaal processen in het grote-schaal model: dit verfijnt de model dynamiek en de stratigrafie die eruit voortkomt.
De processen welke in het model gesimuleerd worden zijn: Fluviatiele rivier dynamiek en oeverwal afzettingen, mariene rivier uitstroom afzettingen, open mariene stromingen, golf resuspensie, golf beinvloede kustwaartse en kust-parallelle sediment transport. Deze manier van gecombineerd modelleren laat inzichten toe in de processen welke de flux van energie en gerelateerd transport van clastisch materiaal en het effect van externe invloeden in alle sedimentaire milieus. Veel belangrijke processen werken op een relatief kleine schaal, bijvoorbeeld in rivier processen is een avulsie een locaal fenomeen, maar de invloed ervan op fluviatiele architectuur is verstrekkend. Dit betekent dat het model deze processen wel moet incorporeren, maar ook nog redelijk efficent (cq snel) moet kunnen zijn. In combinatie met de, relatief grote gridcellen zorgt dit voor een lastig dillema. Wij lossen dit probleem op door de belangrijkste, lokale processen te implementeren als subgrid schaal routines in the grote-schaal model. Deze parameterizatie verfijnt het morphodynamisch gedrag en uiteindelijk de stratigrafie. SimClast simuleert realistisch geomorfologische en stratigrafisch delta gedrag in rivier- en kust-gedomineerde milieus.

Toepassingen
Ontwikkeling van het rivier netwerk (Hoofdstuk 2)
Onze studie van de ontwikkeling van rivier-gedomineerde, lage-gradient deltas laat duidelijk zien dat een initiele toename van het aantal uitvloei geulen. Echter het aantal uitvloei geulen kan ook afnemen gedurende de progradatie van de delta, specifiek na een grootschalige bovenstroomse avulsie. Op de schaal van de gehele delta (effectief

een combinatie van deltalobben) is een quasi-cyclische, autogene toename en afname van uitvloeikanalen te verwachten en ook gevonden in de model uitkomsten.

Correlatie tussen mariene en continentale afzettingen (Hoofdstuk 6)
De meest distale reden waarom rivieren hun loop verleggen is gravitatief voordeel. Echter, rivieren behouden hun stabiliteit veel langer dan men zou verwachten vanuit puur diffusief transport. Een toename in de lengte van actieve riviergeulen door progradatie leidt direct tot bovenstroomse afzettingen op de delta in vergelijking tot de afzettingen op de delta front en prodelta. Na een avulsie wordt, door de lage gradient, veel sediment afgezet in de nieuwe loop van de rivier, net benedenstrooms van het avulsiepunt. Tegelijkertijd kan er erosie plaatsvinden net bovenstrooms van het avulsiepunt door lokale terugschrijdende erosie totdat de nieuwe geul een stabiel evenwichtsprofiel heeft bereikt. Dit fenomeen zal het sterkste zijn in gebieden waar de riviergeulen relatief stabiel zijn, bijvoorbeeld in gebieden met een hoge gradient, sterke vegetatie en beperkte overstromingen. In gebieden met een lage gradient en gemakkelijk erodeerdbare oevers, zal de hoge avulsie frequentie waarschijnlijk deze sediment ophopings gebeurtenissen lastig te vinden zijn in de afzettingen.
Post-avulsie erosie in de bovenstroomse geulen kan dus terrasvorming in de hand werken, welke tegelijkertijd benedenstrooms lokale aggradatie toelaat. Dit zal dan ook de progradatiesnelheid aan de nieuw deltalob verminderen door de afgenomen sediment toevoer. Deze model-resultaten wijzen naar fases van bovenstroomse terrasvorming door geulinsnijding. Voorbeelden van dit proces in de echte wereld zouden zeer interessante inzichten kunnen geven in dit complexe gedrag (cf Bull, 1991) van delta-lob verplaatsingen en geulverleggingen. Dit autogeen sedimentair terugkoppelings mechanisme geeft ons een potentiele methode om fluviatiel en mariene processen en afzettingen te correleren op een zeer korte tijdschaal.
Echter de uitkomsten van dit onderzoek vergroot wel de mogelijke oorzaken voor sedimentaire fenomen. Incisie of aggradatie kan niet automatisch worden toegeschreven aan veranderen in bovenstroomse, of benedenstroomse sturing, het kan ook een compleet inherent, autogeen proces zijn. Dit mechanisme produceert dan ook een inherente variatie van fluviatiel profielen, zonder dat daar veranderingen in de allogene sturing voor nodig is, dit lijkt dan ook een logische verklaring voor hoge-frequentie incisie-aggradatie cycli in delta afzettingen.

Clinoform gedrag onder invloed van golven (Hoofdstuk 7)
In deltas die door golven worden beinvloed zal de erosieve kracht van de golven erosieve vlakken produceren en als gevolg daarvan het sediment redistribueren door fluctuaties in de zeespiegel. Om dit mechanisme en het effect op delta morfologie en sedimentaire architectuur te beoordelen modelleren wij verschillende zeespiegel cycli. Uit deze experiment blijkft dat de lokale curvatuur van de kustlijn toeneemt tijdens relatieve zeespiegelstijging door de toegenomen discrepantie tussen eroderende kustsegmenten en de kustsegmenten die direct sediment aangevoerd krijgen door rivieren. Zelfs onder relatief lage amplitude zeespiegel fluctuaties transporteren golven forse hoeveelheden sediment naar de foreset van de onderwater delta. Dit mechanisme veroorzaakt snelle progradatie van de onderwater delta en vergroot de

lengte van de onderwater topset. De erosie van de kust en de topset neemt toe en dit extra sediment wordt afgezet op de foresets van de onderwater delta.
Dit principe ontkoppelt de ontwikkeling van de "droge" delta front (de kustlijn) en de onderwater deltafront gedurende zeespiegelfluctuaties. Gedurende de start van golf erosie bij zeespiegelstijging, zal de kustlijn zich terugtrekken maar kan de onderwater deltafront nog steeds prograderen door de aanvoer van sediment door de golferosie. Dit ontkoppelen van het gedrag van de samengestelde (onder- en bovenwater) clinoform maakt verdere studie van delta gedrag onder zeespiegelfluctuaties noodzakelijk. Aangezien zeespiegelstijging gecorelleerd wordt met transgressie van de kustlijn, maar aggradatie of non-depositie van de onderwater topset. Daarom is de correlatie tussen de onderwater knickpoint en zeespiegelcurve lastig te kwantificeren. Om de zeespiegel te kunnen bepalen uit stratigrafie, kan dus eigenlijk alleen de kustlijn gebruikt worden aangezien zeespiegelstijgingen niet, of niet in voldoende mate worden weergegeven als men de onderwater knickpoint gebruikt.
Deltas met een sterke invloed van golven maken een onderwater platform door de continue golfwerking. Dit lage gradient plat staat een snelle progradatie van het "droge", fluviatiele deel van de delta toe gedurende hoge en vallende zeespiegels. Langlevende, golfgedomineerde deltas ondergaan waarschijnlijk minder periodes van insnijdingen dan meer fluviatiel gedomineerde systemen. Grootschalige insnijdingen vinden alleen plaats onder zeer grote zeespiegeldalingen als de zeespiegel onder het onderwater delta platform valt. Fluviatiel gedomineerde systemen maken inherent een hogere gradient platform aan , waardoor een zeespiegeldaling eerder tot insnijding zal leiden.

Dankwoord

Om natuurlijk niemand teleur te stellen hierbij de obligate dankjewels. Mocht ik iemand vergeten zijn, hierbij mijn welgemeende excuses. Hopelijk komt er een tweede editie, opdat ik het kan rectificeren ;).

Als initiator en directe begeleider van dit project is Gert Jan natuurlijk de onmisbare factor in dit onderzoek geweest. Onze soms zeer relevante, soms minder, maar immer fascinerende gesprekken zijn van grote invloed geweest op de ontwikkeling van het model en de experimenten alsmede op mijn persoonlijke ontwikkeling.
Mijn promotor Salle heeft gedurende en na het promotiewerk altijd het volste vertrouwen in mij gehad. In de latere fases van het onderzoek hebben zijn enthousiasme en revisies van de hoofdstukken veel verbeterd aan het proefschrift.

Daarnaast hebben Marcel Stive, Ad van der Spek, Irina Overeem, Rick Donselaar Joep Storms met nuttige discussies mij geholpen ideeen te formuleren en te onderbouwen.

Perceptive reviews of chapter 2 by Quintijn Clevis, Rudy Slingerland, Eric Hutton, John Tipper & Bob Hoogendoorn have been very helpful in shaping the paper.

Geertje Strijker heeft een prachtig stuk conceptueel en toegepast werk geleverd tijdens haar afstuderen, waaruit een groot deel van hoofdstuk 3 is voortgekomen. Alina en Meron zijn momenteel bezig met toepassingen van SimClast in de "echte wereld", hun enthousiasme en praktische vragen hebben de bruikbaarheid van het model zeker verbeterd.

Het grootste deel van het werk is verricht in ons oude gebouw aan de mijnbouwstraat, vandaar nog een speciale dank aan mijn kamer/lunchgenoten Jan Kees en Rick voor de broodnodige koffie en lunchpraat. Daarnaast wil ik Rick ook nog speciaal danken voor de kans om te beginnen bij Toegepaste Geologie.

Behalve al het staren naar een computerscherm, mocht ik ook af en toe naar buiten om studenten te begeleiden. Vooral het veldwerk in Vesc met Jan Kees en Remco is voor mij een prachtige onderbreking geweest.

Daarnaast wil ik alle (ex-)collegas van Geotechnologie bedanken voor koffie/lunch en andere bijeenkomsten, ik hoop dat ik iedereen noem: Joep, Tine, Bob, Stefan, Remco, Marit, Wiebke, Albert, Irina, Kees, Jose, Israel, Duddy, Wieske, Adriaan, Gerrit, Ralf, Lydia, Margot, Hannie, Anke .

Daarnaast wil ik ook nog Jan Willem, Annelies, Marc, Lenneke, Anton en Nicolien bedanken voor de traditionele hemelvaartuitjes. En natuurlijk Gerben, Thijs, Pieter,

Joost, Janneke, Linda, Iris, Eefje, Arnold en Sebas voor de nodige bierbijeenkomsten in concertzaal, Belgie of de Huppeldepub.

Zonder mijn ouders zou er natuurlijk helemaal geen proefschrift zijn, en zij hebben ook direct bijgedragen door regelmatig te helpen met het oppassen. Mijn schoonmoeder Els heeft heel veel opgepast op Findlay en ons daar geweldig mee geholpen. Dankjewel.

Mijn zoontje Findlay, was in het geheel niet behulpzaam, maar ik zou het niet anders wensen.

Christa, onze simultaan promotie was een mooi experiment, het begin en middentraject liep voorspoedig, ook rond de geboorte van onze Zoon.. Het heeft voor mij altijd stimulerend gewerkt om de inhoudelijke en praktische kanten van de promotie met Christa dagelijks te bespreken. Zonder mijn lieve Christa's interesse, steun en hulp was het proefschrift er als zodanig niet geweest.

CV

Born in The Hague (1976), Rory grew up in Alphen aan den Rijn and graduated from the Groene Hart Lyceum in 1995. After this he started the study Science and Policy at the Utrecht University, he finished his propedeuse in 1996 but switched to Geology at the same university. He graduated in 2001 on an experimental sedimentological subject at the Sedimentology Group.
The first year of his professional career was spent at Fugro-Robertsons in Leidschendam and Llandudno, Wales. Most work focussed on regional seismic interpretation, with some log interpretation and paleoreconstruction. In 2002 Rory started working at Applied Geology, DUT, on the integrated sedimentological and forward seismic modelling of the Cook formation (Oseberg field, offshore Norway).
In 2004 he started this PhD research, also at the department of Applied Geology, on numerical modelling of fluvio-deltaic and shallow marine stratigraphy.
Since 2008 Rory has been working at the same department on the Holocene development of the Mahakam Delta, Indonesia.